POLITECNICO DI TORINO

College of Chemical and Material Engineering

Master's Degree

in Chemical and Sustainable Processes Engineering

Master Thesis

Design of prototype-biotech devices for anticancer drugs targeting

Supervisor

Prof. Marco Piumetti

Candidate

Elena Antoniono

November-December 2023

Table of contents

Riassunto in italiano

Nonostante il continuo calo del tasso di mortalità associato all'insorgenza del cancro dall'inizio degli anni 90', esso rappresenta ancora un importante problema di salute pubblica a livello globale. Si stima infatti che esso colpisca quasi il 40% della popolazione nel corso della propria vita. [1] La formulazione di nuovi possibili farmaci antitumorali è quindi di primaria importanza, ma il processo tradizionale di sperimentazione per la scoperta di nuove possibili molecole è altamente costoso e complesso. Nel presente lavoro di tesi, viene presentata l'immobilizzazione della Lattato Deidrogenasi (LDH, numero di commissione enzimatica EC 1.1.1.27) su supporti di silice mesoporosa come nuova tecnica per il rapido e riproducibile test di potenziali composti antitumorali. Misurando l'attività dell'enzima, immobilizzato in un biosensore, in presenza di diversi potenziali farmaci, è possibile infatti investigare la loro efficacia nel ridurre l'attività della Lattato Deidrogenasi nel metabolismo tumorale.

Con l'obiettivo di individuare il supporto di immobilizzazione più adatto, sono stati testati quattro diversi materiali mesoporsi: SBA-$15_{0.25}$, $MCF_{0.75}$, DPS e $DPS_{0.75}$. Essi sono stati analizzati sia nella loro forma non funzionalizzata che etero-funzionalizza. La funzionalizzazione è stata effettuata con due diverse molecole organosilane, l'APTES (3-aminopropiltrietossilano) e il GPTMS (3-glicidilpropiltrimetossilano). Tale processo ha permesso la successiva immobilizzazione dell'enzima scelto, tramite la formazione di legami covalenti tra i residui proteici, in particolare la lisina, e i gruppi funzionali introdotti tramite funzionalizzazione. I biocatalizzatori così sintetizzati sono stati studiati tramite l'ausilio di diverse tecniche di caratterizzazione: spettroscopia infrarossa a trasformata di Fourier (FTIR) e microscopia elettronica a scansione a emissione di campo (FE-SEM). La tecnica analitica di fisisorbimento di azoto liquido a 77K è stata impiegata per l'analisi comparata dei campioni funzionalizzati e non funzionalizzati. Infine, la microscopia a fluorescenza è stata effettuata sui campioni di supporto funzionalizzato e su quelli con enzima immobilizzato.

Dopo l'immobilizzazione della Lattato Deidrogenasi sulla struttura mesoporosa dei materiali scelti, l'attività dell'enzima libero e del biocatalizzatore sintetizzato sono state misurate tramite analisi spettrofotometrica UV-vis. L'attività residua relativa del biocatalizzatore rispetto al corrispettivo libero si è rivelata variabile dal 1,7% al 14,4%, all'interno dei diversi processi di immobilizzazione effettuati. La diminuzione dell'attività enzimatica successivamente al processo di immobilizzazione è ben documentata in letteratura e generalmente associata ad un irrigidimento della proteina.[2] Infatti, tramite la formazione di legami covalenti tra il supporto e l'LDH, esso risulterà localmente irrigidito e non potrà adattarsi al substrato, in questo caso il piruvato, con il caratteristico meccanismo

mano-guanto. Il suddetto meccanismo prevede infatti un mutuo adattamento del substrato e dell'enzima, per la formazione del fondamentale complesso enzima-substrato, tramite cui la reazione catalitica potrà procedere verso la formazione dei prodotti. [3]

Attraverso l'analisi FTIR di ognuno dei campioni citati, è stato possibile individuare i gruppi funzionali coinvolti nel legame covalente tra la proteina e il supporto scelto. Per ogni supporto sono stati analizzati due campioni con enzima immobilizzato: nel primo è stato impiegato il PEG (polietilenglicole) come agente stabilizzante, mentre nel secondo è stato utilizzato il trealosio. I diversi campioni analizzati si differenziano principalmente nella zona detta 'dell'impronta digitale' a numeri d'onda inferiori a 1300 cm^{-1}. Questa zona, come suggerito dal suo nome, è caratteristica di ogni materiale, ma non fornisce alcuna informazione riguardo i legami che il supporto instaura con le molecole utilizzate nel processo di funzionalizzazione o con l'enzima. Per questa ragione e per una maggiore chiarezza nelle immagini, si è preferito escludere suddetti numeri d'onda dalla rappresentazione grafica degli spettri ottenuti attraverso l'analisi FTIR. Viene di seguito descritto il risultato dell'analisi del campione di SBA-$15_{0.25}$, supporto che si è dimostrato essere il più adeguato all'immobilizzazione della Lattato Deidrogenasi.

Dalla prima delle due immagini presenti in *Figura 1* sono stati facilmente individuati diversi picchi, caratteristici del campione non funzionalizzato (curva nera), presenti a numeri d'onda intorno a 3740 cm^{-1}. Questi picchi sono associati alla presenza di gruppi silanolici isolati Si-OH, caratteristici della superfice non funzionalizzata dei materiali mesoporosi utilizzati. Inoltre, picchi di intensità minore possono essere individuati nell'intervallo compreso tra 3650 e 3750 cm^{-1}, sempre per il campione di supporto non funzionalizzato. Essi sono stati associati allo stretching dei legami ossigeno-idrogeno presente nei suddetti gruppi funzionali idrossilici. Entrambi i segnali descritti non sono individuabili negli spettri relativi ai campioni funzionalizzati con ATPES e GPTMS. Questo indica che i gruppi idrossilici dei materiali studiati ricoprono un ruolo fondamentale nella formazione di legami covalenti con le molecole organosilane utilizzate nel passaggio di funzionalizzazione.

Sempre analizzando l'immagine (A) in *Figura 1,* nell'intervallo compreso tra 2930 e 2880 cm^{-1}. Sono stati individuati degli intensi picchi, per gli spettri relativi ai campioni funzionalizzati e quelli relativi ai biocatalizzatori studiati. Questi picchi sono dovuti alla presenza del gruppo -CH, tipico delle molecole organosilane precedentemente citate. La presenza di segnali poco intensi in questo intervallo, per i campioni non funzionalizzati, è da imputarsi ad una non completa rimozione dell'agente templante utilizzato durante il processo di sintesi.

Osservando invece l'ingrandimento rappresentato nell'immagine (B), si può notare che lo spettro del materiale funzionalizzato è caratterizzato dalla presenza di un picco a numeri d'onda intorno a 1710 cm^{-1}, non più presente dopo l'immobilizzazione dell'LDH. Esso è stato identificato da letteratura come corrispondente al doppio legame C=O, gruppo funzionale presente nella struttura del GPTMS. La scomparsa di questo segnale negli spettri relativi ai biocatalizzatori è indice che il doppio legame C=O è coinvolto nella formazione del legame covalente tra la superfice del supporto utilizzato e la proteina.

Un altro picco rappresentativo è quello individuato intorno a 1600 cm^{-1}, relativo al legame ammidico. Questo segnale identifica la presenza dell'enzima ed è pertanto presente solo negli spettri dei biocatalizzatori analizzati. Il picco identificabile intorno a 1640 cm^{-1} è invece relativo al gruppo N-H, ed è quindi presente in tutti gli spettri presentati in (B). Per questa ragione i segnali riportati in questo secondo ingrandimento sono stati normalizzati in corrispondenza di tale picco, fornendo così una più chiara visualizzazione delle spalle a 1710 e 1600 cm^{-1}. [4]

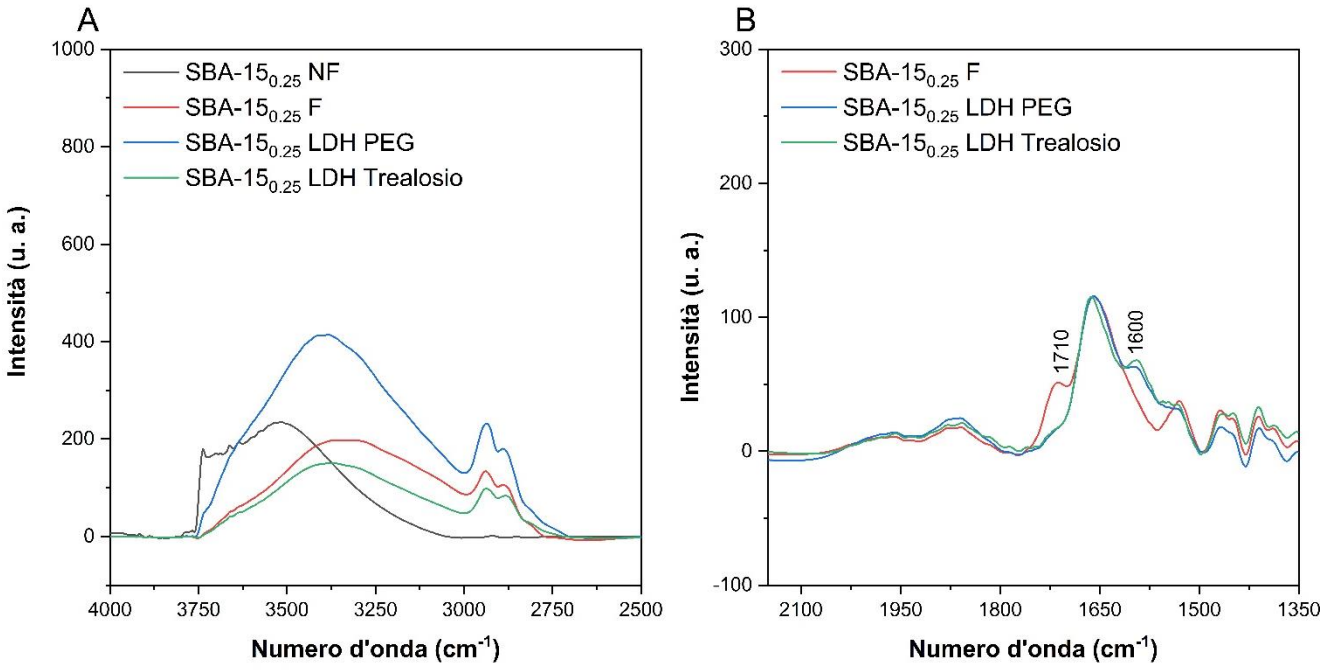

Figura 1. Particolare degli spettri ricavati dall'analisi di SBA-15$_{0.25}$ tra numeri d'onda compresi tra (A) 4000 e 2500 cm^{-1} e (B) tra 2150 e 1350 cm^{-1}. Le abbreviazioni usate si riferiscono a: NF, non funzionalizzato, F, funzionalizzato.

Per valutare la maggiore resistenza dell'enzima immobilizzato rispetto alla sua forma libera, sono stati eseguiti test di attività enzimatica in presenza di diversi agenti denaturanti: solvente organico (etanolo) e una soluzione tampone a pH 10.

Le attività residue misurate sono riportate in *Figura* 2, prendendo come valore di riferimento per il 100% di attività, l'attività della Lattato Deidrogenasi, libera o immobilizzata su SBA-$15_{0.25}$, non inibita. Si può facilmente notare come l'enzima nella sua forma libera raggiunga un'attività residua pari a zero durante i primi 15 minuti circa di prova, sia nel caso di incubazione con il solvente organico che nel caso di incubazione in un buffer pH 10. Contrariamente, l'enzima immobilizzato sul supporto mesoporoso di SBA-$15_{0.25}$ mantiene un'attività residua anche dopo 180 minuti di prova. In entrambi i casi, infatti, la forma immobilizzata di LDH ha mostrato un'attività residua finale del 40-50% superiore rispetto alla corrispondente forma libera. Si ritiene quindi che l'immobilizzazione covalente dell'enzima Lattato Deidrogenasi sul supporto mesoporoso SBA-$15_{0.25}$ sia efficace nell'aumentare la resistenza della macromolecola alla denaturazione.

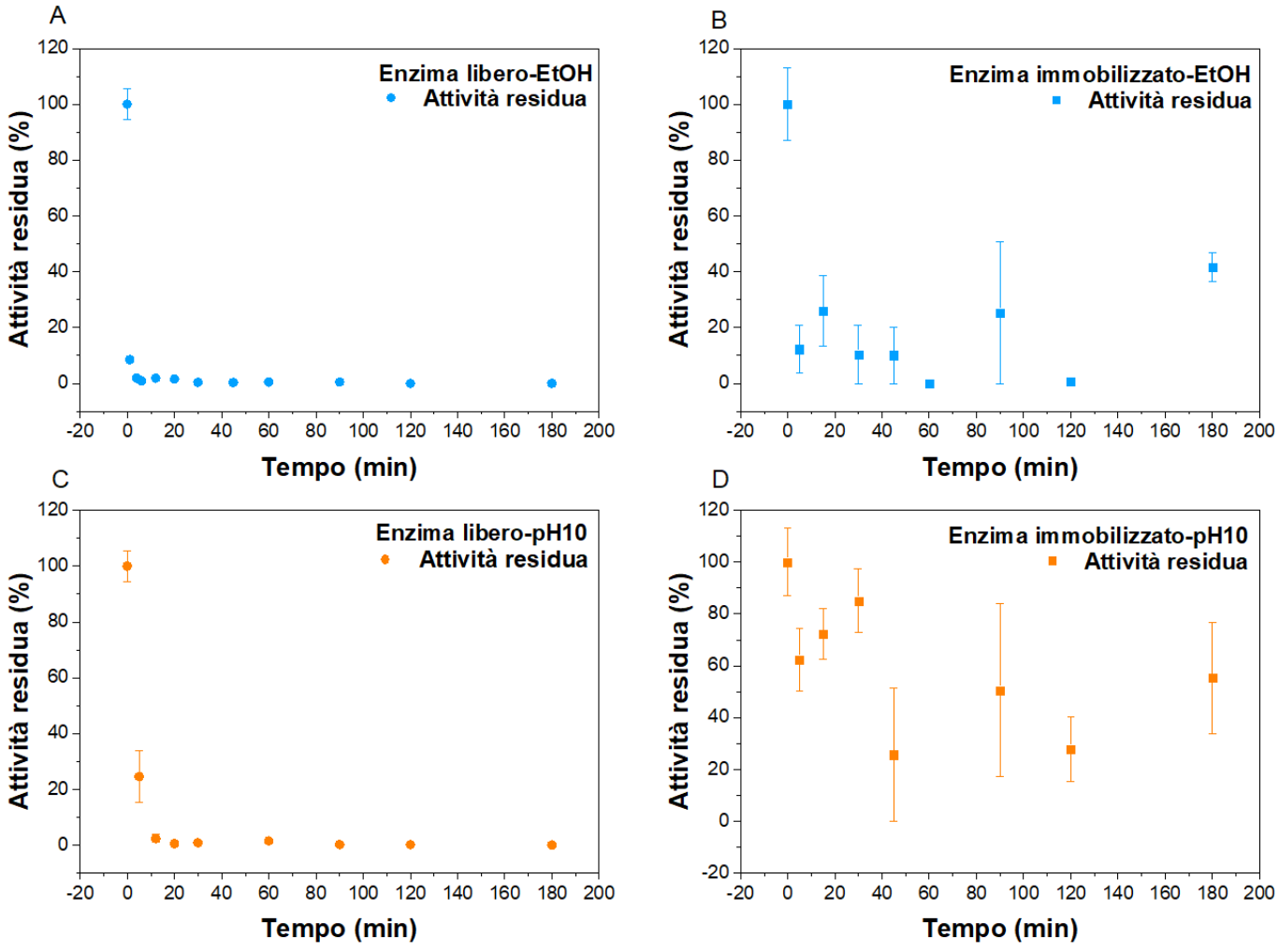

Figura 2. Attività della soluzione di enzima libero e dell'enzima immobilizzato incubati con una soluzione con etanolo (A e B) o con una soluzione buffer pH 10 (C e D). In questo caso, per la forma immobilizzata è stato utilizzato SBA-$15_{0.25}$ come supporto.

Infine, sono state misurate le attività sia dei biocatalizzatori sintetizzati che dell'enzima nella sua forma libera, in presenza del farmaco antitumorale, l'NHI-2, un inibitore dell'isomero A dell'LDH, basato su N-idrossiindolo (NHI). [5] Questa prova è di fondamentale importanza in quanto, per un'applicazione del biocatalizzatore in un sensore per lo screening di farmaci antitumorali, il processo di immobilizzazione su supporto non deve ridurre l'efficacia dei potenziali farmaci analizzati.

Le suddette prove di inibizione sono state effettuate in condizioni di concentrazione di substrato enzimatico (piruvato) variabile, e concentrazioni variabili di cofattore (NADH, nicotinammide adenina dinucleotide) della reazione catalitica. Lo studio cinetico ha permesso l'analisi delle costanti cinetiche coinvolte, dimostrando che l'inibitore scelto è competitivo sia con il substrato dell'enzima LDH, sia con il NADH. Tale competitività è stata anche dimostrata attraverso l'utilizzo di tecniche di modellazione computazionali, secondo il procedimento indicato da Granchi et al. [5].

Per il suddetto studio è stato utilizzato il software BIOVIA Discovery Studio, che ha permesso l'individuazione, sulla struttura tridimensionale dell'enzima Lattato Deidrogenasi, dei residui proteici coinvolti nel legame con le seguenti molecole: NHI-2, NADH e piruvato. È riportata in *Figura 3* la rappresentazione bidimensionale ottenuta attraverso tale software per quanto riguarda il complesso formato dal legame tra il farmaco antitumorale e l'enzima. Il software utilizzato ha permesso di individuare anche i residui proteici con cui il ligando forma delle interazioni sfavorevoli, evidenziati in rosso nell'immagine citata.

L'analisi computazionale dell'interazione tra LDH e piruvato ha permesso di dimostrare come il sito di legame del substrato sull'enzima coinvolga il residuo proteico Ser119, ugualmente coinvolto nel legame dell'enzima con il farmaco. Allo stesso modo, si è visto come il sito attivo del cofattore enzimatico comprenda il residuo His148, anch'esso coinvolto nel legame con l'NHI-2.

Questa analisi computazionale è quindi a supporto di quanto ricavato sperimentalmente durante le prove di inibizione descritte nel seguente lavoro di tesi, che dimostrano la competitività del farmaco antitumorale scelto sia con il cofattore che con il substrato della reazione enzimatica studiata.

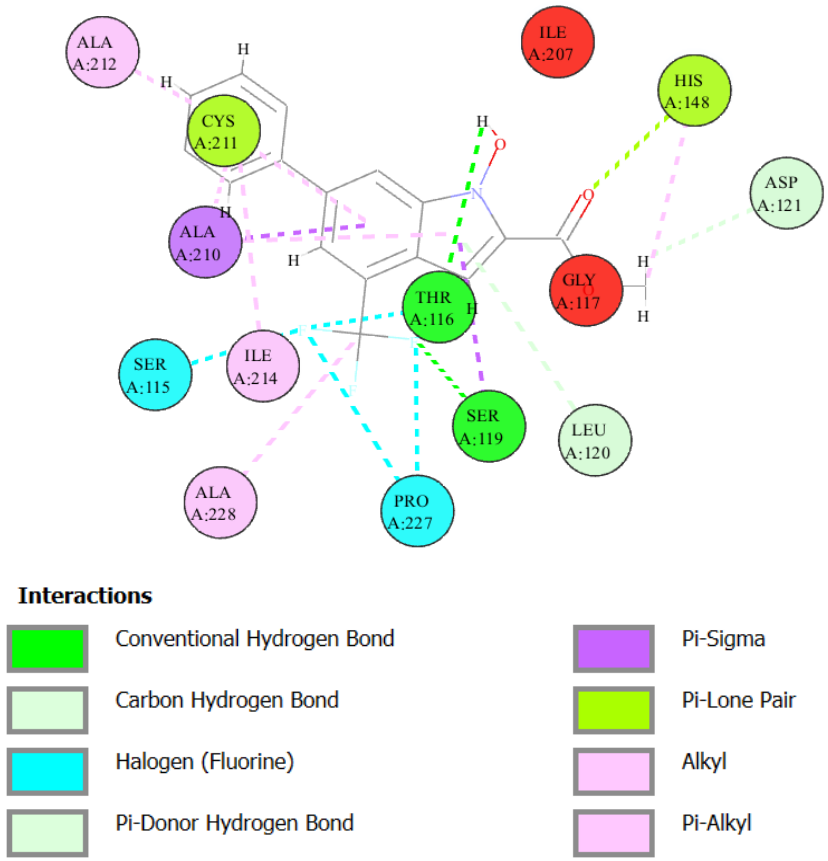

Figura 3. Rappresentazione schematica in due dimensioni dell'interazione tra il farmaco antitumorale NHI-2 e l'enzima Lattato Deidrogenasi (LDH), ottenuta tramite l'uso del software BIOVIA Discovery Studio.

1. Introduction

1.1 Lactate Dehydrogenase (LDH)

Lactate dehydrogenase (LDH), enzyme commission number EC 1.1.1.27, is an H^+ transfer enzymes, belonging to the class of oxidoreductase. LDH plays a fundamental role in anaerobic glycolysis, where it catalyses the conversion of pyruvate (final product of glycolysis) to lactate (lactic acid) and vice-versa, with the simultaneous oxidation of NADH to NAD^+ (Nicotinamide adenine dinucleotide), LDH cofactor. A schematic representation of the described catalytic reaction is shown in *Figure 4*. This reaction is known as anaerobic homolactic fermentation and plays an important role in ATP (adenosine triphosphate) generation when the organism is in anaerobic or hypoxic conditions [6]. As detailed in the next section of the present thesis work, LDH plays a pivotal role in cancer cells metabolism and its study is therefore of great interest for the development of innovative cancer treatments.

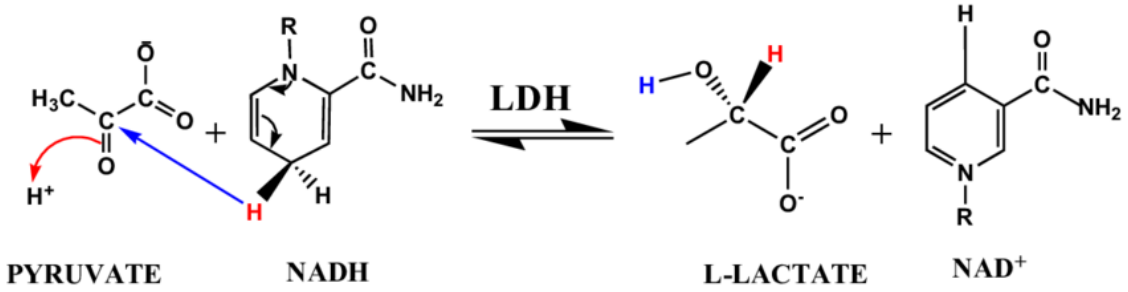

Figure 4. Lactate dehydrogenase catalytic reaction scheme [7].

LDH is fundamental in the metabolism of a wide range of living being, including humans, plants and animals. It can be found in every human tissue, but it is particularly abundant in muscles, kidneys and liver. [8] Lactate dehydrogenase presents five different isomers, named from LDH-1 through LDH-5, each one composed of four subunits. These can be either of the two types: M, predominantly found in muscle tissue, and H, mainly found in cardiac muscle. Isozyme LDH-1, also known as LDH-B, is composed solely by heart subunit and is, in fact, the major isozyme presents in the heart and other oxygenated tissues. Isozyme LDH-2 has three H and one muscle subunit. The LDH-3 isozyme consists of two heart and two muscle subunits (mainly found in lungs tissue). Isozyme LDH-4 has one H and three M subunits (mostly found in kidneys). The LDH-5 isozyme, also called LDH-A, has four muscle subunits and is expressed in liver and skeletal muscle. [8], [9]

In humans, the prevalent isomeric forms are *h*LDH-A and *h*LDH-B. Although sharing 75% of the total sequence and catalysing the same general reaction depicted above, they present different affinity to the substrate, different isoelectric points, and inhibition concentration [10]. In particular, LDH-A kinetically favours the conversion of pyruvate to lactate, while the opposite is true for LDH-B.

LDH-A from UniProt [11] was analysed using VADAR 1.8 online server, which revealed the percentage distribution of the different secondary structure present: helix 109 residues (43%), beta sheets 55 residues (22%), coil 86 residues (34%) and 56 residues of turns (22%). It is of great interest to investigate Lactate Dehydrogenase secondary structure, as it plays a fundamental role in the protein biological activity. The secondary structure of a protein is the result of the formation of different weak bonds, e.g. hydrogen bonds, between the different amino acids composing the polypeptide chain. The creation of said weak bonds determine the folding of the protein backbone, forming the secondary structure. The unfolding of this three-dimensional configuration, due for example to the protein exposition to organic solvents, high temperatures or extreme pH values, will result in the loss of catalytic activity. [12]

Lactate Dehydrogenase schematic secondary structure is shown in *Figure 5*. The two images were obtained through the use of BIOVIA Discovery Studio, a protein modelling tool.

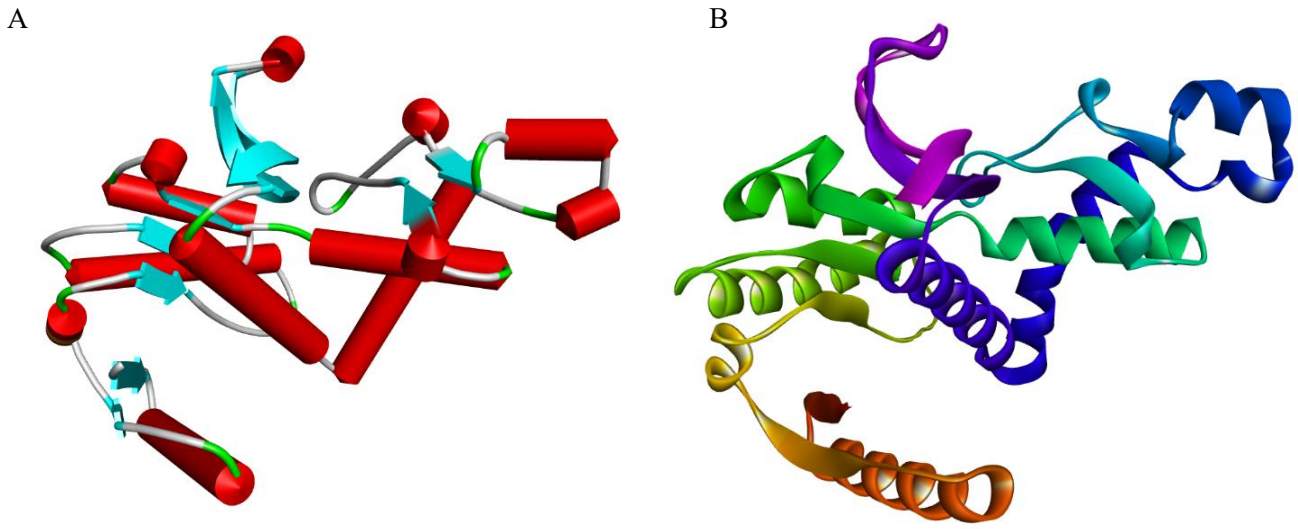

Figure 5. A) Schematic representation of the secondary structure of a human LDH-A, in red: helixes, light blue: β-sheets, grey: coils, green: turns. B) Three-dimensional representation of the same protein. Images obtained via BIOVIA Discovery Studio Visualiser.

1.1.1 hLDH-A role in tumoral cells

Healthy cells derive their energy primarily from glucose, in the form of adenosine triphosphate (ATP) molecules. Through glycolysis, cells convert each glucose molecule into pyruvate, yielding two ATP molecules. In normally functioning cells, pyruvate can then follow one of two metabolic pathways depending on the availability of oxygen.

Under aerobic conditions, pyruvate enters the citric acid cycle, also known as Krebs cycle or the tricarboxylic acid (TCA) cycle, that takes place in the cell mitochondria. This cycle produces two additional ATP molecules and fully oxidizes pyruvate into carbon dioxide (CO_2) and water (H_2O). The reducing power generated in earlier stages of the respiratory chain is crucial for oxidative phosphorylation (aerobic respiration), which yields 34 ATP molecules. Each step in this metabolic pathway is catalysed by a distinct enzyme, essential for cellular energy production.[13]

However, in anaerobic conditions, pyruvate cannot reach complete oxidation due to the absence of oxygen, which is needed for the oxidative phosphorylation final step. Consequently, pyruvate bypasses the TCA cycle and is enzymatically converted into Lactate by Lactate Dehydrogenase. This alternative metabolic pathway, also called lactic fermentation, enables the production of an adequate amount of metabolic energy even in absence of oxygen. Therefore, the activity of LDH is central for the correct functioning of glycolysis under anaerobic conditions. Even in healthy cells, partial lack of oxygen is not uncommon, as it could be for example the result of intense exercise, leading to an abnormal consumption of oxygen in muscular tissues.

In the 1920s, Otto Warburg reported a preferential production of energy through lactic fermentation rather that via mitochondrial oxidative phosphorylation in cancer cells, even under aerobic condition. This unique metabolic behaviour, depicted in *Figure 6*, called ‘Warburg effect’, is characterised by high glucose avidity and lactate production, and it is a now well-known metabolic reprogramming techniques, employed by a great variety of different tumoral tissues. [14]

Even if aerobic glycolysis is not as efficient as mitochondrial respiration for the generation of ATP, it results in a higher fermentation of glucose to lactic acid. The Warburg effect provides the tumoral cells with ATP and lactic acid, thanks to an overexpression of Lactate Dehydrogenase (LDH-A). Lactate, in particular, cumulates in the tumoral tissues, contributing to their rapid growth. This phenomenon leads to the acidification of the cancer microenvironment and plays an important role in suppressing the immune response of the hosting organism. [15], [16]

The in-dept understanding of the Warburg effect has important implications for the development of new cancer therapy. The altered metabolism of cancer cells is, in fact, currently emerging as a potential strategical target for cancer treatment drugs. The Warburg effect could be inhibited by targeting the activity of Lactate Dehydrogenase, as it plays a pivotal role in Lactate synthesis, with the result of a reduced tumoral metabolic activity.[17]

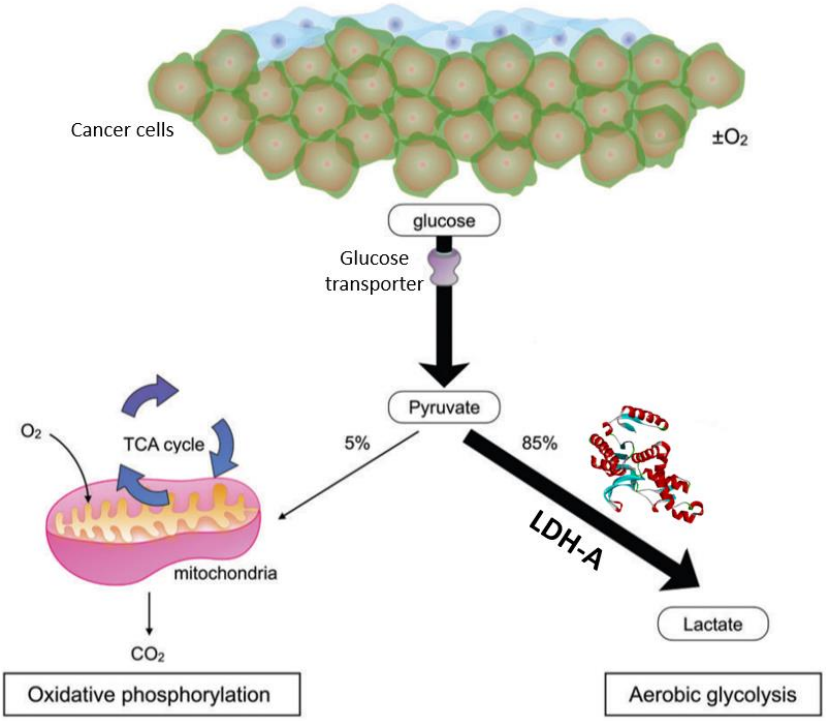

Figure 6. Scheme of the Warburg effect displayed by cancer cells. Adapted from Kobayashi et al. [18]

1.1.2 Biosensor for anticancer drugs testing

Despite the continuous decrease in cancer death rates since the beginning of the 90s, cancer still represents a major public health issue worldwide. It is in fact estimated that, throughout their life, almost 40% of the population will be diagnosed with a form of cancer. In 2023, 1.958.310 cancer cases occurred in the United States, with 609.820 deaths, making tumours the second cause of death in the country. [1] The fast growth of cancer cases number is particularly alarming. The graph below, *Figure 7,* displays the percentage of diagnosed cases increase expected in 2040, compared to the total number of cancer cases in 2020, per geographical region.

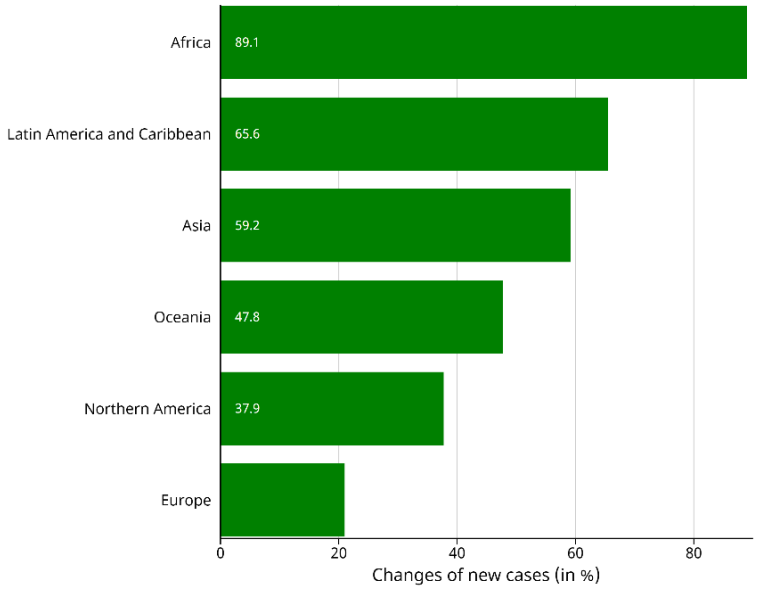

Figure 7. Percentage increase in cancer cases in 2040 compared to 2020, for each geographical region. [19]

Although there has been remarkable advancement in biotechnologies and medicine and there is now a deeper understanding of tumours biology, finding new small molecules that can act as anticancer drugs continues to be a challenge. Moreover, discovering new anticancer drugs is a time-consuming and costly quest, with around 12 years and 2.7 billion US dollar needed on average for each new drug found. Furthermore, around only the 10% of the tested molecules eventually reaches the market. [20], [21]

The present research aims to contribute to making the discovery of new drugs easier and less expensive, drastically reducing the waiting time for a new efficient drug to start trial *in vivo.* Traditionally, in fact, the effectiveness of a new compound is tested on a few tumoral cell lines, in order to evaluate its activity *in vitro*. This methodology required a huge resources consumption and limits the number of compounds tested. [22] In this research, the immobilisation of Lactate Dehydrogenase for the design of a Biosensor is presented as a new technique for the quick and reproducible testing potential anticancer compounds. By measuring the enzyme activity in presence of different potential drugs, it would be possible to investigate their effectiveness in reducing LDH catalytic role in tumour metabolism. The proposed enzyme immobilisation could significantly improve the enzyme reuse over time, permitting the fast and efficient testing of different compounds.

1.2 Enzymes immobilisation

Enzymes are the most efficient biological catalysts, having a turnover frequency number several orders of magnitude higher than the ones of heterogeneous and homogeneous non-bio catalysts. [23] Enzymes' importance derives from their very elevated stereo- and chemo-selectivity to their substrates, that enables the catalysed reaction to take place at a considerably high speed at ambient temperature and with limited substrate availability. Their industrial large-scale employment is however hampered by their low stability when extracted from their natural medium, the cell. To overcome this major disadvantage, various immobilisation techniques have been developed, making thus possible their usage in many industrial fields, such as: food technologies, water treatment, fine-chemicals synthesis and pharmaceuticals. [2]

Enzyme immobilisation consists in the biocatalyst attachment into or on different types of supports, that can be either organic (e.g. polysaccharides such as agarose, polyvinyl or polyacrylic materials) or inorganic (e.g. silica-aluminate). [24]

The most significant benefits of enzyme immobilisation are:

1. The enzyme *stabilisation towards harsh working condition*. In particular, an immobilised enzyme is more resistant to denaturation at high temperature, extreme pH and the presence of organic solvents (e.g., ethanol) or other inhibitors, compared to the enzyme in its natural form. The attachment to the support, and especially its entrapment in a porous support, will substantially hinder the modification of the enzyme 3D structure caused by the surrounding environment. [25]

2. The enzyme *reusability* and its *fast recovery from the reaction medium*. When the enzyme is successfully immobilized onto a rigid and unreactive structure, it will be able to perform its catalytic role without being released in the liquid medium containing the substrate(s), the product(s) and cofactors. The immobilisation will therefore enable the physical separation of enzyme and the reaction products, hence reducing the separation costs linked with downstream treatment of a conventional catalytical reaction. This particularity of enzyme immobilisation could be especially beneficial to their employment in fixed bed reactors. [26]

3. *Enhanced process controllability*. The enzyme immobilisation in a reactor allows for a more precise monitoring of the catalytic process parameters, such as the enzymatic load,

the contact time, the reaction temperature. [2] Finally, the advanced control over the process parameters makes possible the implementation of co-immobilisation and co-location techniques. In other words, the immobilisation of two or more different enzymes on the same support. These techniques are particularly interesting for substrate and co-enzymes regeneration. [27]

1.2.1 Immobilisation strategies

Enzyme immobilisation is an interesting method to overcome the major drawbacks associated with enzyme use in their natural form and it has consequently been investigated thoughtfully over the last three decades [28]. However, the attachment of an enzyme on a support can also result in a series of drawbacks that need to be accounted for when choosing the support material and the immobilisation method. The latter particularly requires a careful analysis since it will influence drastically the final enzyme activity. The main immobilisation strategies are here described, with a focus on the benefits and challenges of each method:

1. *Physical absorption* or physisorption is characterized by the formation of non-specific bonds between the attached enzyme and the support surface. The typical interactions occurring in this type of immobilisation are non-covalent ones such as: Van der Waals, hydrogen bonding, ionic and electrostatic interactions. Due to the weak nature of the cited bonds, physisorption is characterised by the possible leakage of the organic molecule, as a consequence of even slight changes in working condition. On the other hand, physisorption presents also a significant advantage: the weak bonding between enzyme and support material will generally not lead to any structural modification of the protein, that will maintain its original 3D configuration. Hence, this technique conveniently ensures a very high residual catalytical activity of immobilized enzyme [25].

2. *Covalent bonding* is a more complex technique compared to the previous one, since it normally requires a chemical modification of the support surface. A preparation of the material is needed to obtain functionalisation groups that will lead to a strong covalent bond between some enzyme residue, generally Lysine (Lys) and support. This method is thus efficient in minimising enzyme leaching and maximising the biomolecule resistance in presence of high temperature, extreme pH and organic solvents. Enzymes are complex structures with numerous functional groups that could form covalent bonds with the surface, meaning that an incorrect orientation of the protein could occur, shielding the

active sites. In worst cases, this phenomenon could result in enzyme rigidification, activity loss, and enzyme denaturation, as schematised in *Figure 8* [24]

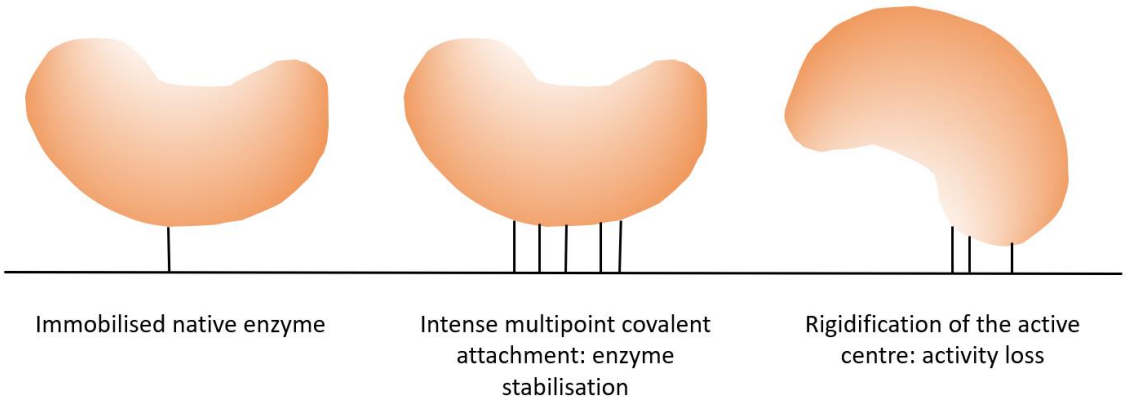

Figure 8. Schematic representation of covalent bonding as an immobilisation strategy and its possible drawbacks. [2]

3. *Cross-linking* between enzymes is originally a carrier-free technique for the synthesis of the so-called *cross-linked enzymes aggregates* (CLEAs). The linking between the different enzymatic polymeric chain is obtained via a two steps process and it is therefore a simple and unexpensive method. The first step is the formation of water-insoluble enzymes aggregates and their precipitation through the addition of e.g. salts or organic solvents. Secondly, the aggregates are linked together using a bifunctional cross-linking agent such as glutaraldehyde (GTA), hexamethylene diisocyanate or bidiazobenidine.[29] The formation of strong covalent bonds stabilizes the enzymes thus ensuring their high catalytic activity. As depicted in *Figure 9,* CLEAs are usually entrapped in large support cavities, to maximise the enzyme reusability and enable their practical use within a reactor. One of the drawbacks of this immobilisation strategy is the fact that, due to the formation of large aggregates, that can have a diameter up to 100 μm, a large amount of enzyme molecules will be located in the centre of the aggregate, with no access to the reaction medium. During the immobilisation, special attention should therefore be given to the aggregates size, in order to minimise mass and heat transfer limitation. [25] Additionally, the formation of covalent bonds can lead to the deformation of the enzyme active site.

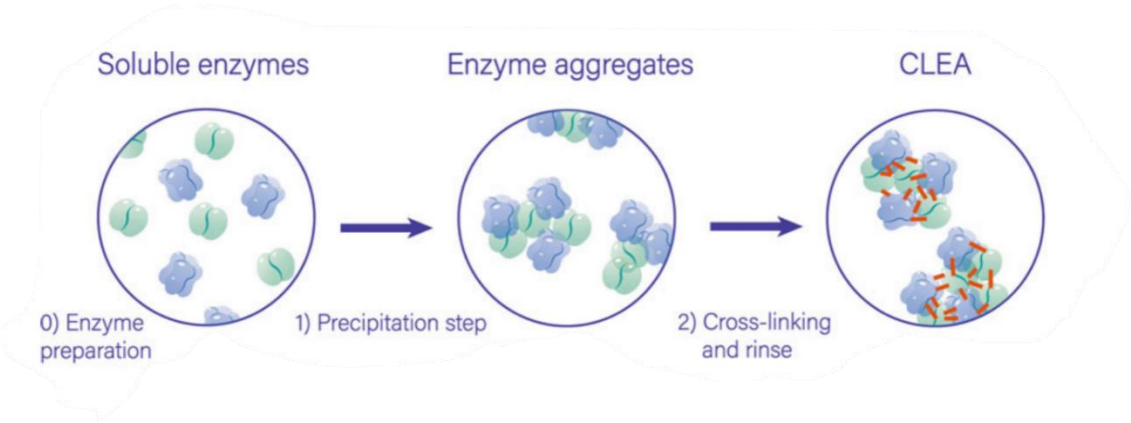

Figure 9. Schematic procedure for the synthesis of cross-linked enzymes aggregates (CLEAs). [30]

From this brief presentation of the main immobilisation techniques, it should be clear how each technique has its own particular advantages and disadvantages, and great caution should be taken when choosing which strategy to implement. All the previously described immobilisation techniques are summarised in *Figure 10* below.

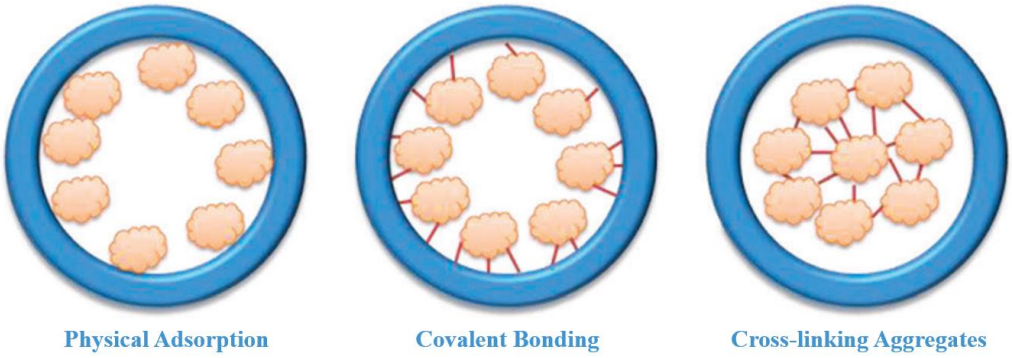

Figure 10. Prime techniques applied for enzyme immobilisation of mesoporous silica. [28]

1.3 Supports for enzymes immobilisation: mesoporous silica

As seen in the previous section, the selection of the suitable support for enzyme immobilisation is of critical importance. The chosen support will play a fundamental role in maintaining the enzyme activity throughout the reaction process and allowing its reuse. The key parameters to evaluate for the correct selection of a support material are: its stability at the reaction conditions, the pore volume, the pore diameter distribution, the cost of production, its hydrophobicity, and the possibility of an easy and tuneable functionalisation of its surface. [31] The non-toxicity of the material is also a requisite for its implementation as a catalysis support on industrial scale. Physical properties of the support such as mechanical stability and rigidity are also important parameters that should be

considered when choosing the right material for the immobilisation. Porous supports allow a higher enzyme loading per unit mass thanks to their high surface area and pore volume and they are therefore the preferred choice. The immobilisation of the enzyme inside the cavities of the selected material grants the protection of the molecule from the external environment, thus increasing its stability and activity at varying pH, temperature and in presence of organic solvents. [32] A high pore volume is desirable since it will increase the binding capacity of the enzyme. The pore dimension should be tuned during the material synthesis, due to the fact that too narrow pores would prevent the inclusion of the enzyme, thus undermining the immobilisation advantages, and larger pores would significantly decrease the material surface area but also decrease diffusion limitations.
The chosen support should have minimized hydrophobicity since it could lead to unwanted protein adsorption and denaturation on the material surface. The only known exception is shown by the enzyme lipase, which presents hydrophobic behaviour. [24]

The inherently stability of the material itself under working conditions is essential for its reuse, considering that the degradation of the support would lead to the irreversible loss of the enzyme activity [33]. Among different inorganic supports, silica-based ones, and in particular mesoporous silicates (MPS), are the most widely used as biocatalysts supports since they encompass all the previously mentioned necessary characteristics. [24]

Mesoporous materials are described by IUPAC as porous inorganic solids with a pore diameter range from 2 nm to 50 nm, as summarized in *Figure 11*.

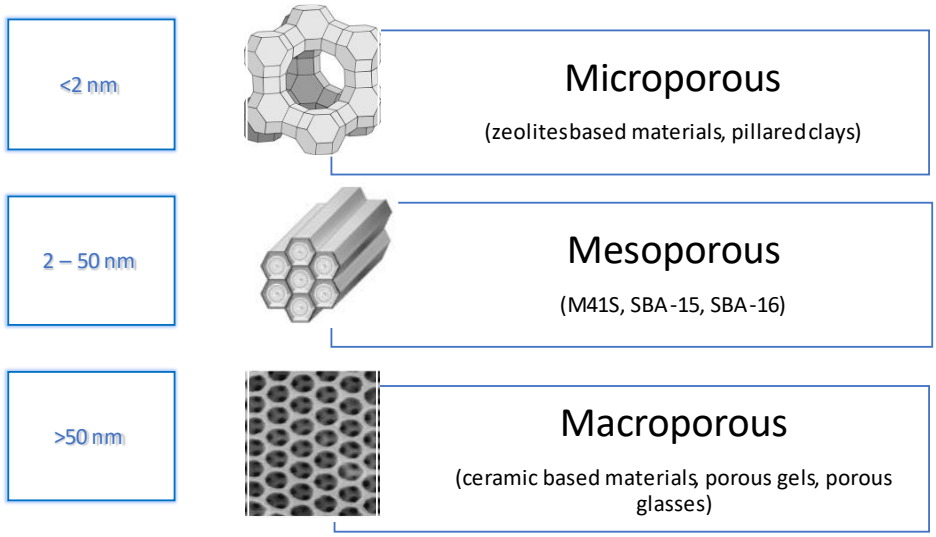

Figure 11. IUPAC classification of porous materials, adapted from [34].

A turning point in the study of mesoporous material was reached in 1992, with the synthesis of the so called “M41S” family, by the Mobil Corporation Laboratories. [35] This family of nanostructured materials is characterised by an ordered repeating structure and rigid walls. The cited family includes three different mesophases: lamellar (MCM-50), hexagonal (MCM-41), and cubic (MCM-48) phases, as depicted in *Figure 12*. MCM-41 (Mobil Composition of Matter No. 41) is characterised by hexagonal non-intersecting channels, with a diameter that can vary from 1.5 to 10 nm, depending on various synthesis characteristic, such as the used template and the synthesis time and temperature. [36], [37] This honeycomb-like structure is the most widely used between the materials of the M41S family, since the cubic and lamellar nanostructures are unstable and therefore not found in any relevant application. MCM-41 on the other hand, has already been employed as support for the adsorption of small molecules [38], immobilisation of several enzymes [39] and even for retaining entire cells. [40]

Figure 12. Schematic refiguration of the materials of the M41S family, MCM-50 (layered), MCM-41 (hexagonal) and MCM-48 (Cubic). [41]

MCM-41 was originally synthetised using the liquid-crystal templating (LCT) mechanism, which is based on the formation of aggregates of a templating agent or surfactant in a polar solvents, e.g.water. [42] The surfactant molecules cluster together as micelles; their hydrophobic tails tend to agglomerate, and their hydrophilic heads remain exposed to the polar solution. This spontaneous mechanism tends to form rod-like structures, which reduce the system entropy and act as structure directors for the formation of the mesophase, enabling the condensation on their external surface of a silica-containing reagent. This precursor, added after the formation of the self-assembled template, will polymerize, creating an inorganic network, as summarised in *Figure 13.* In the MCM-41 synthesis, the formation of this composite material is possible thanks to the electrostatic interaction between the positively charged organic surfactant molecules and the inorganic negatively charged silica. [42]

The accurate choice of the templating agent's chain length allows for the tuning of the final pores dimension, since these will be obtained by the subsequent elimination of the surfactant, leaving intact only the rigid silica-based structure. In the case of M41S, the hydrophobic alkyl chains of the template have between 8 and 22 carbon atoms, making MCM-X part of the lowest mesoporous size range. [32] The pore size can also be modified using auxiliary organic compounds (i.e., trimethylbenzene) as spacers and swelling agents. [43], [44]

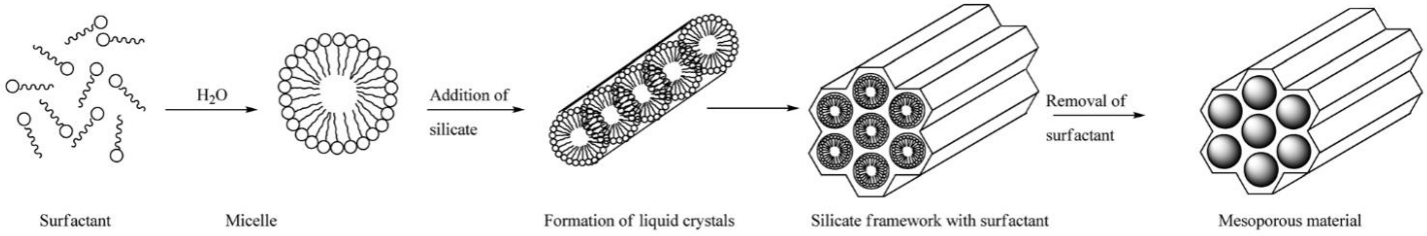

Figure 13. Proposed schematic procedure for the synthesis of mesoporous materials. [42]

Micelles will only form if the templating agent is present in a concentration higher than the so called critical micellization concentration (CMC). The high concentration of these randomly ordered composite structures will allow their spontaneous hexagonal arrangement, coupled with the before mentioned precursor condensation. The final step of the liquid-crystal templating technique is the template removal, which will lead to the formation of ordered porosities in the previously formed 3D structure. This can be performed by washing the organic-inorganic network with water, through solvent extraction or calcination. [41]

The most interesting aspect of the implementation of liquid-crystal templating technique is the possibility to vary the result of the synthesis adjusting the conditions used. Changing the length of the templating agent hydrophobic carbon tail or adding a swelling agent are the best known and already mentioned methods to modify the pore size in the final mesoporous structure. [41], [43], [45]

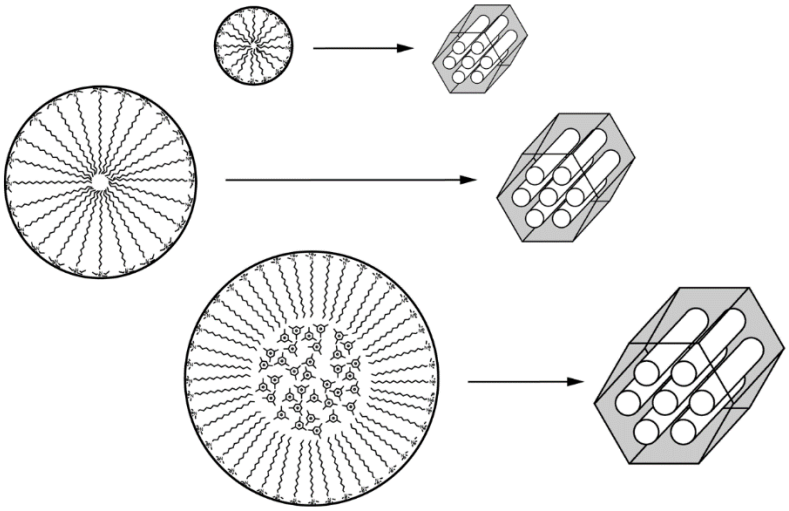

Figure 14. Tuning of the pore size in porous material synthesis with liquid crystal technique, varying the template chain length (first and second case) or adding a swelling agent (third case). [46]

1.3.1 Santa Barbara Amorphous no 15 (SBA-15)

A wide variety of other ordered mesoporous material have been subsequently synthetised following the method proposed for M41S. In fact, the previously mentioned mechanism, although being described in regard to the synthesis of MCM-X supports, can be carried out using different templating agents and synthesis conditions, in order to obtain mesoporous materials with different and improved characteristics.

As already mentioned, MCM-41 is obtained via alkaline hydrolysis with a cationic surfactant as cetyltrimethylammonium Bromide (CTAB). Replacing the structure directing agent with a non-ionic one, such as P-123 (Pluronic®) in an acidic solvent (pH~1), will lead to the synthesis of one of the most used mesoporous support, SBA-15. [24] The strong acid synthesis conditions are fundamental for the condensation of silica, which would not occur at a pH higher than its isoelectric point (pH 2-6). [47]

Typically, SBA-15 is synthetised using the aforementioned P-123, a symmetric triblock copolymer constituted of alternating poly(ethylene oxide) (PEO) and poly(propylene oxide) (PPO), in the form PEO-PPO-PEO. It is in fact well known that PPO is strongly hydrophobic at the synthesis temperature, while PEO is hydrophilic. P-123 con therefore be used in the LCT composite material synthesis, being it able to self-assembly, forming micelles in the aqueous medium used. [48] The most common silica-source used for SBA-15 synthetises are: tetramethyl orthosilicate (TMOS), tetraethyl orthosilicate (TEOS), tetrapropyl orthosilicate (TPOS).

SBA-15 presents an ordered repeating structure, with a sharp pore size distribution, adjustable in the range of 4.6-30 nm, depending on the synthesis conditions. The major advantage of this material are the thick silicate walls (~3 nm), that make it more hydrothermally stable compared to MCM-41 (< 2nm). [44] Additionally, SBA-15 is thermally and chemically resistant and its larger pore size, compared to MCM-41, make it the preferred choice for enzymatic immobilisation. SBA-15 synthesis will thoughtfully be described in the following chapter, as the main support chosen for this work. Particular attention will also be given to its functionalisation, as a way of tuning the material characteristics for the studied application.

1.3.2 $MCF_{0.75}$

$MCF_{0.75}$ (Mesocellular Foam) silica is a unique form of mesoporous silica known for its three-dimensional 'spongy' structure. This structure is achieved by employing a procedure similar to that used for SBA-15, but with the addition of a swelling agent, such as 1,3,5 trimethylbenzenexylene (TMB), combined with a surfactant, in this case Pluronic P123, in a specific ratio of 0.75. Normally, the inclusion of the swelling agent increases micelles expansion, but its addition to the mixture in a high concentration leads to the formation of a foam-like porous structure. [43] The surfactant, on the other side, is used to stabilise the material structure and to control the pore sizes distribution. $MCF_{0.75}$ framework consists of a three-dimensional lattice of uniformly sized spherical cells of between 20 and 40 nm. This structure, contrary to SBA-15, does not present hexagonal shaped rod-structures but is characterised by regular so-called ‘windows’ of approximately 10 nm, which are suitable for protein inclusion. A graphical representation of said 3D structure can be found in *Figure 15*, where the cell structure from which the material gains its name is also highlighted. [46]

Similarly to the other mesoporous silica materials discussed in this study, it presents a high specific surface area, exhibits excellent thermal stability, and offers customizable pore sizes. Furthermore, its surface can be tailored to meet specific research requirements, facilitating the formation of covalent bonds between the support and the target molecule under investigation.

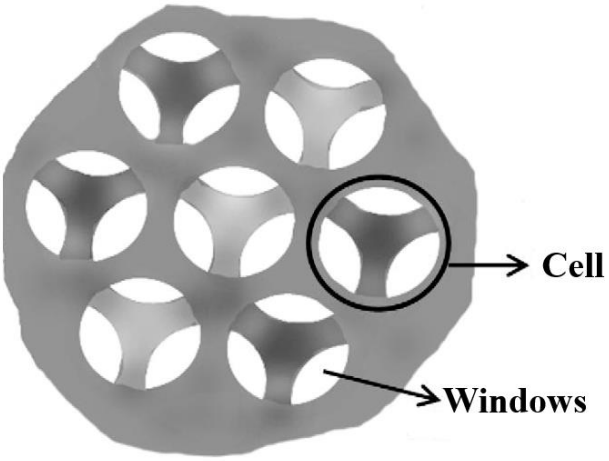

Figure 15. Schematic representation of Mesocellular Foam silica from Qian et al. [49]

1.3.3 Dendritic fibrous nanosilica (DFNS)

The previously mentioned support candidates for enzyme immobilisation, MCM-41 and SBA-15, both present a two-dimensional pore geometry, in rod-like shape. These particularities can lead to a significant disadvantage when biological particles are loaded on their surface. In fact, the small pore 1mouth can be blocked by larger molecules, limiting the total quantity of enzyme deposited. [25] The inability of the guest molecule to be allocated on the whole cavities of the porous structure can be a drawback for the employment of MCM-41 and SBA-15 when working with molecules with big dimensions. For overcoming this downside, dendritic fibrous nanosilicates (DFNS), also referred to as Dendritic porous silica (DPS), can be used.

They consist in thin fibres of 3.5 to 5.2 nm, that converge in the central part of the nanoparticle, creating radially oriented channels that increase in diameter from the centre of the particle to its outer surface. This unique conformation enables the penetration of guests' molecules inside the pores, without mass transfer limitation. A graphical representation of this phenomenon can be found in *Figure 16*, a comparison between DFNS and conventional mesoporous silica with tubular pores. As with the other silica materials studied, DFNS also presents a tuneable pore size distribution, that can be modified by controlling the fibres concentration in the synthesis solution. Due to the particular pore geometry (to be intended as the distance between adjacent fibres) the pore distribution will not be a sharp one, but it usually ranges between 3, in the internal portion of the particle, and 25 nm, at the particle surface.

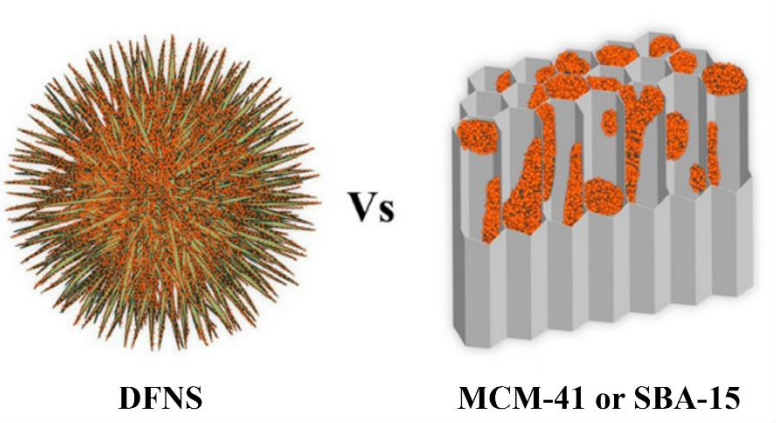

Figure 16. Advantage of the use of DFNS materials, compared to the most common mesoporous silica supports. The red dots represent guest molecules such as organometallic complexes, enzymes, polymers and carbon. [50]

Although having a reduced surface area compared to MCM-41 and SBA-15, dendritic fibrous nanosilicates are appreciated for their easily accessible large pores and are therefore employed in various application, such as: drug delivery, bioimaging, extraction and detection of pollutants and enzyme immobilisation. [51]

1.4 Support functionalisation

One of the requirements for a support material to be suitable for enzyme immobilisation is its stability at reaction conditions, since it is of crucial importance that the support does not interact with the surrounding medium. A certain degree of reactivity is however needed to implement the covalent-bonding immobilisation strategy. As seen, covalent bonding has numerous benefits, and it is therefore the selected technique. In particular, the aim of the immobilisation strategy is to obtain a multipoint enzyme coupling, an enzyme molecule linked with multiple covalent bonds to the support surface. This type of linkage is particularly advantageous because it will prevent the dissociation of enzyme subunits, a typical denaturation mechanism. On the other hand, excessive interconnection between support and organic molecule would result in the rigidification of the enzyme and possibly a conformational change of its active side. This strong multipoint coupling is undesired, as it would greatly decrease the enzyme activity. [2]

For most covalent immobilisations, a chemical modification of the silica surface is required to introduce organic groups capable of interacting with selected enzyme residues. The silica-based support presents a high quantity of silanol groups (Si-OH), that are the key to the support functionalisation techniques. In fact, the most widespread procedure for surface modification is the

"silanization", a nucleophilic attack between a silanol group on the support and a silica atom of the functionalisation molecule, usually an organosilane.

Organosilanes play the role of a functionalisation reagent, creating the link between the support surface and the biological molecule. Their general formula is $(RO)_3Si–(CH_2)_3–X$, where R usually is either $–CH_3$ or $–C_2H_5$, and X is a suitable chemical function. [24] The latest needs to be carefully selected, as it will react with $-NH_2$ groups of the enzyme in the subsequent immobilisation reaction. The most well-established techniques for the functionalisation of silica-based materials are:

1. *Co-functionalisation:* direct-synthesis method that allows the support synthesis and its functionalisation in a single step. In this method, organosilanes are added to the TEOS and surfactant solution and take part to the liquid-crystal templating mechanism. The organosilanes will be incorporated in the growing micelles and the resulting structure will present a very homogeneous distribution of the desired organic function on its surface. However, high concentration of organisilanes added to the synthesis solution would lead to the formation of a deeply disordered final structure, loss of specific surface and pore volume. [24]

2. *Grafting:* In this case the support is functionalised post-synthesis, throughout reaction with the selected organosilane. The final support will present a less homogeneous distribution of organic group compared with one obtained via co-functionalisation. In fact, it has been highlighted how the organosilanes will mostly allocate on the support surface of the mesopores, without penetrating in the core structure, and therefore causing pore-blocking and a diminished enzymes loading capacity. Nonetheless, grafting does not modify the material original structure. [52]

1.5 LDH immobilisation

In most immobilisation processes, the targeted residues of the enzyme molecule, are lysine, cysteine or histidine [25]. Lysine (Lys) is the most aimed protein residue: it presents a highly reactive $-NH_2$ group and it is extremely common in all enzymes. Moreover, Lys is usually present on the protein surface and therefore easily accessible and in most cases, it is not directly linked with the enzyme catalytic activity. Cysteine and histidine residues are less common and will not be taken into consideration in the present work.

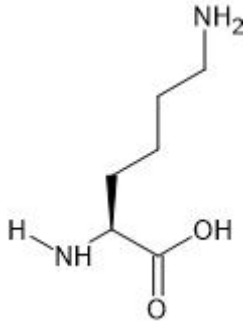

Figure 17. Lysine

In particular, it has been shown how LDH is a promising candidate for multipoint covalent immobilisation through the link between a support functionalised with aldehydic groups and deprotonated amino groups from Lysine [26]. *Figure 18* shows the high concentration of Lys residue on LDH surface, fundamental parameter for the application of covalent bonding technique.

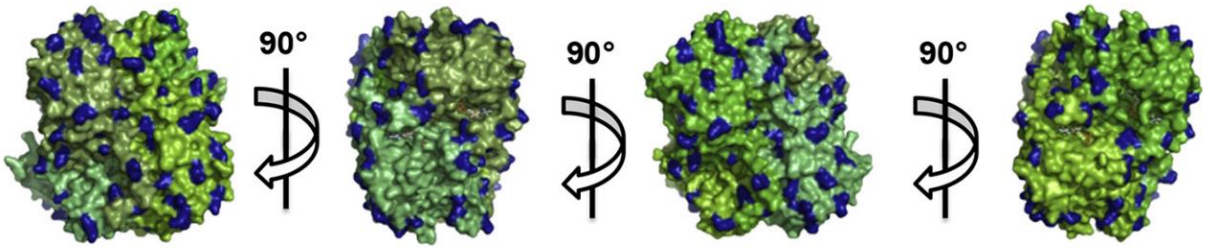

Figure 18. Crystal structure of LDH-5 from rabbit muscle, where Lys residues are highlighted in blue. [26]

Since the activity of protonated amino groups $-NH_3^+$ is almost negligible, the immobilisation of the enzyme should take place in an alkaline solution with pH > 10, as this reaction condition would lead to the deprotonation of amino groups from Lysine residue, that presents a pKa equal to 9.2 [26]. These basic immobilisation conditions could easily resolve in the enzyme denaturation and are therefore not always applicable. It has however been shown how, even a low percentage of unprotonated Lysine residue could be suitable for the enzyme attachment on the functionalised support. Even if a high residue concentration plays an important role on the feasibility of the coupling, it is advised not to adopt pH lower than 6 for covalent enzyme immobilisation. [24]

Due to the need of alkaline or semi-alkaline solution in the immobilisation process, the used enzyme needs to be stabilised, for example through the use of trehalose. Trehalose is an organic osmolyte and it has been extensively studied for its stabilizing properties towards proteins, against denaturation

induced by high temperature or extreme pH. When in solution, trehalose elevates the surface tension of medium, leading to a heightened preferential hydration of the protein, protecting it against dehydration and desiccation. Specifically, a higher surface tension of the solvent is known to increase the energy required to create cavities in the medium, needed to accommodate the enlarged surface area of the protein caused by its denaturation. It is still unclear how trehalose interacts with the protein structure, but it is hypothesized that it can form 3D structures in close proximity to protein surfaces, establishing numerous stabilising peptide-sugar hydrogen bonds. However, it is crucial to note that the effectiveness of these stabilizing agents may vary depending on the specific enzyme, support material, and experimental conditions. Consequently, a case-by-case approach is necessary to establish the optimal conditions for enzyme stabilization. [53]

The chemical reaction involving aldehydes on the support material and amines derived from the protein, culminates in the formation of a very unstable imine bond, also called Schiff's bases.

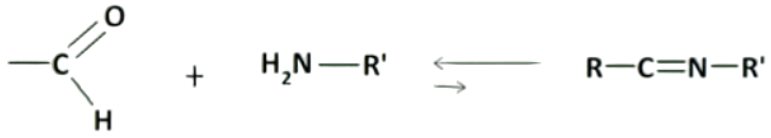

Figure 19. Formation of a Schiff's base. [2]

For the formation of a strong covalent linkage, Schiff's bases need to undergo a reduction reaction. This reduction step holds considerable importance in facilitating a stable interaction between the protein and support material; however, it could potentially influence the catalytic activity of the protein. The imine bond reduction can be performed using different mild reducing agents, such as cyanoborohydride or borane. [2], [26]

1.6 Enzyme kinetic

As previously mentioned, enzymes play a fundamental role in allowing reaction to proceed at lower temperatures and more rapidly than in their absence. Their particularity is to be incredibly selective through the substrate, allowing the formation of the so-called enzyme-substrate complex (ES), a strong interaction that enables the utilisation of the substrate at a rapid rate, to form the desired product. The complex formation is the key element for the acceleration of the desired reaction, in fact, its formation will lower the reaction activation energy needed. This will therefore result in a diminished temperature and amount of time required to conduct the analysed reaction. [54]

An enzymatic catalysed reaction follows the general scheme below:

$$E + S \rightleftarrows ES \rightleftarrows EP \rightleftarrows E + P \qquad \textit{Equation 1}$$

It is clear from the given reaction path, that after the product formation, the enzyme is free to take part in another catalytic reaction, through the interaction with a new substrate molecule. If there are not inhibitor effects, the enzyme results unchanged after the reaction.

The study of enzyme catalysed reaction kinetic is pivotal for the complete understanding of the enzyme structure and function. It consists in the correct assessment of the reaction rate and its variations in response to experimental parameter alterations. [55]

Under typical conditions, the reaction rate is directly proportional to the enzyme concentration, owing to an excess of substrate molecules in relation to the enzyme concentration. For a specific enzyme concentration, the reaction rate initially escalates with an increase in substrate concentration. Ultimately, a maximum rate is reached, and further addition of substrate essentially exerts no influence on the reaction rate, that will remain constant. The shape of a reaction rate graph (V) plotted against substrate concentration [S] takes the form of a rectangular hyperbola, terminating in a plateau, a characteristic feature of the majority of enzymes. These dependencies on enzyme and substrate concentrations gave rise to a renowned algebraic equation that accounts for most enzyme catalysed reactions. This model was conceived in 1913 by Leonor Michaelis and Maud Menten and serves as a mathematical representation for enzyme-catalysed reactions. It is based on the idea that the enzyme binds rapidly to the substrate, forming an enzyme-substrate complex (ES), which subsequently will result into the product and the original enzyme, in a second, considerably slower, step. [56]

$$V = \frac{V_{max}[S]}{K_m + [S]} \qquad \textit{Equation 2}$$

This equation represents the catalytic reaction velocity dependence to the substrate concentration and it is therefore suitable for the description of reaction where only one of the substrates is varying. It is also important to note that, the equation characterise the initial reaction rate, as [S] will progressively be consumed by the reaction. This is the reason why, the accuracy of estimating the speed of an enzymatic reaction increases as the time interval, in which the concentration of the reaction product is determined, decreases. [13] The Michaelis-Menten equation can be visualised in *Figure 20*, for a general enzymatic reaction.

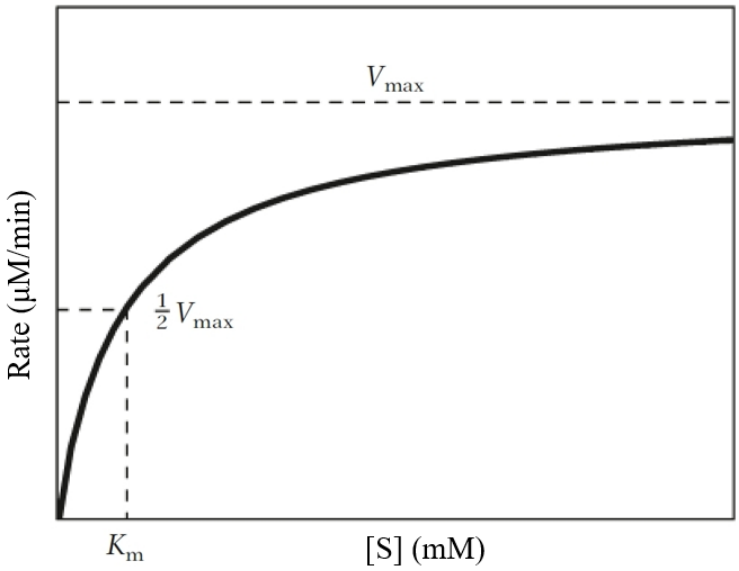

Figure 20. Graphical representation of Michaelis-Menten equation. Adapted from [13]

It is important to specify the meaning of the two kinetic constants present in the given equation.

- V_{max}, the maximum conversion rate reached by the reaction. Generally, it is directly proportional to the total amount of enzyme present.
- K_M, Michaelis constant, the substrate concentration at which the reaction shows a rate equal to half of the maximum one ($V_{max}/2$). Its value is of crucial importance since it represents the affinity between the analysed substrate and the enzyme. In fact, a low value of K_M, indicated that an exceedingly small amount of reagent is needed to reach $V_{max}/2$. As a result, K_M can vary considering different substrates for the same enzyme.

The evaluation of these kinetic parameters is of crucial importance to compare different catalytic activities, different reaction conditions and the effect of inhibitors. These two constraints are in fact used to describe the interaction between the enzyme and its substrate. [13] To calculate these constants, many approaches are possible. The more straightforward and used method was implemented by *Lineweaver and Burk* in 1934. This linearisation, also known as double reciprocal plot, is a graphical representation of the Michaelis-Menten equation. In fact, starting from the already cited equation, it is possible to obtain the Lineweaver-Burk plot by taking the reciprocal of each side of the formula. [57]

$$\frac{1}{V} = \frac{K_M}{V_{MAX}} \cdot \frac{1}{[S]} + \frac{1}{V_{MAX}}$$ *Equation 3*

By replacing the experimentally found values of V for each used substrate concentration in the Lineweaver-Burk equation, a line will form. The plot presents a slope that corresponds to K_M/V_{MAX}. As can be seen in the graph below, the plotted line intersects the ordinate axis at the value $1/V_{MAX}$ and, when extrapolated, intersects the negative abscissa axis at the value $-1/K_M$. The interpolation of the experimental data with this method will enable to find the values of the two kinetic constants.

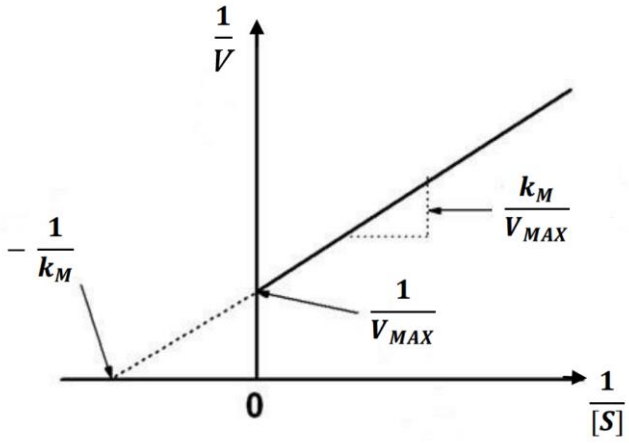

Figure 21. Lineweaver-Burk plot. Adapted from [13]

The double reciprocal plot, however, is not the preferred choice. This method is, in fact, known for its susceptibility to experimental errors. This linearization process can magnify minor inaccuracies in the measurement of reaction velocity V, leading to amplified errors in 1/V values. Nonetheless, Lineweaver-Burk plot was implemented in this work, due to its simplicity and ability to clearly show the undergoing inhibition mechanism when applied in the study of inhibition kinetics. *Figure 22* shows how the use of Lineweaver-Burk plot for the representation of enzyme kinetics can be advantageous in differentiating the various inhibition mechanisms possible.

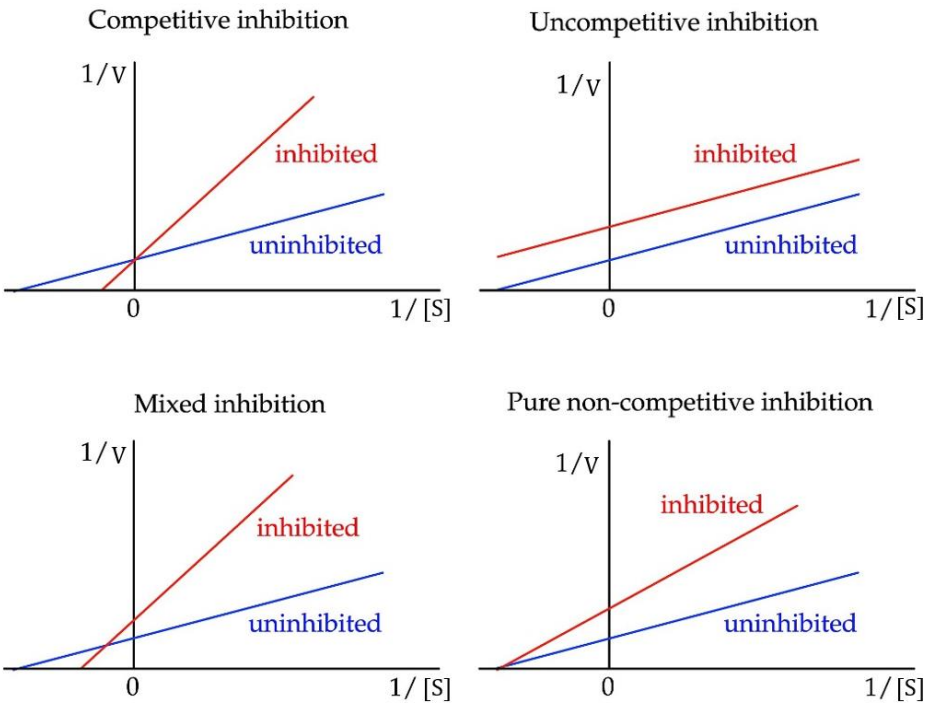

Figure 22. Representation of how different types of inhibition mechanisms effect the Lineweaver-Burk plot. [58]

By multiplying each term of the Lineweaver-Burk equation it is possible to obtain a second linearisation method, known as the *Hanes* method. As for the first method, it can be used to easily calculate the two kinetic constants of interest, K_M and V_{max}. [55]

$$\frac{[S]}{V} = \frac{K_M}{V_{MAX}} + \frac{[S]}{V_{MAX}} \qquad \textit{Equation 4}$$

The graphical representation of the Hanes plot in *Figure 23* shows how the two constants can be extrapolated from the slope and the intersection with the y-axis, when plotting [S]/V versus the substrate concentration. Hanes linearisation is generally considered more precise, however, the use of this plot is discouraged when analysis the reaction rate as a function of coenzyme concentration, due to its more precise approximation when [S] refers to the substrate.

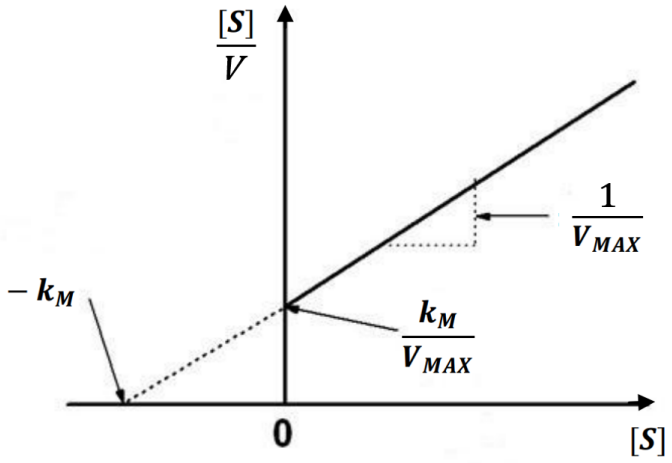

Figure 23.Hanes plot. Adapted from [13]

1.7 Enzyme inhibition

Enzymatic inhibitors (I) are a class of molecules that interact with enzymes, leading to a decrease in their activity. Some inhibitors may also interact with the coenzyme, indirectly influencing the catalytic reaction rate. They can be classified as either reversible or irreversible, depending on the type of bond formed with the targeted enzyme (E). Reversible inhibitors form weaker bonds with the protein, polar or ionic ones, allowing the resulting complex (EI) to dissociate easily. In contrast, irreversible inhibitors bind with the protein forming a stable, inactive complex, due to the formation of covalent bonds. [59] In both cases, the enzyme does not undergo a denaturation process, since the interaction with the inhibitors, whether strong or week, only alters a portion of the protein. In fact, enzyme inhibition is not to be confused with protein denaturation by high temperature or extremes pH values, that modify the enzyme structure in a non-specific way.

When an irreversible inhibition mechanism takes place, the reaction rate cannot be described using Michaelis-Menten equation. A sigmoidal curve-like equation better describe this type of trend. On the contrary, the presence of a reversible inhibitor modifies the Michaelis-Menten curve, but the reaction rate trend is a rectangular hyperbole, as for the noninhibited one. As irreversible inhibitors were not investigated in this work, the focus will be on reversible inhibition mechanisms.

Reversible inhibition processes can be classified in 4 different categories: [13], [60]

- *Competitive*: the inhibitor is characterised by a high affinity with the substrate binding site. Most of the competitive inhibitors are synthetised to be conformationally similar to the enzyme substrate. The link between the competitive-type inhibitor and the protein forms an

inactive complex, EI. As a consequence of the inhibitor presence, the affinity between the substate and the protein will be reduced, meaning the kinetic constant K_M will increase. However, since the inhibitor does not interact with the ES complex, V_{max} will remain unchanged. The presented inhibition mechanism is schematised in *Figure 24*. In this work, as discussed in more dept in the following chapter, Lactate Dehydrogenase was tested using an inhibitor competitive with both the substrate, pyruvate, and the cofactor.

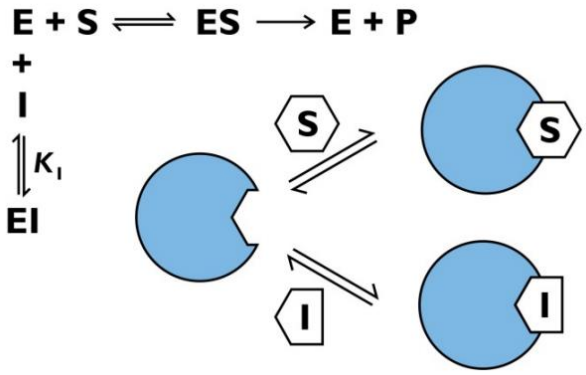

Figure 24.Schematic representation of competitive inhibition. [61]

- *Uncompetitive*: the inhibitor binds solely the enzyme-substrate complex. This results in a decrease of the reaction maximum velocity, due to the consumption of the active complex. K_M decreases, accordingly with Chatelier's principle.

- *Noncompetitive*: reduce enzyme activity without affecting substrate binding. They bind away from the active site, altering enzyme conformation. This binding, however, compromises H-bonds and weak interactions, changing the 3D shape of the protein. Noncompetitive-type inhibitors differ for their equal affinity for the free enzyme and the enzyme-substrate complex. As a result of their attachment, V_{max} decreases, but K_M remains unchanged, as the substrate is still able to bond to the enzyme. Consequently, the inhibitor presence hampers the substrate conversion.

- *Mixed*: as for an uncompetitive inhibition, the enzyme can simultaneously bind the inhibitor molecule and the substrate, but the two phenomena are not unrelated. Mixed-type inhibitors, in fact, bind to a site different from the active site where the link between the protein and the substrate takes place. However, the inhibitor binding affects the affinity of the substrate for its active site, reducing it. This effect is due to the change of the enzyme structural conformation after the inhibitor attachment.

2. Materials and methods

This chapter is comprehensive of all the procedures followed to synthetise the needed materials and the punctual description of every characterisation method employed for their analysis.

Evaluation of Lactate Dehydrogenase dimension

In order to adequately select the more suitable mesoporous material for Lactate Dehydrogenase immobilisation, it is important to evaluate the dimensions of the enzyme. In the present work, human LDH-A was used for every assay successively described. In particular, recombinant hLDH-A, produced via *E.coli* expression, was purchased from Merck in an aqueous solution form.

The volume occupied by the protein was calculated using the following equation:

$$V_{Prot} = \frac{V_2}{N_A} \times M \qquad \textit{Equation 5}$$

Where:

- V_{prot}, Volume occupied by the protein (in nm^3)
- V_2, Partial specific volume, the reciprocal of the protein density. Knowing from literature that the majority of the protein have a V_2 that varies from 0.70 to 0.76, for the present work, the average, 0.73 cm^3/g, was used. [62]
- N_A, Avogadro's number
- M, total average enzyme mass (in Dalton, Da)

To be able to calculate the volume occupied by Lactate Dehydrogenase, M must be assumed. In this case, the total average enzyme mass was calculated from the average mass of one subunit, that, accordingly to the literature, is approximately equal to 35 kDa. [11] The total protein mass used was therefore 140 kDa. This estimation allowed for the calculation of $V_{prot.}$ Since this result is not directly comparable with the pore dimension that characterises the material used, it was assumed that the protein presents a globular shape. This enabled the calculation of its average radium, using the following formula:

$$R_{min} = \left(\frac{3}{4\pi} \times V_{prot}\right)^{\frac{1}{3}} \qquad \textit{Equation 6}$$

The obtained R_{min} is equal to 3.43 nm.

2.1 Support synthesis

2.1.1 SBA-$15_{0.25}$

As previously described in the introduction section, SBA-15 presents various advantages, the main one being its large porosities compared to the more common MCM-41 and its high hydrothermal stability. Taking into consideration the size of lactate dehydrogenase, and the porosimetry results obtained for this mesoporous silica in the characterisation section, SBA-$15_{0.25}$ was chosen as inorganic support for this thesis work. The subscript 0.25 indicates the chosen ratio between the amount of swelling agent and of template used. This parameter is of crucial importance for the tuning of pore size and distribution in the final product. [43] To facilitate the positioning of the studied protein in the material cavities, said parameter was set at 0.25.

For the preparation of this material, 31.53 mL of HCl and 128.47 mL of purified Milli-Q water were mixed in a graduated cylinder, to obtain 160 mL of acid solution 2M, with the help of a magnetic stirrer. This solution was placed in a round-bottomed flask, under hood. After homogenisation of the solution occurred, 4 grams of P123, the templating agent, were added and left stirring for 1 hour at 40 °C. In these conditions, the triblock co-polymer auto-aggregates to form micelles. The second step is the slow incorporation of 1.16 mL of swelling agent, 1,3,5-Trimethylbenzene or TMB. The solution was then left at 40°C for 1 hours, to complete the organic template arrangement, obtain a high specific surface and the desired pore size distribution. Subsequently, 9.11 mL of tetraethyl orthosilicate (TEOS) were added to the solution and left stirring always at the same temperature for 24 hours. During this period, TEOS, the silica source, will condensate on the previously formed 3D structure, forming an inorganic interconnected network. The described liquid-crystal synthesis method is summarised below in *Figure 25*.

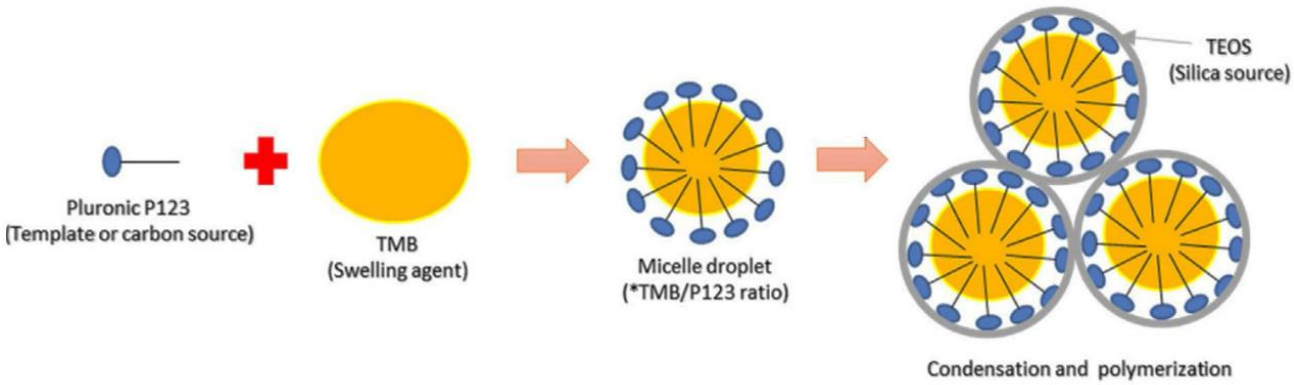

Figure 25. Schematical synthesis of SBA-15. Adapted from Klinthongchai et al. [43]

At the end of the condensation time, a gel-like white solution was recovered from the flask and placed for 24 hours in autoclave at 100°C. The next step was then to wash the solution a total of 10 times, the first two using ethanol and the last eight times with Milli-Q water. In between each washing stage, the solution was centrifuged until the supernatant turned clear, which required approximately 10 minutes at ambient temperature, using a centrifuge. The synthesis process was completed by one night on drying at 100°C and a final step of calcination at 550°C for 5 hours. This last step is particularly important to eliminate the template and obtaining the silica network without any unwanted carbon residue.

2.1.2 $MCF_{0.75}$

The procedure followed for the synthesis of Mesocellular Foam silica, MCF, is equivalent to the one described in the previous chapter for Santa Barbara Amorphous no 15. The only different is the chosen ratio between the concentration of amount of swelling agent (TMB) and of template employed. In fact, to obtain the desired typical 'spongy-like' structure of the MCF, a higher amount of TMB is needed. The ratio used is therefore equal to 0.75. This difference in the synthesis process will lead to substantial morphological differences in the final products, that will be highlighted in the third chapter of the present work. [43]

2.1.3 Dendritic fibrous nanosilica DPS and $DPS_{0.75}$

Dendridic fibrous nanosilica particles were synthetises following a procedure very similar to the one employed previously for the other chosen mesoporous supports. a combined. Through this process, TEOS was again employed as the silica source (similarly to the previous syntheses described), CTAB was employed as a surfactant, and urea was used to catalyse and modulate the reaction speed. As characteristic of every catalyst, urea intervened in the reaction, facilitating it, without becoming part of the final product's composition.

As a first step, a solution of Urea and CTAB was prepared by blending 1.2 g of urea, 5.6 g of CTAB together with 60 ml of Milli-Q water. Secondly, a solution of butanol and cyclohexane was created by mixing 3 ml of butanol and 60 ml of cyclohexane. During the synthesis process, cyclohexane, in conjunction with butanol, established an organic phase environment, leading to the formation of reverse micelles. This step is particularly important since these reverse micelles served as templates

for the creation of mesoporous dendritic structures during silica polymerization. Finally, cyclohexane is removed from the solution, through either evaporation or thermal treatment. This removal contributed to enlarging the pores within the final support three-dimensional structure.

8 ml of TEOS were then gradually added drop by drop to the solution of butanol and cyclohexane. Eventually, the solution of urea and CTAB was introduced to the mixture of TEOS, butanol, and cyclohexane. The formed mixture was then left stirring at room temperature for 30 minutes and subsequently conveyed to an autoclave and subjected to thermal treatment at 130°C for 5 hours.

A final filtering and thoughtful washing of the prepared suspension with ethanol and water was performed to eliminate all the present impurities. This separation process was carried out using a centrifuge and repeated ten times. Post-washing, to eliminate any residual moisture from the synthetised material, it was dried overnight at 60°C.

As a last step, the material underwent a calcination process at 550°C for 5 hours, with a gradual temperature increase of 0.75°C/min, equal to a 45°C increase in one hour, in order to attain the desired morphology of the final product. [45]

The synthesis procedure followed for the $DPS_{0.75}$ sample mirrored the one exemplified for DPS. The only difference lies in the diverse volume of the organic solvents employed, which in this second case were 0.2715 ml for the butanol and 5.43 ml for the cyclohexane; the formed solution however served as organic phase for the formation of reverse micelles, the core part of this synthesis process. The ratio 0.75 was obtained from the quantities of butanol and cyclohexane employed, expressed in grams. The rest of the process was repeated unchanged.

2.2 Silica support functionalisation

Once the silica supports have been synthesised, they were functionalised with amino and aldehyde groups, employing two organosilanes molecules, APTES ((3-Aminopropyl)triethoxysilane) and GPTMS ((3-Glycidyloxypropyl)trimethoxy silane), which form covalent bonds with the -OH groups on the surface of silica.

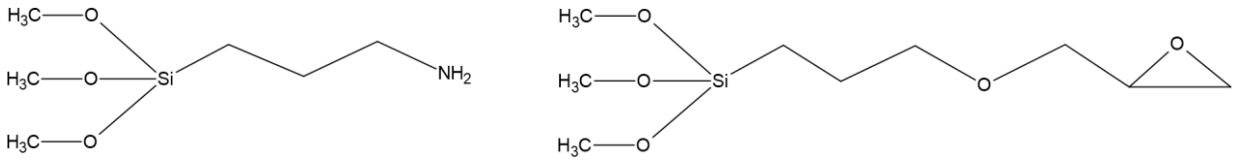

Figure 26. APTES molecule on the left and GPTMS molecule on the right.

The used grafting technique consists in three different steps: the first one is the reaction between the silica support, APTES and GPTMS, that will lead to functionalisation of the silica with epoxy and amino groups. Whereas the second and third steps will involve the activation of the surface to generate diols initially and subsequently forming glyoxylic groups.

Generation of amino and epoxy groups: 6 mL of APTES and GPTMS each were slowly added in 120 mL of ethanol in a round-bottomed flask under magnetic stirring to obtain a homogeneous solution containing 5%v/v of each organosilane. Then, 4 grams of the previously synthetised support were weighted and added to the solution, under hood. The reacting mixture was kept at ambient temperature for 5 hours. At the end of this reaction time, the solution was centrifuged for 10 minutes at 5000 rpm. The support was washed 10 times, first with ethanol and then using Milli-Q water. At the end of this washing procedure, the obtained product was filtered via Buchner funnel. The result of this operation is the functionalised silica support, with amino and epoxy group on its surface, as represented in the scheme below. The material was placed on a paper filter and dried overnight.

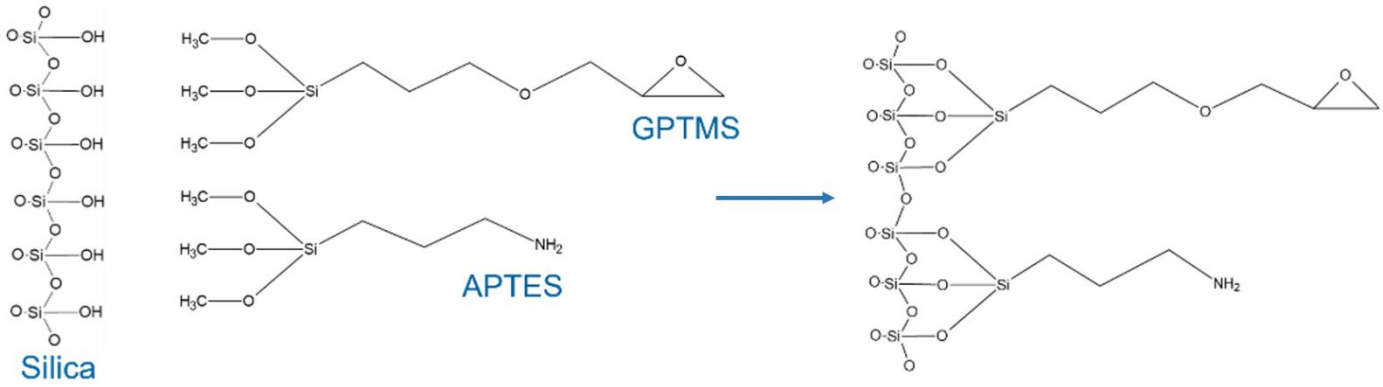

Figure 27. Generation of amino and epoxy groups.

Generation of diols groups: The support obtained at the end of the first step was introduced in a 0.1M H_2SO_4 solution. This was prepared by combining 120 mL of Milli-Q water with 0.66 mL of H_2SO_4 (96.5%). Sulfuric acid will react with the epoxy groups previously forms, to create diols groups, as depicted in *Figure 28*. The primary amino groups formed due to the linkage of APTES molecules on the support surface are not as reactive as the epoxy groups and will therefore be left unchanged by the performed reactions.

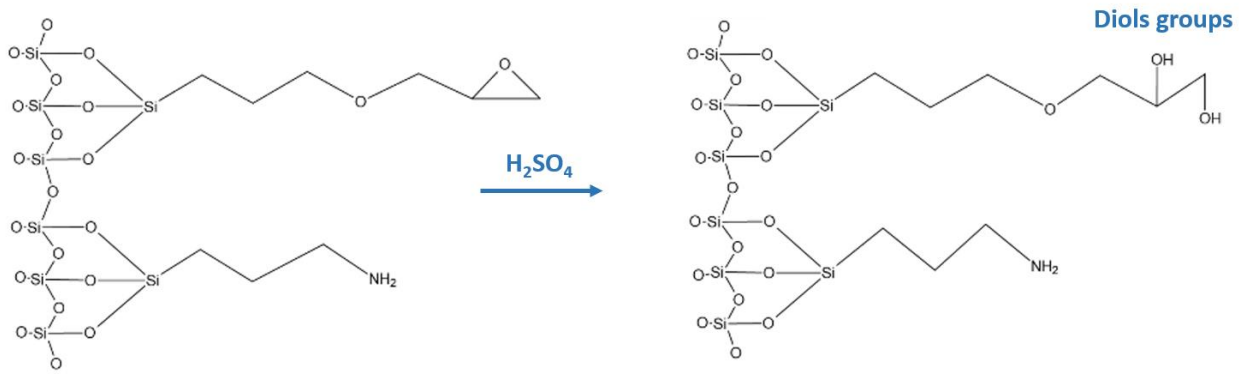

Figure 28. Generation of diols groups.

The reagents were thoroughly maintained at 85°C and mixed for 2 hours. Once the reaction had completed, the mixture was left to cool down to an appropriate handling temperature. The exceeding liquid and reagents were separated from the support through centrifugation and subsequent abundant washing with Milli-Q water. As for the past step, the obtained mixture was filtered and then placed in a dried overnight.

The third and last functionalisation step was the *generation of glyoxyl groups.* For this reaction a $NaIO_4$ 0.1M solution was prepared mixing 2.61 g of sodium periodate and 121.98 mL of Milli-Q water. Sodium periodate is here used to activate the previously formed hydroxyl groups; this reaction will form aldehydic groups on the support surface, which will be essential as binding sites for the enzyme immobilisation. The silica support was slowly added to the reagent's solution, previously placed in a round-bottomed flask, under magnetic stirring. All the operations were performed under the hood. The solution was let stirring at room temperature for two hours. After the reaction time, the mixture was once again centrifuged and washed with Milli-Q water, before filtering with Buchner funnel and drying.

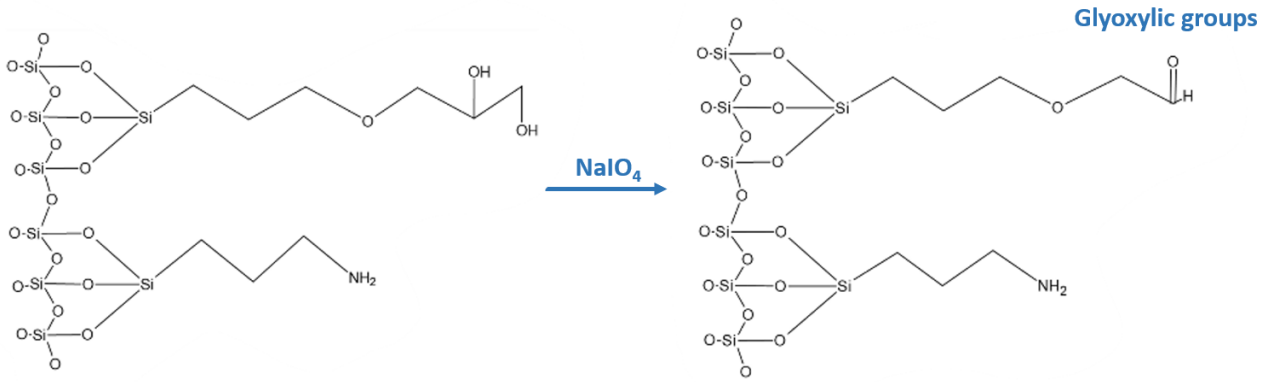

Figure 29. Generation of glyoxylic groups.

At the end of the described functionalisation process, two different active groups are present on the surface: glyoxylic and amino groups. Their relative concentration was investigated with appropriate techniques, subsequently described.

Since the support material properties and ability to subsequently bind the chosen enzyme highly rely on the material surface chemistry, it is pivotal to correctly analyse the functional groups present at the end of the functionalisation process of every mesoporous material employed in the present study. The comprehensive understanding of the studied material surfaces will allow a correct analysis of the conformation of LDH after the immobilisation. For this reason, two different quantification procedures were implemented: glyoxyl group quantification via retro-titration and $-NH_2$ groups quantification using a copper sulphate solution.

2.2.1 Aldehydic groups quantification

To quantify the aldehyde (glyoxyl) groups, present on the support surface after the third functionalisation step, a retro-titration procedure was followed. For this analysis two solutions were needed: a 10% potassium iodide (KI) solution, that was prepared by mixing 1 g of KI with 10 mL Milli-Q water, and a sodium bicarbonate ($NaHCO_3$) solution, prepared by mixing 1.5 g of sodium bicarbonate with 10 mL of Milli-Q water. This last solution was saturated. The technique employed allows to indirectly measures the quantity of aldehyde groups formed on the silica surfaces by exploiting the generation of IO_4^- ions during the substrate activation reaction. This analysis was performed on all the mesoporous materials functionalised: $SBA\text{-}15_{0.25}$, $MCF_{0.75}$, DPS and $DPS_{0.75}$. To measure the concentration of IO_4^- ions in the reaction solution, two samples were collected: one before the reaction started and one at the end of the diol oxidation reaction to aldehyde groups. They were successively diluted to a 1:50 ratio by adding 20 µL of the taken sample to 980 µL of Milli-Q water. This dilution allows for an appropriate concentration for subsequent analysis. The samples for analysis were prepared by adding 0.2 mL of the diluted sample prepared in the previous step to a solution containing 1 mL of the 10% potassium iodide solution and 1 mL of the saturated sodium bicarbonate solution. For the blank sample, 0.2 mL of Milli-Q water were added instead.

The analysis was performed using a UV-vis spectrophotometer set to "Fixed Wavelength" mode at 420nm, wavelength at which the compound formed by the reaction between sodium periodate and potassium iodide can be correctly measured. Therefore, by measuring the absorbance of the solution before and after the epoxidation reaction took place, it was possible to determine the amount of aldehydic groups generated on the support surface by using the given equation: [63]

$$\frac{\mathrm{mol_{ald}}}{\mathrm{g_{sup}}} = \frac{\mathrm{V_{IO4^-}}[\mathrm{IO_4^-}]_{\mathrm{in}}\left(1-\frac{\mathrm{Abs_{fin}}}{\mathrm{Abs_{in}}}\right)}{\mathrm{g_{sup}}} \qquad \textit{Equation 7}$$

Where:

- mol_{ald}, quantity of aldehydic groups formed on the support surface;
- g_{sup}, support mass;
- V_{IO4^-}, initial volume of sodium periodate solution;
- $[IO_4^-]_{in}$, sodium periodate solution initial concentration;
- Abs_{fin}, measured absorbance at 420 nm of the tested solution at the end of the reaction;
- $Abs_{in,}$ measured absorbance at 420 nm of the tested solution before reaction.

2.2.2 Amino groups quantification

For the quantification of the amino groups formed on the support surfaces after the last step of the functionalisation process, the following procedure was applied to all the synthetised supports: SBA-$15_{0.25}$, $MCF_{0.75}$, DPS and $DPS_{0.75}$. Firstly, 11,72 mg of sodium borohydride ($NaBH_4$) were used to prepare a 5 mM solution with Milli-Q water. 15 mL of this solution were subsequently mixed with 50 mg of each support, in its hetero functionalised form, for one hour using a magnetic stirrer. The reaction between this reagent and the silica material is fundamental for the reduction of the double bond C=O of the functional aldehydic group. In fact, $NaBH_4$ is a source of hydride ion (H^-), fundamental to reduce the very reactive double bonds of the glyoxylic groups in this preliminary phase of the amino groups' quantification assay. [64] Otherwise, the aldehydic groups will react with the reagent ($CuSO_4$) used for the quantification.

After the described reaction was let take place under the hood, each sample was centrifuged and washed with abundant Milli-Q water. This step allowed for the complete removal of all the residual reagent. Consequently, a 300 mM copper sulphate ($CuSO_4$) aqueous solution was prepared. 1.5 mL of this solution were added to each support, recovered after the centrifuge treatment, and each suspension was placed in an Eppendorf. The reaction between $CuSO_4$ and the $-NH_2$ groups present of each material surface was let proceeding for approximately one hour in gentle mixing conditions. After this reaction time, the obtained suspensions were centrifuged vigorously, until the complete sedimentation of the contained silica support. The fast adsorption of Cu^{2+} on silica materials functionalised with amino groups is well documented in literature; it was employed in this study for the quantification of $-NH_2$ groups through the comparison between the $CuSO_4$ concentration in the

initial reagent solution and its concentration in the supernatant obtained via centrifuge for each solution after the reaction took place. [65], [66] Each initial and final concentration was measured using a UV-vis spectrophotometer set to "Fixed Wavelength" mode at 750 nm. The ratio between the absorption of the initial and final concentration was correlated to the amino group concentration on each silica material using the following equation.

$$\frac{\mathrm{mol_{NH2}}}{\mathrm{g_{sup}}} = \frac{\mathrm{V_{CuSO4}[CuSO4]_{in}}\left(1-\frac{\mathrm{Abs_{fin}}}{\mathrm{Abs_{in}}}\right)}{\mathrm{g_{sup}}} \qquad \textit{Equation 8}$$

Where:

- mol_{NH2}, quantity of amino groups formed on the support surface;
- g_{sup}, support mass;
- V_{CuSO4} , initial volume of sodium periodate solution;
- $[CuSO_4]_{in}$, copper sulphate solution initial concentration;
- Abs_{fin}, measured absorbance at 750 nm of the tested solution at the end of the reaction;
- $Abs_{in,}$ measured absorbance at 750 nm of the tested solution before reaction.

2.3 Support Characterisation

After the complete synthesis and functionalization of the selected supports, various techniques were employed for their characterization. This crucial step allowed for the complete understanding of the structural and chemical attributes of the studied mesoporous silica supports: SBA-$15_{0.25}$, $MCF_{0.75}$, DPS and $DPS_{0.75}$. For this thesis work, the following methods were employed: Fourier-transform infrared spectroscopy (FTIR), high-resolution scanning electron microscopy (FE-SEM), and nitrogen physisorption at 77K (BET analysis). The coupled application of these analytical tools enabled a thorough examination of the selected supports, permitting an in-dept study of their crystalline structure, chemical composition, surface morphology and absorption properties.

2.3.1 Fourier-Transform Infrared Spectroscopy (FTIR)

The Fourier-transform infrared spectroscopy (FTIR) is a commonly employed analytical technique for the determination of a material superficial and bulk chemistry. This technique relies on the interaction between electromagnetic radiation, emitted by a primary light source, and the selected sample. The radiation used in this type of spectroscopy belongs to the electromagnetic spectrum's infrared region, which extends between the visible and microwave regions, with wavelengths from

around 1 millimeter (300 GHz) to around 700 nanometers (430 THz). [64] The interaction between the infrared beam and the sample leads to the selective absorption of the radiation at specific wavelengths, resulting in a change of the vibrational energy of the sample bonds. The infrared radiation can induce two different forms (or modes) of vibration in the targeted sample: stretching or bending vibration. In particular, stretching vibration can be symmetric or asymmetric, while bending vibrations are subdivided in: wagging, rocking, twisting, and scissoring. [65] The cited vibration modes are summarised in *Figure 30.*

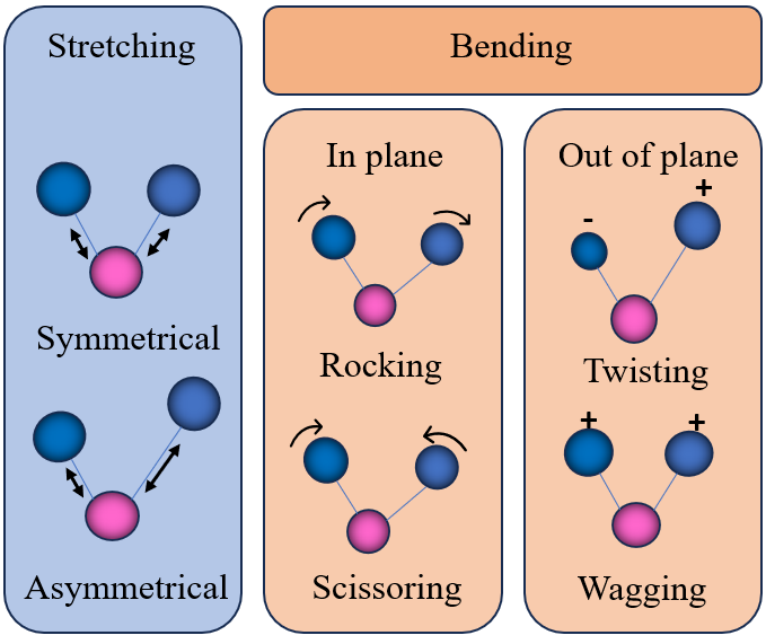

Figure 30. Possible vibrational modes of a molecule. Adapted from [66]

What cause the absorption of the infrared radiation is the net change of their dipole moments during the vibration. Some molecules are not able to absorb infrared radiation and change their vibrational mode and therefore they are called IR inactive molecules, while the molecules that do absorb IR radiation are called IR active. The latter are characterised by highly polar covalent bonds, which enable a vigorous stretching or bending of the molecule when subjected to IR radiation. [67]

On the other hand, bonds that do not present a change in dipole moment are IR inactive and hence do not correspond to a peak in the molecule spectrum. Some examples of IR inactive bonds are the completely symmetrical ones: C=C, C≡C and O=O. [68]

The transmitted radiation will be collected by a detector that will enable a detailed characterisation of the covalent bonds present in the analysed sample. The resulting signal at the detector presents as

a spectrum, typically from 4000 cm^{-1} to 400 cm^{-1}, which is characteristic of the covalent bonds presents. More specifically, the region between 400 and 1400 cm^{-1} presents a pattern of absorbance peaks that is peculiar for each molecule, and it is therefore called the molecular fingerprint region. [67] Exactly like a human fingerprint, no two molecular structures generate the same infrared spectrum. This particularity is what renders infrared spectroscopy the preferred choice for chemical composition analysis.

In the present thesis work, FTIR analysis was used to determine the changes underwent by the various mesoporous silica supports, after their functionalisation with APTES and GPTMS and after the enzyme immobilisation on their surface. The samples were prepared starting from the dried powder suitably compacted in the form of thin wafers and placed in a gold sample holder, given that gold is an IR inactive material. This operation is essential to avoid the holder material interference on the measurements. All the previously mentioned supports were analysed using Bruker INVENIO spectrophotometer equipped with liquid nitrogen cooled Mercury Cadmium Telluride detector (LN-MCT). Both water vapour molecules and CO_2 are IR active, meaning that their absorption on the analysed sample would result in a visible peak on the final spectrum. To avoid the interference given by these molecules, void was applied to each sample before its spectrum was taken. All the analysis were performed at room temperature.

2.3.2 Field emission scanning electron microscopy (FE-SEM)

Scanning electron microscopy (SEM) is a widely used electron microscope technique for the analysis of material structure and surface. It can be applied to provide information about the surface morphology of different classes of material, such as crystals, amorphous solids and electronic devices, without damaging the sample. High resolution images can be obtained with a magnification up to 900000x. It differs from the conventional and more commonly used optical microscopy because of the use of a beam of electrons instead of visible light (400 to 700 nm) to interact with the sample. This enables to overcome the resolution limit of the optical microscopy, which is linked with the wavelength of the employed light source, allowing the nanoscale imaging of the samples. [23]

What distinguishes Field emission scanning electron microscopy (FE-SEM) from SEM is the electron beam source. FE-SEM instruments use a Field Emission Gun (FEG), placed in a vacuum environment, as an electron source, while in SEM a thermionic emission is used. Thermionic Emitters use electrical current to overheat a filament, mainly made of tungsten, up to the temperature at which the filament electron gain enough energy to escape from the material. On the other hand, a FEG does not use heat to excite the electron source but applies a strong electrical potential gradient. The

electrical field is concentrated thanks to the peculiar shape of the tungsten rod, which terminates in a pointed sharp tip. The high-energy electrons of the tip will be able to escape and will form the so-called primary electrons beam. [69], [70]

The two instruments then follow the same operating principle. The primary electrons are focussed and deflected through a lenses system to produce a narrow electron beam that will interact with the first atomic layers of the prepared sample. The interaction between the beam and the solid surface will result in a series of detectable signals, summarised in *Figure 31*.

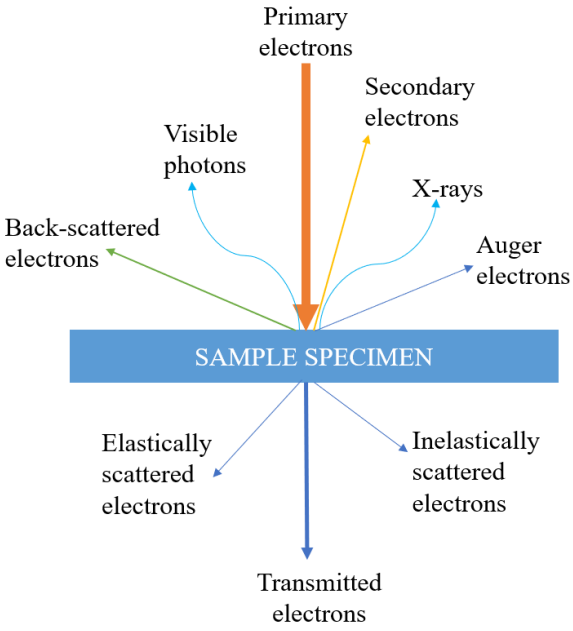

Figure 31. Representation of electrons formed as a result of the interaction of the incoming electron beam on the sample. Adapted from [70]

In particular, the secondary electrons scattered from the surface are low-energy electrons that carry an enormous amount of information about the topography of the sample. In fact, the secondary electrons present a different velocity and diffraction angle from the primary source, closely related to the specimen morphology. Through the collection of the emitted electrons, the instrument will be able to convert the signals into electrical currents. The electrical signals from the detectors are then amplified, processed, and converted into an image that can be displayed on a screen. [71]

To be able to analyse the material, a pre-treatment of the sample is needed. Each sample was in fact compacted to form a thin layer, which was subsequently covered with a conductive film (in this case platinum was used but it is also possible to use gold), to allow the electrons diffusion. The conductive film in fact prevents electrons from accumulating on the solid surface, a phenomenon that would lead to a less precise imaging of the sample. The presence of a thin layer of platinum does not modify the

morphology of the samples. As for the other characterisation techniques, the analysis was performed on four different samples: SBA-$15_{0.25}$, $MCF_{0.75}$, DPS and $DPS_{0.75}$.

2.3.3 Surface area and Porosimetric analysis

As previously mentioned, having a large surface area is a fundamental attribute for silica supports, as it will allow the deposition of a greater amount of enzyme in its porosities. It is however also true that, while small cavities grant a wider surface, it might not result in an available surface for enzyme immobilisation, since the narrow pores increase mass transfer limitation of the protein. Consequently, a detailed analysis of the porosities present in the sample is needed. An easy and established technique for determining the internal surface area and porosities distribution of porous material is based on the physisorption of liquid nitrogen at 77K. Physisorption analysis using different substances as adsorptive is also possible, but the use of nitrogen is the standardised choice for mesoporous and microporous materials analysis. [72]

As for every physisorption, this analysis relies on the formation of weak Van der Waals bonds between the adsorbate, N_2 in this case, and the material surface at low temperature. This type of adsorption is non-specific, reversible, non-activated and leads to the formation of multiple layers on the material surface.

During the adsorption process, the gas molecules will be admitted to the material surface under increasing pressure, and, via accurate data treatment techniques, it will be possible to calculate the quantity of gas forming the first adsorbed layer. The measurement of the adsorbed, and consequently desorbed, volume of gas at constant temperature as a function of gas pressure, is described by a curve called isotherm. The shape of the isotherm is indicative of the pores shape and dimension. IUPAC classifies isotherms in six different possible groups, schematised in *Figure 32*. [73]

For the study of mesoporous silica material, such as the ones utilised in the present work, the most relevant isotherm group is type IV, which describes the gas monolayer formation followed by the filling of mesopores. This particular morphology is characterised by the presence of a hysteresis in the obtained isotherm curve. The hysteresis loop depends upon the non-overlapping of the adsorption and desorption branches, generally associated with capillary condensation of nitrogen. [74]

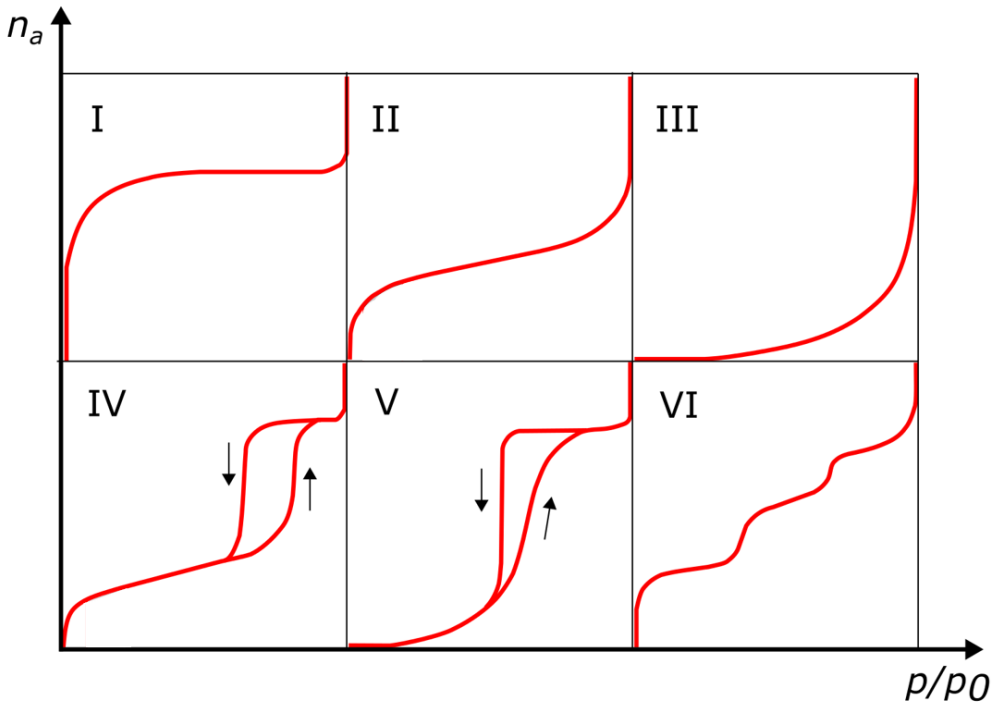

Figure 32. Adsorption and desorption isotherms, according to IUPAC classification. n_a, on the y-axis, stends for Volume Adsorbed. Scheme modified from [75]

It is well known that the particular shape of the analysed hysteresis can be correlated to the material pore geometry. IUPAC classifies the different types of hysteresis in six classes, reported in *Figure 33*. A brief description of each pore structure correlated to a type of hysteresis loop is given. [76]

- *Type H1 hysteresis loop* is typically observed in materials with a narrow pore size distribution, with well-ordered cylindrical pores. This network is exhibited by ordered silica material like MCM-41, MCM-48, and SBA-15, as well as some controlled pore glasses and ordered mesoporous carbons.
- *Type H2 hysteresis loops* are characteristic of more intricate pore structures, where pore blocking effects can play a significant role. The hallmark of H2 loops is the steep desorption branch. In fact, the presence of bottle-neck shaped pores will result in the delayed desorption of vapour from the wide pores. A lower relative pressure is needed to desorb nitrogen from the narrow necks. This particular hysteresis loop can also indicate the presence of evaporation induced by cavitation. Silica gels and porous glasses often exhibit H2 loops. The major difference between H2a and H2b types of hysteresis, is the larger neck width exhibited by the latter.

- *The Type H3 loop* is characterised by the location of the lower limit of the desorption branch in the cavitation-induced region of the p/p0 axis. This type of loop is easily observed in non-rigid aggregates with slit-shaped pores. [41]
- *Type H4 loops* share similarities with H3, but the more marked adsorption at low relative pressure is associated with the filling of micropores present in the analysed material. H4 loops are typical of various mesoporous zeolites and micro-mesoporous carbons.
- *Type H5 hysteresis loop* is very uncommon and shows a peculiar shape, associated with specific pore structures that contain both open and partially blocked pores.

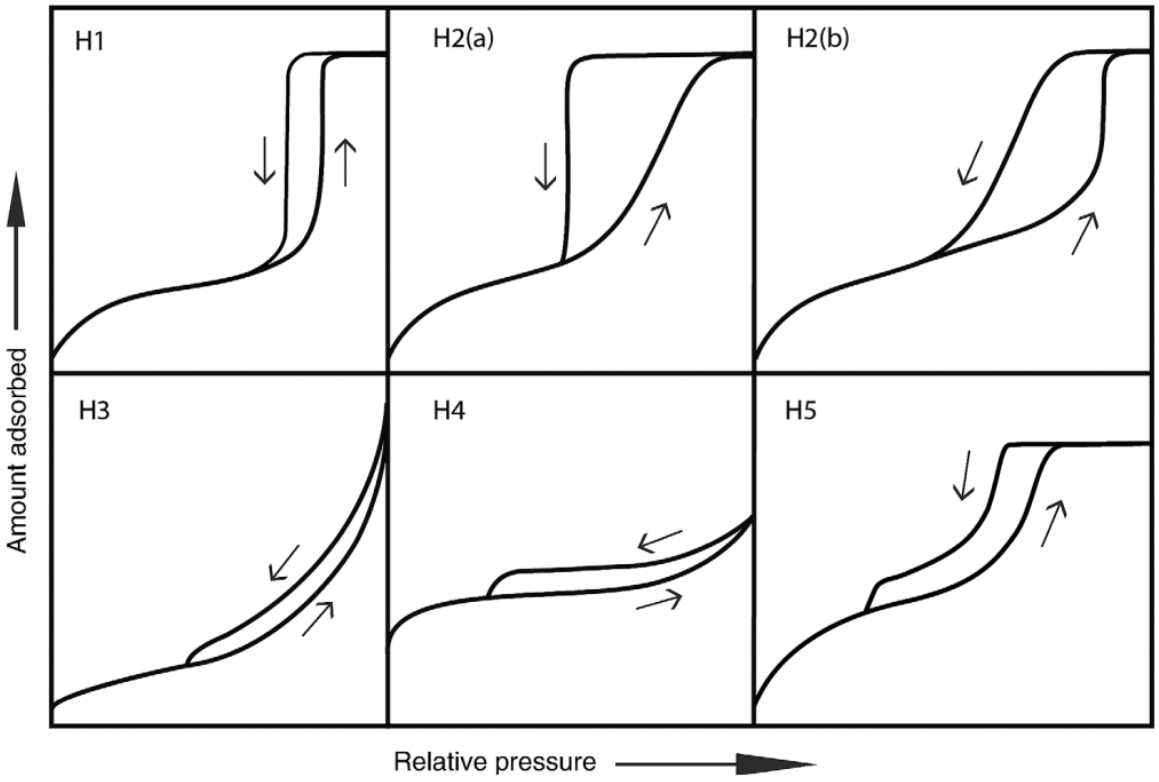

Figure 33. IUPAC classification of hysteresis loop in six distinct categories. [76]

The other isotherm types are: type I, typical of microporous materials (pores < 2nm), type II, that describes nonporous and macroporous solids (> 50 nm) and type III, that represents the absence of multilayer formation and therefore describes materials where adsorbate molecules are preferentially adsorbed on other adsorbate molecules instead of on the solid surface. Type V and VI are highly uncommon and will not be discussed. [74] To summarise the main parts composing a general isotherm curve, the following scheme in *Figure 34* is given.

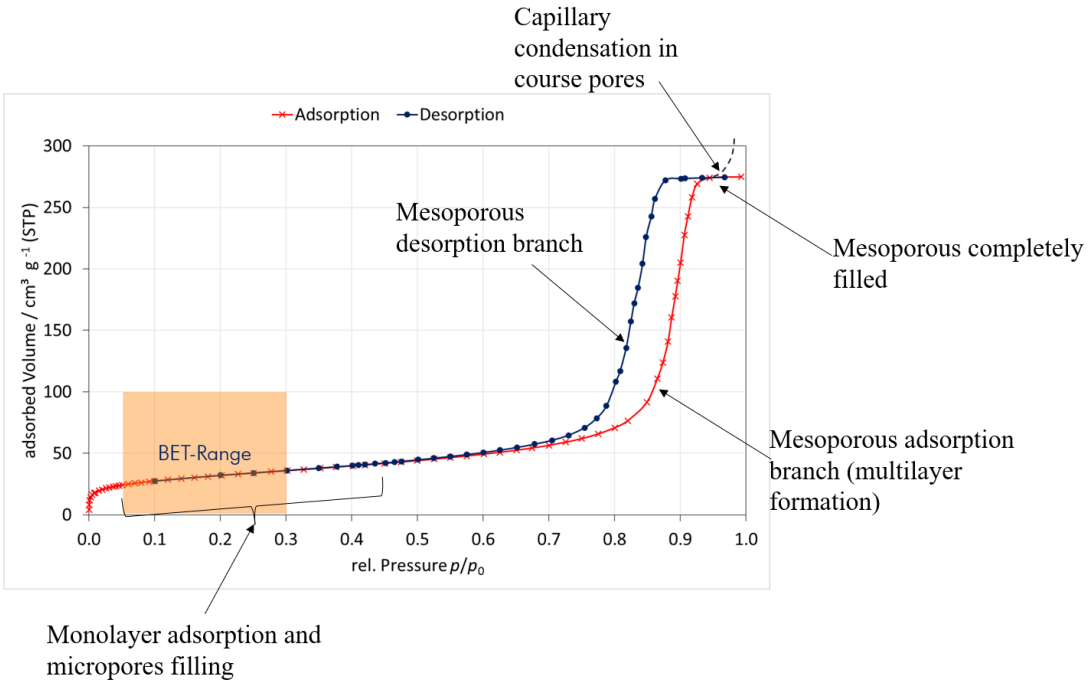

Figure 34. General Isotherm curve type IV, where main adsorption and desorption ranges have been highlighted. Adapted from [77]

The most common mathematical model used to describe multilayer adsorption in mesoporous materials is the Brunauer-Emmett-Teller (BET) equation, reported below in its linear form. [78]

$$\frac{P}{V\cdot(P^0-P)} = \frac{C-1}{V_m\cdot C}\left(\frac{P}{P^0}\right) + \frac{1}{V_m\cdot C} \qquad \textit{Equation 9}$$

Where:

- V, total adsorbed volume
- V_m, volume of gas required to form a monolayer
- P, pressure of the adsorbed gas
- P_0, saturation pressure of the gas
- C, BET constant, related to the affinity of the solid with the adsorbate, it is calculated as:

$$C = \exp\left(\frac{\Delta H_1 - \Delta H}{R\cdot T}\right) \qquad \textit{Equation 10}$$

- ΔH_1, heat of adsorption for the first layer
- ΔH, heat of vaporization

Knowing the adsorbed gas (nitrogen) volume linked with the pressure variation, it is possible to use the BET equation to estimate the number of N_2 molecules present in a monolayer. This equation differentiates between the first adsorbed monolayer at the following ones, taking into account the different values of adsorption enthalpies, through the constant C. The BET equation is the generalisation of the widely known Langmuir equation, which can be used to describe type I isotherm. BET equation, on the other hand, can be applied to the analysis of mesoporous solids, being able to describe accurately type II and IV isotherms.

From the monolayer absorbed gas volume (V_m), it is possible to determine total and specific surface area St, using the equation below:

$$S_t = \frac{V_m \cdot s \cdot N_A}{V} \qquad \textit{Equation 11}$$

- S_t, total surface area of sample material
- V_m, monolayer absorbed gas volume
- N_A, Avogadro's number = $6.023 \cdot 10^{23}$ molecules/mol
- s, cross-sectional area of adsorbed gas molecule
- V, molar volume of adsorbed gas

Therefore, knowing the volume of the gas monolayer used (in this case N_2) and the cross-sectional area of the N_2 molecule (0.162 nm^2), it is possible to derive the specific surface area S_{BET} (m^2/g) by dividing the previously calculated S_t by the mass of the sample. [75]

As regards for the calculation if pore volume and pore size distribution, they can be derived from the previously calculate V_m, using the Kelvin equation, which gives the pressure ratio for cylindrical pores of r radius.

$$ln\frac{P_0}{P} = \frac{2 \cdot \gamma \cdot \widetilde{V} \cdot \cos\theta}{r \cdot R \cdot T} \qquad \textit{Equation 12}$$

Where:

- γ, surface tension of the liquid
- cosθ, contact angle between liquid and gas
- $\widetilde{V}$, molar volume of the adsorbed total liquid
- r, radius of a cylindrical pore

In order to gain relevant information about the material specific surface area and pores distribution, the described physisorption analysis was performed on SBA-$15_{0.75}$, $MCF_{0.75}$, DFNS and $DFNS_{0.75}$

samples, both functionalised with APTES and GPTMS and not functionalised. Each sample was degasified in a dedicated station, where the samples were kept at 200°C for 2 hours, to evacuate the residual water vapour present. The samples were then analysed using a Micromeritics TriStar II.

2.4 Lactate Dehydrogenase immobilisation

Once the support was completely functionalised, Lactate dehydrogenase immobilisation was carried out following the guideline given by Cocuzza et al. [79] for the immobilisation of human Lactate Dehydrogenase on MCM-41.

The immobilisation solution was prepared adding trehalose to a 25 mM pH 9 carbonate buffer. The optimal trehalose concentration of 300 mM was chosen according to the results of Jackson et al. [26]. A proper amount of LDH, was added to the prepared buffer-stabiliser solution, to achieve a final protein concentration of 1 mg of protein per gram of support. 1 mL of the prepared solution was collected and kept in an Eppendorf to be able to monitor the activity of the free protein at the reaction conditions. In the remaining 8 mL of solution, 200 mg of the prepared hetero functionalized support ($SBA\text{-}15_{0.25}$) were added. The reaction was carried out on a magnetic plate to guarantee a gentle agitation. Reaction temperature was kept in a range from 4°C to 10°C. The reagent solution containing LDH, buffer and the stabilising agent was left stirring for 15 minutes before the first sample (500 µL) was taken. A fraction of this sample (100 µL) was immediately analysed, while the remaining part was centrifuged at 500 rpm for 2 minutes. This separation step enabled to test the enzymatic activity of the supernatant solution. Simultaneously, a second activity test was also carried out on the blank solution containing the free enzyme. All the enzyme activity tests were evaluated adding to the extracted samples:

- 100 µL of NADH 7 mM
- 100 µL of Pyruvate 49 mM
- 2.7 mL of 0.1 M pH 7.5 phosphate buffer

For every sample (free enzyme, supernatant solution and support suspension) the enzyme activity was analysed monitoring the variation of NADH concentration with a UV-vis spectrophotometer in "Time Course" mode over 60 seconds at 340 nm. The same analysis was replicated for the three sample, which were taken with 15 minutes intervals until the enzymatic activity in solution (in the supernatant) approached zero or until two successive measurements showed the same absorbance.

For the evaluation of the immobilisation of Lactate Dehydrogenase of the supports, the activity results collected during the described procedure have been analysed with the following equation.

$$I\% = \frac{\text{Initial activity} - \text{Supernatant activity}}{\text{Initial activity}} \cdot 100 \qquad \textit{Equation 13}$$

Where:

- I%, the enzymatic immobilization percentage
- Initial activity, the initial activity of the free enzyme
- Supernatant activity, at the end of the immobilisation process

The enzyme immobilisation percentage is an indicator of the successful bonding of the free enzyme on the silica support used. In fact, it compares the activity of the free enzyme solution at the beginning of the process (time zero) and the final activity measured for the supernatant. A low supernatant activity at the end of the procedure indicates that a high amount of the free enzyme initially present in solution is now linked to the support, and therefore is collected in the support suspension sample or separated via centrifuge.

Upon completion of this initial immobilisation phase, the aldehydic groups present on the support surface enabled the physical adsorption of Lactate Dehydrogenase through weak imide bonds (Schiff's bases). These interactions would not be sufficient to ensure the durable stabilisation of the enzyme on the material surface and this would result in the protein leaching [2].

To create stable covalent bonding between the protein and the silica support, a second immobilisation step was performed. An adequate amount of sodium borohydride ($NaBH_4$) was added to the previously studied immobilised enzyme mixture, in order to obtain a final concentration of 0.1 mg/mL. $NaBH_4$ acted as a reducing agent on the previously formed Schiff's bases, as described in *Figure 35* below.

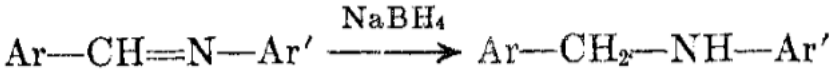

Figure 35. Mechanism of formation of a Schiff's base, where Ar indicates generic amine groups. [80]

The reaction was allowed to progress for about 15 minutes under magnetic stirring, in a temperature within the range of 4°C to 10°C. At the end of this reaction period, the substrate and the enzyme will result covalently linked through a single stable bond. The biocatalyst solution was then filtered using a Buchner funnel, washed with a generous amount of Milli-Q water and eventually placed in a drier. The described procedure is summarised schematically in *Figure 36.*

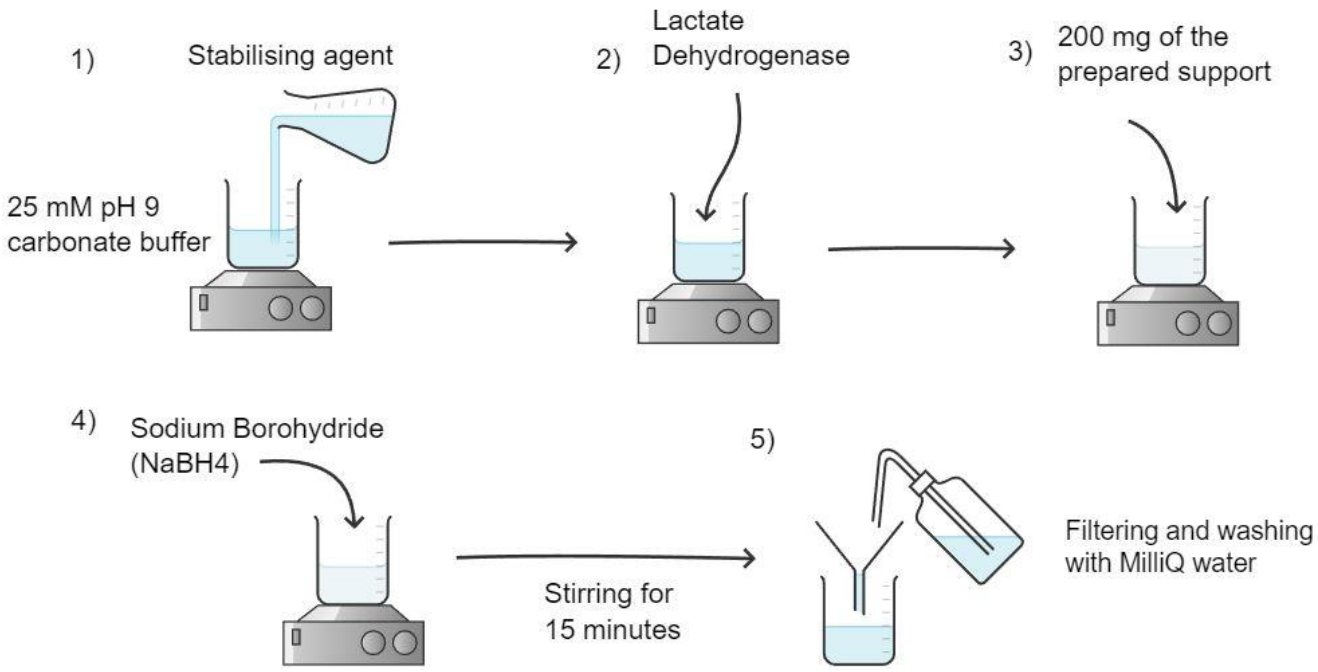

Figure 36. Schematic representation of the procedure followed for the immobilisation of human Lactate Dehydrogenase (LDH) on the previously synthetised mesoporous silica support.

The same procedure was repeated using the different mesoporous silica supports previously described: $MCF_{0.75}$, DPS and $DPS_{0.75}$. For each material, along with the explicated procedure employing trehalose as stabilising agent, PEG was employed. In this second case, 50 ppm of PEG were used for each synthesis process.

2.4.1 Fluorescence Microscopy

Fluorescence microscopy is a powerful imaging technique that relies on the use of fluorophores, particular molecules that are capable of adsorbing light at a certain wavelength and emitting it at a longer one, as a result of the decreased energy of the emitted photons compared to the adsorbed one. This phenomenon, florescence, can be exploited by labelling the molecule of interest with specific fluorophores. By investigating the labelled sample with light at the appropriate wavelength it is possible to detect its emission spectrum and gain information on the sample's distinctive characteristics. [61]

For the present thesis work, fluorescence microscopy was employed to investigate human Lactate Dehydrogenase correct immobilisation on the chosen silica support. For the proper visualisation of the enzyme, it was dyed in accordance with the instructions outlined in the ATTO 550 labelling kit

(Merck). The fluorescent marker used belongs to the rhodamine family and exhibits the optimal excitation at wavelength in the range of 540 to 565 nm, as shown in *Figure 37*. This dye is particularly well-suited for biological applications owing to its strong adsorption to proteins, facilitated by the presence of a succinimidyl ester group. This enables an efficient reaction with the primary amino groups of the analysed protein. Additionally, the chosen dye exhibits good thermal and photochemical stability. [81]

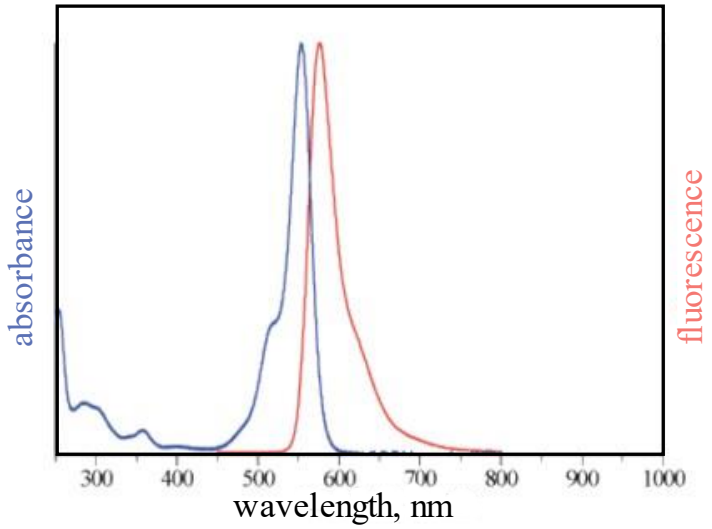

Figure 37. ATTO 550 fluorescent marker absorption and fluorescence spectra. [81]

After creating a dye solution using dimethyl sulfoxide (DMSO), it was introduced in a beaker containing 0.8 mg/mL of LDH, along with a pH 9.5 sodium bicarbonate buffer. The solution was then gently agitated for two hours to enable the bonding between the dye and the enzyme. The whole procedure was conducted in a dark environment to maintain the dye efficiency intact. The fluorescence-labelled enzyme was then filtrated using a gel filtration column, provided in the ATTO 550 labelling kit, which enabled the separation of the residual dye. This procedure was performed only by means of gravity, without applying an external pressure. The so-obtained purified protein was used to synthetise a biocatalyst through immobilisation of the previously mentioned selected support, SBA-$15_{0.25}$.

2.5 Biocatalyst activity

After the biocatalyst was let drying overnight, an activity test was performed, both to evaluate the immobilisation process and to use the activity results as a blank reference for the following inhibition

tests. The enzymatic activity of hLDH-A was measured for its free and immobilized forms. For these analysis, the UV-vis spectrophotometer Jasco V-730 previously used was again employed at a wavelength of 340 nm. In fact, Lactate Dehydrogenase catalytically converts the coenzyme NADH into NAD^+, along with the conversion of pyruvate into lactate and, since NADH absorbs at 340nm, LDH activity was measured indirectly through the monitoring of NADH concentration, which will decrease during the catalytic reaction. [6] The reaction was monitored for a total of 60 seconds, and successively, the absorbance variation was calculated over this time frame. This variation was then correlated to the biocatalyst activity using the following equation.

$$A_{IE} = \frac{m}{\varepsilon \cdot L} \cdot \frac{V_c}{V_e} \cdot \frac{1}{C_p} \quad \left[\frac{\mu Mole}{min \cdot mg}\right] \qquad \textit{Equation 14}$$

- A_{IE}, immobilized enzyme activity
- $m = \frac{dAds}{dt}$, adsorbance variation during the assay (min^{-1})
- ε, molar extinction coefficient (6.22 $mM^{-1}cm^{-1}$)
- L, optical path (1 cm)
- V_c, total volume present in the analysed cuvette (3 mL)
- V_e, volume containing the protein suspension (100 µL)
- C_p, concentration of the suspension of the immobilized enzyme (0.02 g/mL)

The enzymatic activity is expressed in International Units (IU) and represents the amount of enzyme required to catalyse the transformation of 1 µMole of substrate per gram of biocatalyst per unit of time, under specific conditions of temperature, pH, and substrate concentration. The free enzyme activity and the biocatalyst activity will therefore be reported as IU mg_{prot}^{-1} and IU g_{sup}^{-1} respectively.

Each test was performed adding 2.7 ml of pH 7.5 0.1 M phosphate buffer, 100 µL of a 7 mM NADH solution and 100 µL of a 49 mM pyruvate solution to a cuvette. The resulting solution was used as a blank measurement for the spectrophotometer. 20 mg of dry biocatalyst were then added to 1 ml of the previously used buffer solution and mixed vigorously with a vortex.

After adding 100 µL of the prepared suspension to the measuring cuvette, the activity test was carried out at 340 nm, at room temperature, in 'Time Course' mode. Each analysis was performed placing a magnetic stirred at the bottom of every cuvette, in order to prevent the biocatalyst suspension from settling.

The same analysis was implemented on the free form of the enzyme, adding to the NADH, pyruvate and pH 7.5 0.1 M phosphate buffer solution 100 µL of a free LDH solution at 0.1 mg/mL concentration. The downside of the immobilisation process is the partial loss of activity of the enzyme, meaning that the measured A_{IE} will result lower than A_{FE}. To be able to correlate the activities measured for the biocatalyst with the activity of the free enzyme, and compare different immobilisations, the so-called Relative activity was calculated.

$$R_{act} = \frac{A_{IE}}{q \cdot A_{FE}} \cdot 100 \qquad \textit{Equation 15}$$

Where:

- R_{act}, retained relative enzymatic activity (%)
- A_{IE}, immobilised enzyme activity
- A_{FE}, free enzyme activity
- q, enzymatic loading

2.6 Lactate Dehydrogenase inhibition

2.6.1 Lactate Dehydrogenase inactivation via incubation with denaturation agents

As previously mentioned, one of the aims of enzyme immobilisation is to stabilise the protein against harsh environmental condition and presence of inhibitors. To assess the actual effectiveness of the immobilisation strategies against Lactate Dehydrogenase inactivation, enzyme stability tests were conducted using different condition of pH and organic solvent content.

Enzyme inactivation in ethanol

Each test was performed adding 2.7 ml of pH 7.5 0.1 M phosphate buffer, 100 µL of a 7 mM NADH solution and 100 µL of a 49 mM pyruvate solution to a cuvette. The enzyme was incubated in a pH 7.5 0.1 M buffer solution, containing 30% of ethanol (CH_3CH_2OH), according to the assay performed by Jackson et. al [26]. The final enzyme concentration was 0.01 mg/mL. 100 µL of the LDH solution were added at set times to the tested cuvette, while 100 µL of the buffer ethanol solution were added to the cuvette used for the blank measurements. The free enzyme inhibition was monitored spectrophotometrically, measuring the concentration of the coenzyme NADH at 340 nm during the catalytic reaction. Three measurements were performed in the first five minutes from the introduction

of the enzyme in the buffer ethanol solution, while the other essays were performed at fixed times, each 10 or 15 minutes.

Enzyme inactivation in alkaline pH

The inactivation assay was performed in the same way as described in the previous paragraph, but in this case, the enzyme was incubated in 1 mL of pH 10 0.1 M carbonate buffer, instead of in a buffer-ethanol solution. Similarly, the final enzyme concentration was 0.01 mg/mL. 100 µL of the LDH solution were added at set times to the tested cuvette, where 2.7 ml of pH 7.5 0.1 M phosphate buffer, 100 µL of a 7 mM NADH solution and 100 µL of a 49 mM pyruvate solution have previously been added. For the cuvette used for the blank measurements, 100 µL of pH 10 0.1 M buffer were added instead of the free enzyme solution.

Biocatalyst inactivation in ethanol

The procedure employed for the free lactate dehydrogenase inhibition assays was replicated for tests involving the immobilized enzyme. Identical concentrations of organic solvent and incubation times were applied. Additionally, all UV-Vis spectrophotometric analyses were conducted with a magnetic stirrer positioned at the base of each cuvette to ensure continuous suspension of the biocatalyst powder.

Biocatalyst inactivation in alkaline pH

In the case of the immobilised LDH, the inhibition test was performed similarly, using a pH 10 0.1 M carbonate buffer, in which the biocatalyst was incubated before being collected for the spectrophotometric analysis. The analysis was operated measuring the optical absorbance of NADH at 340 nm, both with ethanol and with alkaline buffer.

For each test, the residual activities were calculated, in order to be able to evaluate the enhanced resistance of immobilised enzyme to harsh environmental condition, compared to the one exhibited by free enzyme in the same denaturising conditions. The residual activity was calculated as a percentage of the enzyme activities previously evaluated for the free and immobilised form of Lactate Dehydrogenase. The activities were evaluated as described in paragraph 2.5. For each inhibition assay, the following equation was employed:

$$Residual\ Activity\ (\%) = \frac{A_{LDH\ inhibited}}{A_{LDH}} \cdot 100 \qquad \textit{Equation 16}$$

2.6.2 Lactate Dehydrogenase inhibition with NHI-2

LDH inhibition was parallelly tested in presence and in absence of the anticancer drug NHI-2, at varying concentration of pyruvate, the reaction substrate, and NADH, the LDH coenzyme. NHI-2, N-hydroxyindole (NHI)-based LDH-A inhibitor, depicted in the image below, is known to be a competitive inhibitor against pyruvate and NADH. [82], [83] NHI-based compounds are being intensively investigated due to their simple syntheses, their selective toxicity toward tumoral cells and their proven in vitro and cell culture efficacy. [16]

Other possible LDH inhibitors, not employed in this thesis work, are FX-11 (2,3-dihydroxy-1-naphthoic acid derivative) and galloflavin. [84]

To obtain a comprehensive evaluation of the inhibition kinetic, the test was performed on both free LDH and the immobilized enzyme. An in depth understanding of the biocatalyst resistance against NHI-2 inhibition is fundamental for its application in a biosensor device for anticancer drug testing. Each test was repeated three times and results were presented in terms of the average value.

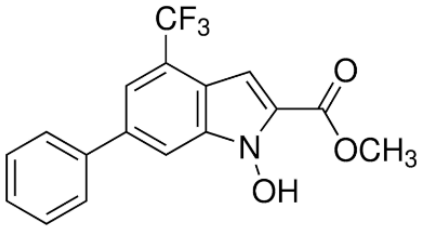

Figure 38. NHI-2 molecule, from Sigma Aldrich.

Enzyme inhibition using NHI-2

To assess the efficacy of the anticancer drug under non-ideal conditions, the free enzyme activity was examined in the presence and absence of the inhibitor, while varying the concentrations of pyruvate and coenzyme. Specifically, different pyruvate concentrations were investigated, ranging from 1 mM to 0.05 mM (final pyruvate concentration in the cuvette), while keeping the NADH concentration constant at 0.232 mM, consistent with the previous inhibition tests.

Regarding assays involving varying NADH concentrations, a narrower range of concentrations was employed. The highest NADH concentration tested was 0.4 mM, as higher levels of coenzyme led to signal saturation in the instrument. Similarly, for this set of experiments, each assessment was conducted both in the presence and absence of the competitive inhibitor NHI-2, while maintaining pyruvate concentration fixed at 1.62 mM.

Each inhibition test was conducted in a spectrophotometer operating in 'Time Course' mode, set at 340 nm. The enzyme activity was assessed by adding 100 µL of a pH 7.5, 1 M phosphate buffer containing 0.01 mg/mL of free LDH to a cuvette. This cuvette also contained 2.7 mL of 0.1 M phosphate buffer pH 7.5, 100 µL of the selected concentration of NADH, 100 µL of the selected concentration of pyruvate, and 20 µL of a 3.02 mM NHI-2 solution in Dimethylsulfoxide (DMSO). The selected concentration of NHI-2, which was used for all inhibition tests, had been optimized in prior studies here not reported for the sake of brevity. Subsequently, the enzyme activity was once again determined using the aforementioned *Equation 14*.

Biocatalyst inhibition using NHI-2

The procedure and concentration employed for inhibiting the free enzyme with NHI-2 were replicated for the biocatalyst assay. However, instead of utilizing 100 µL of a pH 7.5, 1 M phosphate buffer containing 0.01 mg/mL of free LDH, 100 µL were taken from a suspension of 20 mg of dried biocatalyst mixed in 1 mL of phosphate buffer. All the spectrophotometric tests were carried out using a magnetic stirred, to prevent the settling of the suspension, as for the previously described inhibition test using the immobilised enzyme.

For each experiment conducted, while varying the pyruvate concentration and measuring the reaction rate, the experimental data were described using the Michaelis-Menten (MM) equation. The calculation of the kinetic parameters present in MM formula, was enabled by the use of the linearisation method explained in section 1.6, Lineweaver-Burk or Hanes plot.

3. Results and discussion

3.1 Aldehydic and amino groups quantification results

The concentration of aldehydic and amino functional groups presents on the support surface was quantified as described in section 2.2.1 and 2.2.2 and expressed in mmol per gram of silica support, for each material studied: SBA-$15_{0.25}$, $MCF_{0.75}$, DPS and $DPS_{0.75}$.

The concentration of aldehydic and amino group on the support surface is an important indicator of the efficaciousness of the functionalisation technique. Moreover, a high quantity of functionalisation group is fundamental for the subsequent immobilisation step, during which the enzyme will be able to form a considerable amount of bonds with the successfully functionalised support surface. Glyoxylic group have been identified as highly reactive with primary amino groups, homogeneously present of LDH surface, as demonstrated in Chapter 4. The high concentration of glyoxylic groups can lead to the strong attachment of the protein on the support, hence increasing its resistance to denaturation when exposed to harsh reaction conditions. Amino groups, on the other hand, play an important role in the physical adsorption of the enzyme on the silica material surface, enhancing its stability. [2] The obtained concentrations are reported in *Table 1* for each studied mesoporous silica support.

Table 1. Aldehydic and amino groups quantification results

Support	**SBA-$15_{0.25}$**	**$MCF_{0.75}$**	**DPS**	**$DPS_{0.75}$**
Aldehydic group (mmol /g)	1.013	0.691	1.190	1.085
Amino groups (mmol /g)	1.297	1.550	1.090	0.790

Given the fact that the two organosilanes used in the functionalisation process, APTES and GPTMS, were employed in the same concentration, the final concentration of glyoxylic and amino groups on each silica surface was expected to be similar. The results show that the two functionalisation groups are present in the same order of magnitude for every synthetised support. The more pronounced difference found for the $MCF_{0.75}$ and $DPS_{0.75}$ samples is to be researched in their three-dimensional conformation and in the uneven distribution of the organosilanes during the support functionalisation.

3.2 Immobilisation Results

As mentioned in section 2.4, while performing each immobilisation process, three different solutions were simultaneously monitored: the free enzyme, the enzyme-support suspension, and the supernatant of the centrifugated solution. For each solution the activity was measure in order to track the undergoing immobilisation. The results of said measurement are presented in *Figure 39* for the SBA-$15_{0.25}$ sample.

As expected, the supernatant solution decreased its activity over time, while also starting from a low relative activity (43,36 %). This is due to the fact that, being the supernatant the solution that was separated from the support on which the immobilisation process undergoes, it contained free active Lactate Dehydrogenase. With the progress of the covalent binding of the enzyme on the support surface, the concentration of LDH in the immobilisation solution decreases, resulting in a decreased of the supernatant activity. To verify that this decrease in activity was not linked with the denaturation of the enzyme itself, free LDH activity was also tested.

The free enzyme activity, tested concurrently under the immobilisation conditions, exhibited an oscillatory trend. This phenomenon can be a consequence of the low temperature, between 4 and 10 °C, at which the enzyme solution was kept during the activity tests. In fact, at temperatures outside LDH optimal range, deactivation inhibition is possible.

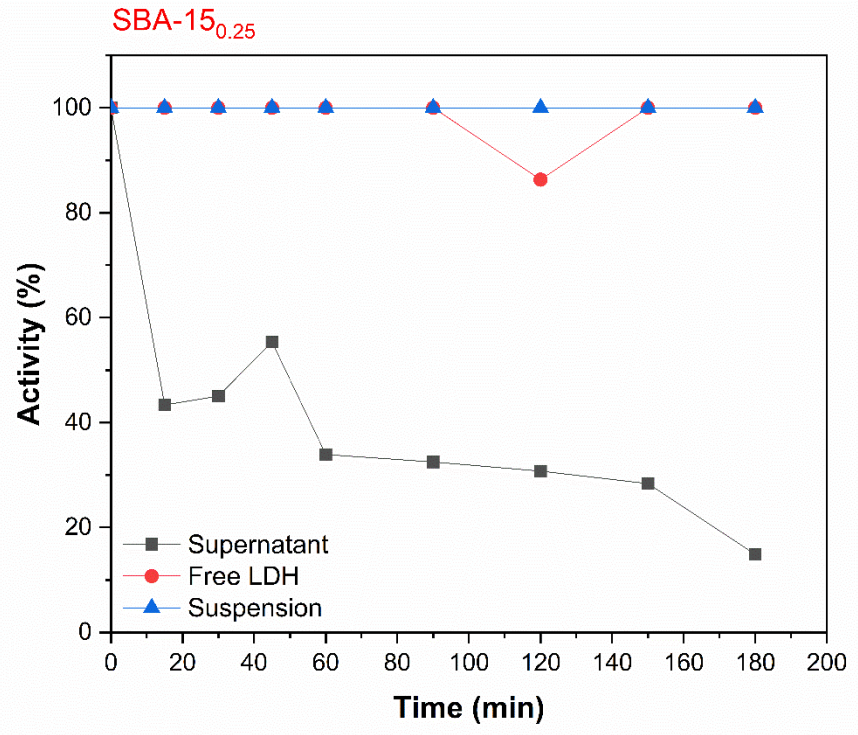

Figure 39. Free enzyme, suspension, and supernatant relative activity during LDH immobilisation process on SBA-$15_{0.25}$ sample, using trehalose as stabilising agent.

Table 2 presents the values of immobilization percentage (I%) and Retained activity calculated for each silica support employed in the immobilisation process, using the formulas presented previously.

It is easily noticeable that the Retained activities of all analysed biocatalysts are below 15%, indicating a decrease in activity after the enzyme immobilisation. This phenomenon was foreseeable, as generally the formation of covalent bonds between the protein and the support can lead to the partial alteration of the protein structure. The modification of the enzyme's three-dimensional structure may result into a reduction in its activity and a modification of its active sites. The immobilisation process can alter the possibility of the enzyme to slightly change its conformation, a fundamental characteristic for correct binding to the substrate. The blockage of the protein in the support pores may result in the LDH becoming more rigid and unable to perfectly bind to pyruvate, with a subsequent decrease in activity.

Additionally, if sodium borohydride ($NaBH_4$) is used in large quantities during the immobilization process, to reduce Schiff bonds, it can cause unwanted denaturation. Moreover, it is commonly known that the immobilisation of a molecule in the pores of a chosen support can lead to mass-transfer resistance phenomenon. The localisation of the LDH inside the support structure can in fact limit the diffusion of the substrate and the cofactor to its active sites, hampering the reaction rate. [85]

Table 2. Immobilisation percentage, Residual retained activity and activity of the immobilised LDH samples, on different silica supports, with two different stabilising agents, PEG and Trehalose.

Sample	**I (%)**	**R_{act} (%)**	**A_{IE}**
SBA-15$_{0.25}$-PEG	97.97	2.64	10.11 ± 6.03
SBA-150.25-TREA	85.13	14.4	62.42 ± 13.5
MCF$_{0.75}$-PEG	89.24	1.85	7.08 ± 0.08
MCF$_{0.75}$-TREA	81.07	2.05	7.85 ± 2.47
DPS-PEG	99.05	1.47	5.64 ± 1.12
DPS-TREA	98.76	6.77	25.96 ± 7.04
DPS$_{0.75}$-PEG	97.97	3.94	15.13 ± 1.76
DPS$_{0.75}$-TREA	98.56	1.68	6.42 ± 1.02

All the presented activity results are reported in IU g_{sup}^{-1}. The average rates were then used to calculate the relative residual activity, through *Equation 15*. It is easily noticeable how the results obtained via LDH immobilisation using trehalose instead of PEG are generally superior.

It is also interesting to notice how the lower activity results measured for the Mesocellular Foam silica, compared to $SBA\text{-}15_{0.25}$, even if the two samples share a very similar synthesis process and surface morphology. This phenomenon could be explained thanks to the results of Surface area and Porosimetric analysis in section 3.3.3. It is in fact reported that the $MCF_{0.75}$ sample presents a higher pore volume and average pore diameter compared to $SBA\text{-}15_{0.25}$. This could result in enzyme leaching from its porosities, and hence in the lower biocatalyst activity.

From this comprehensive study of two different immobilisation process (with PEG or trehalose as stabilising agent) on four different mesoporous silica supports, it can be assumed that the immobilisation of LDH on the $SBA\text{-}15_{0.25}$ sample using trehalose leads to the best activity results. This sample is considered as the best candidate for Lactate Dehydrogenase immobilisation for a biosensor application and it was therefore employed in the following inhibition tests, presented in the final part of the present thesis work.

3.3 Support Characterisation results

This section collects all the results found regarding the characterisation of the mesoporous materials employed, through the use of the different analytical methods described in section 2.3.

3.3.1 Fourier-Transform Infrared Spectroscopy (FTIR) results

Four different mesoposous silica supports were analysed using Fourier-Transform Infrared Spectroscopy: SBA-$15_{0.25}$, $MCF_{0.75}$, DPS and $DPS_{0.75}$. Each material was observed in its non-functionalised form, after hetero functionalisation with APTES and GPTMS and finally after immobilisation of Lactate Dehydrogenase on its surface. For every biocatalyst, two immobilisation mechanisms were investigated. In particular, two different stabilising agents were employed: trehalose and PEG (polyethylene glycol). Each sample was pressed in a wafer shape before being analysed at ambient temperature, at varying decreasing pressures. The minimum pressure reached varies between the different samples, from 0.007 to 0.005 mbar. However, each low pressure reached enabled the desorption of all adsorbed gasses and water vapour from the support's surfaces. This procedure is essential for a correct analysis of the samples. All the presented spectra were normalised using the calculated superficial density of the corresponding wafer and smoothed using the Savitsky-Golay method implemented by Origin.

It is worth noting that in each spectrum corresponding to a non-functionalized (NF) sample (always depicted in black on the presented graphs), there is a distinct peak at approximately 3740 cm^{-1}, which is indicative of isolated silanols. Additionally, multiple peaks in the range of 3665-3375 cm^{-1} can be identified in the non-functionalized spectra shown, attributed to the stretching of Si-OH hydroxyl groups. These groups define the surface properties of silica materials and play a crucial role in the following support functionalization. This accounts for the absence of the mentioned peaks in the spectra relative to the materials functionalized with APTES and GPTMS molecules, as well as in those of the analysed biocatalysts. [4]

When comparing the spectra relative to the non-functionalised materials and the functionalised ones (both with and without immobilised enzyme) it is possible to notice a distinguished peak at wavelengths in the range of 2930 and 2880 cm^{-1}. This peak is relative to the presence of -CH, typical of the organosilanes molecules used: APTES and GPTMS. It is however true that the non-complete removal of the used template during the calcination process may results in the presence on the sample of residual carbon chain. This phenomenon is detected in non-functionalised samples by peaks of

different intensities in the wavelength range of 2900-2850 cm^{-1}. These peaks always appear less pronounced compared to the ones that originate from the functionalisation process and present a characteristic trident-like shape.

Another interesting difference depicted in the analysed spectra is the presence of pronounced peaks at wavelengths around 1665 cm^{-1}. These peaks can be seen in the spectra relative to the functionalised material and those of the biocatalysts and are correlated to the bending of -NH groups. [86]

To facilitate the identification of the previously cited peaks, a magnification of the wavelenghts reagion included between 4000 and 2500 cm^{-1} is presented for each analysed support. An additional magnification of the region between 2150 and 1350 cm^{-1} is proposed, with the aim to better highlight the difference between the spectrum of the functionalised support and the ones where Lactate Dehydrogenase has been immobilised. In this part of the spectrum, in fact, it is possible to notice two interesting peaks. At around 1600 cm^{-1} the two spectra collected for the biocatalyst present a shoulder, indicating the presence of the protein (amide bands). This characteristic shoulder rise from the immobilisation process and it is therefore not present in the functionalised and non-functionalised spectra.

Another particular feature of the biocatalyst spectra is the absence of the shoulder indicated between 1720 and 1710 cm^{-1}. This peak is identified in literature as corresponding to C=O bonds, present in this study case on the surface of functionalised materials as glyoxylic groups, formed from the subsequent reaction of GPTMS molecules. [86]

The absence of this signal in the spectra collected for the biocatalysts can indicate that the C=O group is involved in the formation of covalent bonds between carbonyl groups of the support surface and the $-NH_2$ groups of the protein.

For each of the analysed spectra, the curves represented in the second magnification, from 2150 to 1350 cm^{-1}, have been multiplied by an adequate constant, so that they overlap at wavenumber at around 1650 cm^{-1}. This manipulation allows for a clearer observation of the two cited peaks at around 1710 and 1600 cm^{-1}, that are of great importance for the present analysis.

For a further clarification of this important region of the analysed FTIR spectra, the signal of each functionalised material was subtracted from the spectra relative the synthetised biocatalysts, both immobilised using trehalose and PEG. In every image presented, the wavenumber at which the latter normalisation has been performed, is highlighted with an arrow. At the end of the paragraph, *Table 3* summarise the cited spectra regions and the corresponding assigned functional groups.

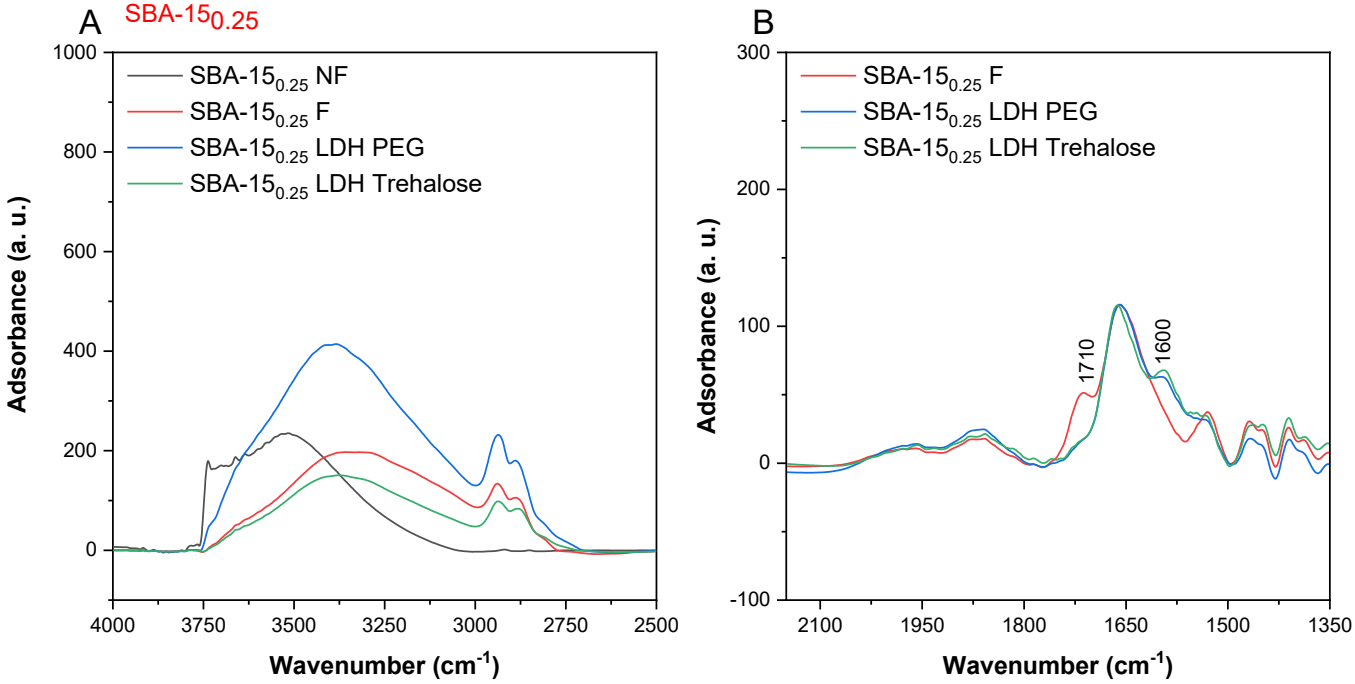

Figure 40. FTIR spectra of SBA-15$_{0.25}$: non-functionalised, functionalised with APTES and GPTMS and of the final biocatalyst, with the enzyme immobilised using PEG or Trehalose as a stabilising agent.

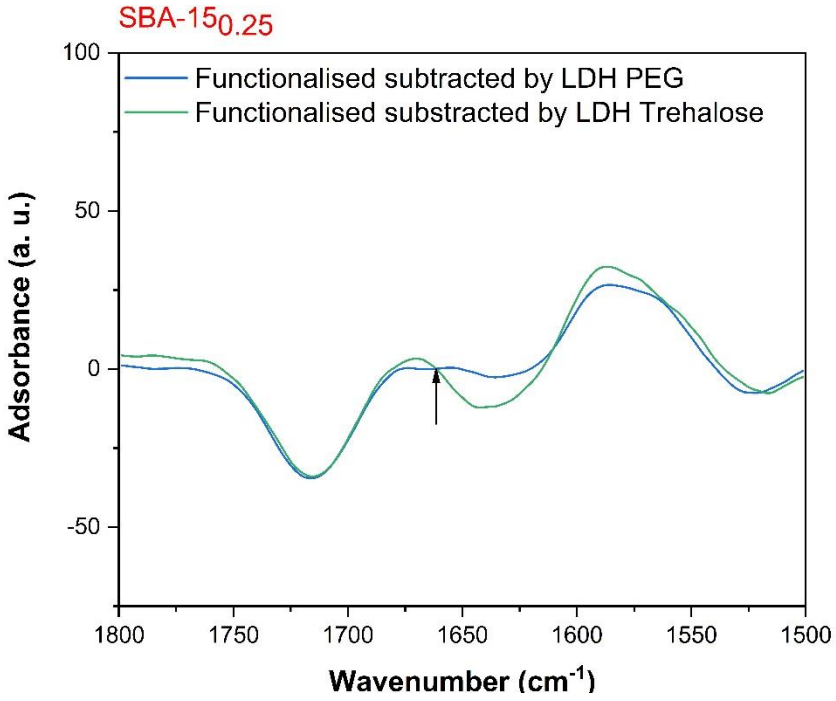

Figure 41. FTIR spectra of LDH immobilised on SBA-15$_{0.25}$ using PEG or Trehalose, to which the spectra of the functionalised support have been subtracted.

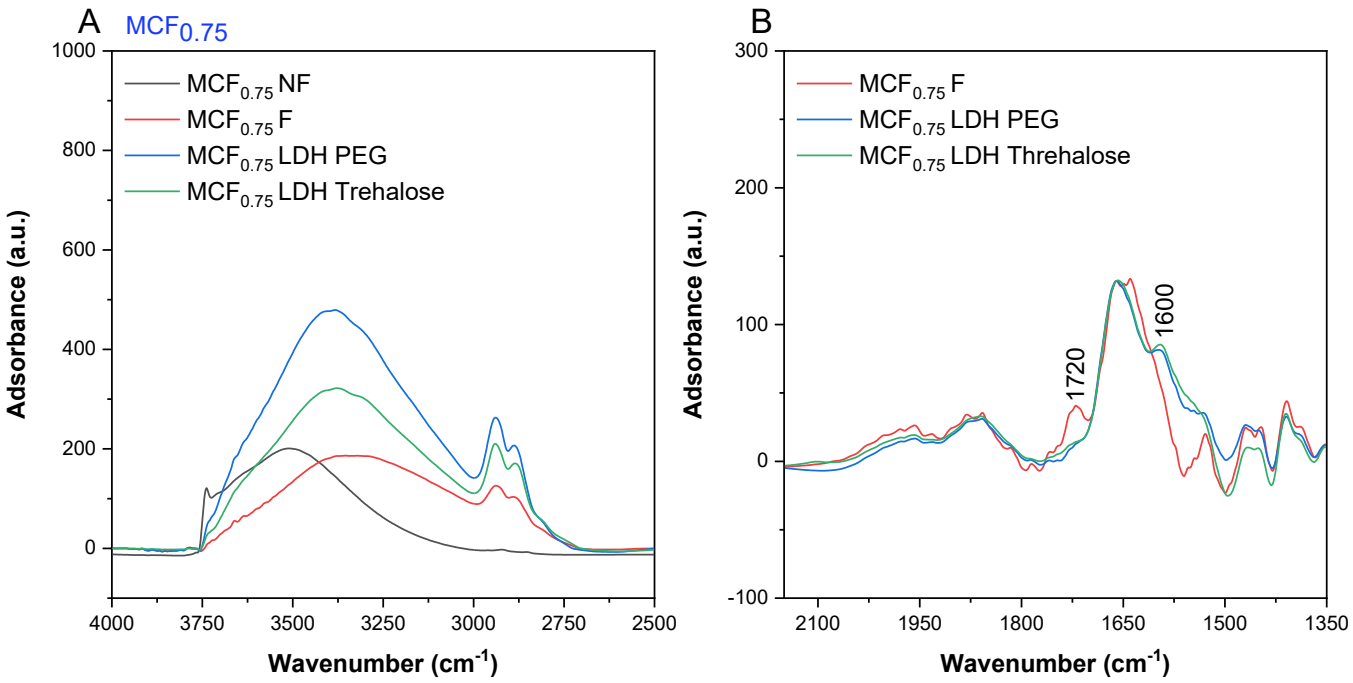

Figure 42. FTIR spectra of Mesocellular Foam silica: non-functionalised, functionalised with APTES and GPTMS and of the final biocatalyst, with the enzyme immobilised using PEG or Trehalose as a stabilising agent.

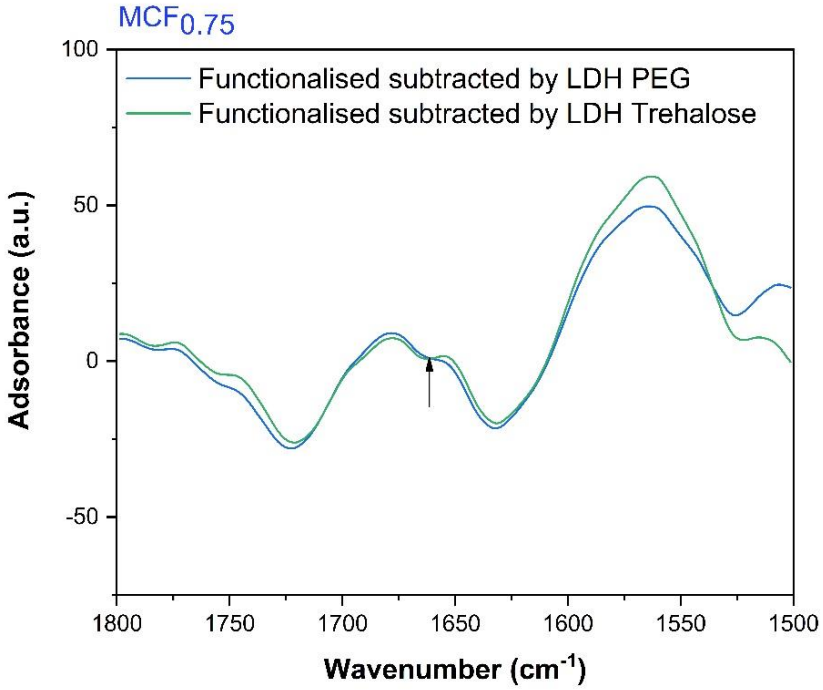

Figure 43. FTIR spectra of LDH immobilised on $MCF_{0.75}$ using PEG or Trehalose, to which the spectra of the functionalised support have been subtracted.

It is possible to notice that the peaks described previously for the SBA-$15_{0.25}$ samples can also be detected on the spectra obtained for the other mesoporous supports. Notably, what differentiate the four silica materials is the region located between 1300 and 500 cm^{-1}, in the so-called fingerprint region, which is relative to the asymmetric stretching modes of the Si–O–Si and the presence of Si–OH functional groups. This wavenumber range is not correlated with the functionalisation or immobilisation processes, and it is therefore not shown.

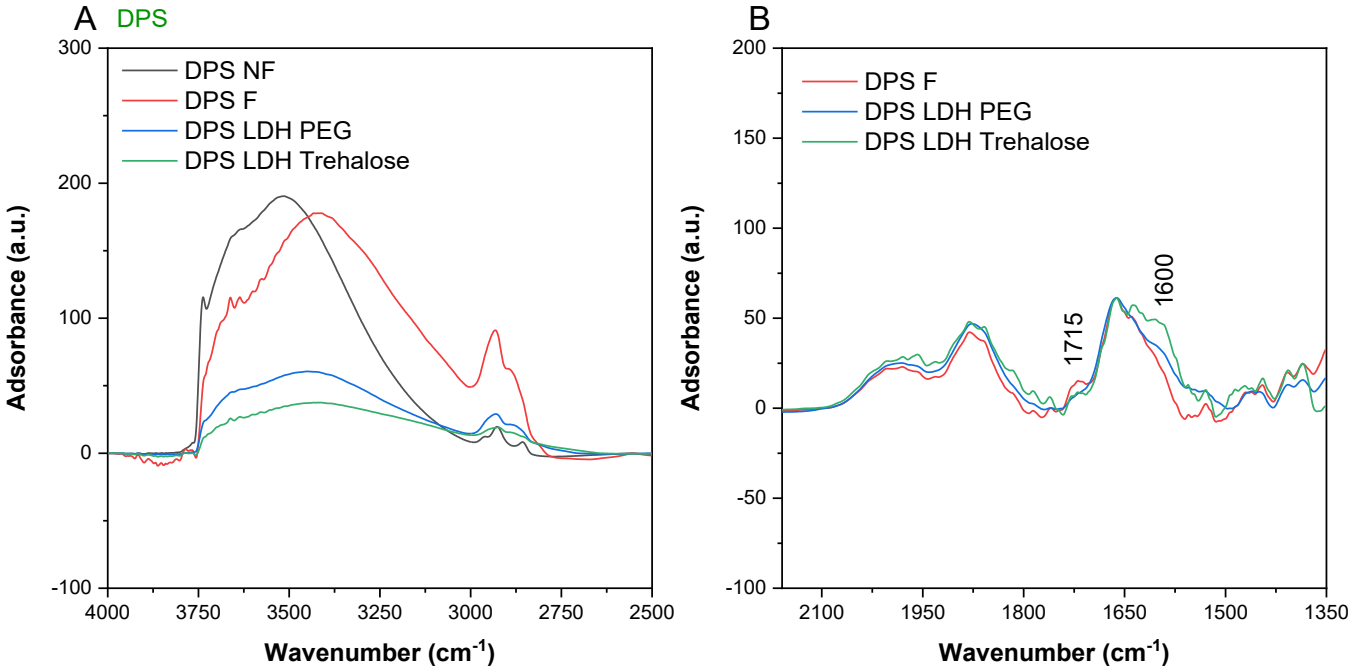

Figure 45. FTIR spectra of Dendritic porous silica: non-functionalised, functionalised with APTES and GPTMS and of the final biocatalyst, with the enzyme immobilised using PEG or Trehalose as a stabilising agent.

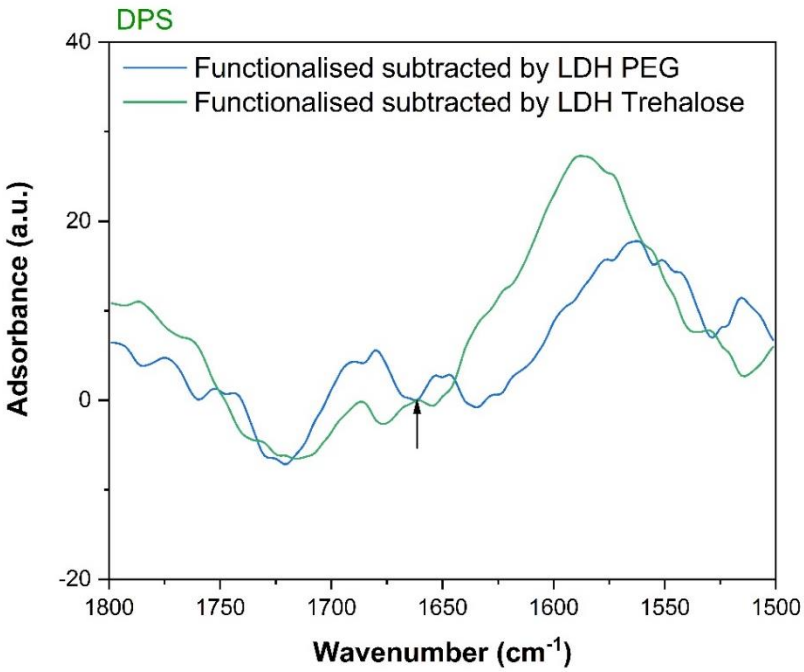

Figure 44. FTIR spectra of LDH immobilised on DPS using PEG or Trehalose, to which the spectra of the functionalised support have been subtracted.

In graph *Figure 45* (B), relative to the DPS sample, it can be noted that, differently from what has been highlighted for the other studied supports, the spectrum obtained for the biocatalyst synthetised using trehalose, presents a peak at around 1700 cm^{-1}. This peak, which is also observed in the spectrum of the functionalised support, was correlated to the presence of C=O functional group. The presence of this peak therefore indicates that the organosilanes group C=O was not completely involved in the formation of covalent bonds with the enzyme and hence emits a detectable signal. This is not the case for the biocatalyst formed via immobilisation with PEG, whose spectrum does not present the mentioned signal. The non complete utilisation of the cited reactive functional group in the case of immobilisation with trehalose on DPS support however, does not interfere with the biocatalyst activity. In fact, it had been shown that the residual retained activity for this immobilised enzyme is higher than the one calculated for the DPS-PEG immobilisation. This could be explained by the fact that, in the case of DPS, the C=O groups that bind the enzyme in the case of PEG, could be too concentrated on the support surface, leading to a too strong interaction with the protein. As already mentioned, the too intense interaction with the enzyme could result in its rigidification and hamper its catalytic activity.

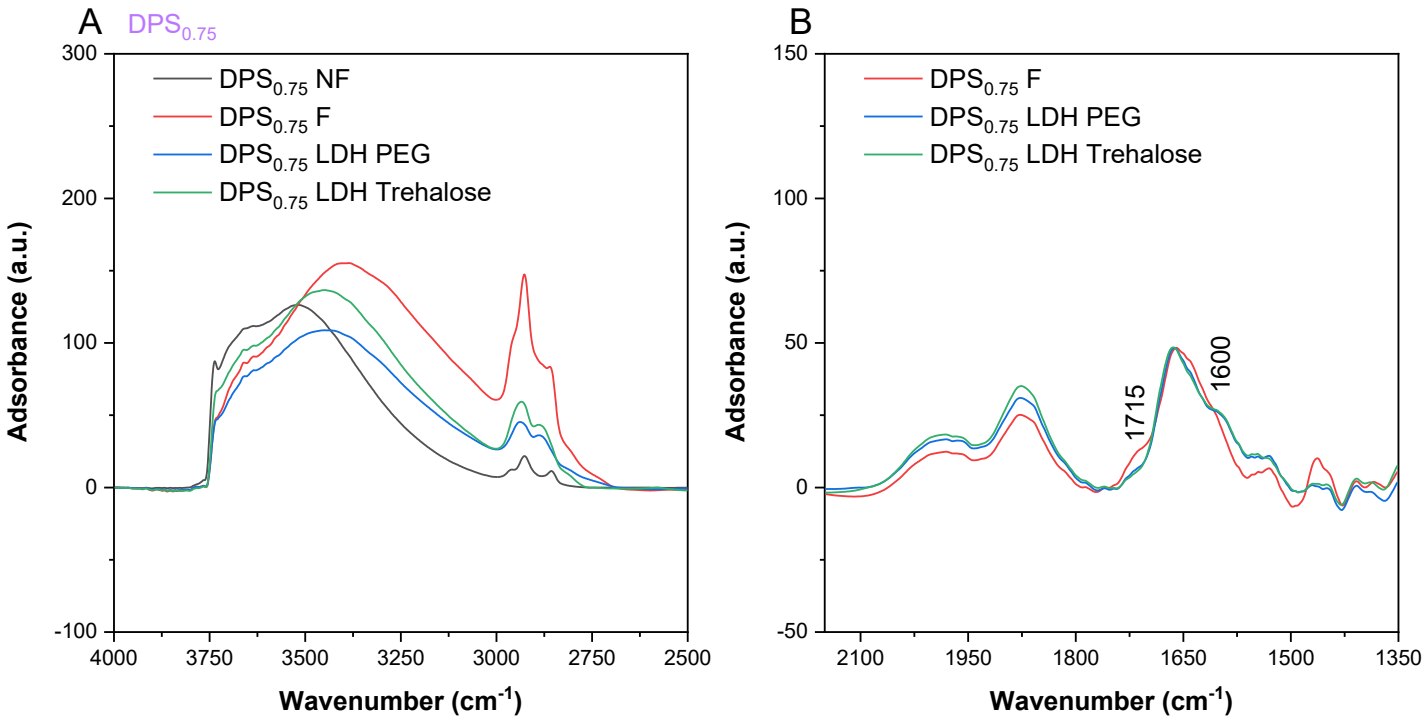

Figure 46. FTIR spectra of Dendritic porous silica ($DPS_{0.75}$): non-functionalised, functionalised with APTES and GPTMS and of the final biocatalyst, with the enzyme immobilised using PEG or Trehalose as a stabilising agent.

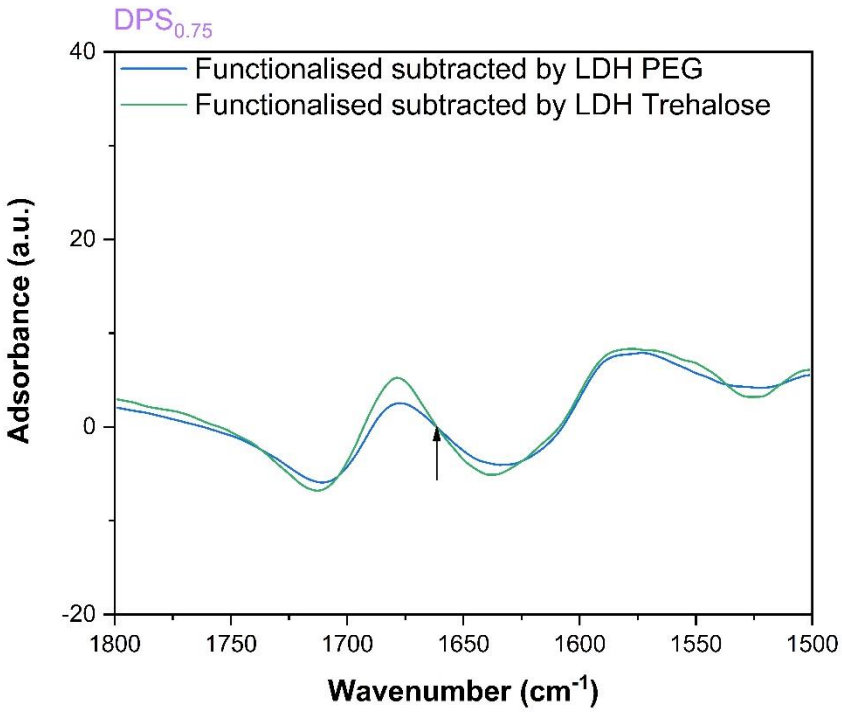

Figure 47. FTIR spectra of LDH immobilised on $DPS_{0.75}$ using PEG or Trehalose, to which the spectra of the functionalised support have been subtracted.

From the analysis of the subtracted spectra displayed for every support sample, it is possible to notice that the peak found at around 1600 cm^{-1}, identified from literature as corresponding to the presence of the immobilised enzyme, is more intense when related to the immobilised sample obtained using trehalose as stabilising agent. This qualitative analysis may indicate that the employment of trehalose instead of PEG result in an increased amount of final immobilised enzyme on the support surface. This observation is in accordance with the experimental activity results presented in section 3.2, which highlighted an increased biocatalyst activity of the samples synthetised using trehalose.

Table 3. Assigned wavelength of the FTIR spectra of the analysed samples

Wavenumber (cm^{-1})	**Vibrational features**
from 3700 to 3200 cm^{-1}	stretching mode of hydrogen in Si–OH groups
2930 $cm^{-1}$and 2880 cm^{-1}	stretching modes of CH
2250 cm^{-1}	O–Si–H
2100 cm^{-1}	Si–Si–H
Around 1710 cm^{-1}	C=O
1641 cm^{-1}	N–H scissoring bending
1600 cm^{-1} and 1484 cm^{-1}	NH_2 deformation modes of the amine groups
1130 $cm^{-1}$and 1044 cm^{-1}	asymmetric stretching modes of the Si–O–Si
795 cm^{-1} and 1177 cm^{-1}	Si–OH functional group

3.3.2 Field emission scanning electron microscopy (FE-SEM) results

In this section are presented the obtained FE-SEM images relative to the four analysed samples: SBA-$15_{0.25}$, $MCF_{0.75}$, DPS and $DPS_{0.75}$. For each material, two different magnifications are presented, a first one at 10.000x and a second one at 200.000x. All the samples were analysed in their non-functionalised form.

It is particularly clear from the images reported in *Figure 50* and *Figure 51* that DPS and $DPS_{0.75}$ present a very similar structure when observed at a lower magnification value. However, the second magnification demonstrates that the use of a higher ratio of swelling agent during the synthesis process leads to considerably larger support aggregates. In particular, the employment of a swelling agent template ratio of 0.75 results in a final support with aggregates almost 10 times larger than the DPS non-modified sample. The FE-SEM image of *Figure 50* in particular, clearly highlights the three-dimensional ramified structure typical of dendritic fibrous nanosilica, shown schematically in the introductive part of this work.

As for the two DPS sample previously described, what differentiate the analysed SBA-$15_{0.25}$ and $MCF_{0.75}$ samples is the ratio between the sweeling agent and the template using during the support synthesis. This reflects on the morphology of the supports, observed via field emission scanning electron microscopy. More specifically, it is possible to notice that the two mentioned samples present a similar structure, especially when comparing the images at 10.000x. Nonetheless, the higher reagent ratio used for the synthesis of $MCF_{0.75}$ is evident from the sample larger pores and aggregates when compared to the SBA-$15_{0.25}$ structure.

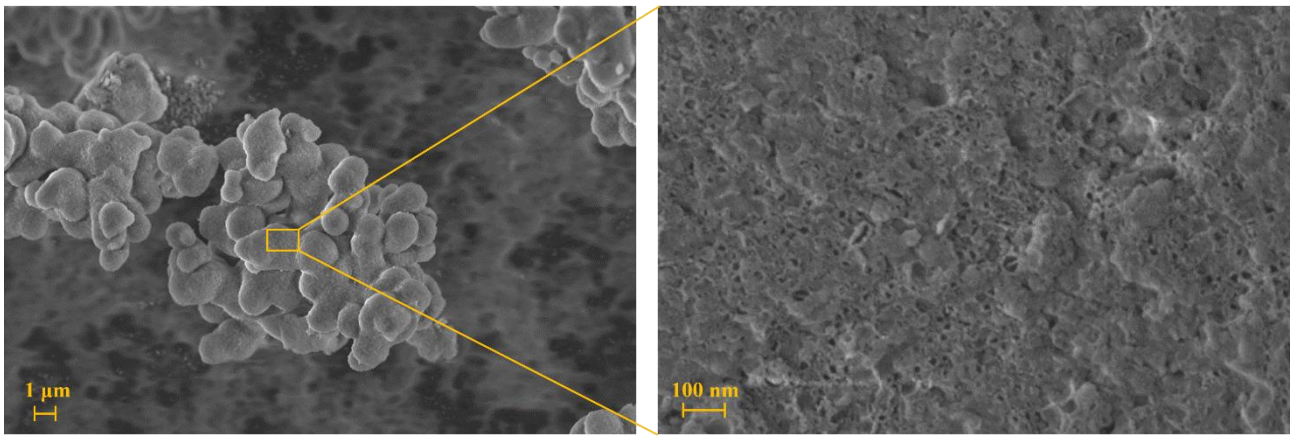

Figure 48. FE-SEM images of SBA-15 sample, metallised with platinum. Magnification: 10.000x on the left and 200.000x on the right. ETH: 3 kV

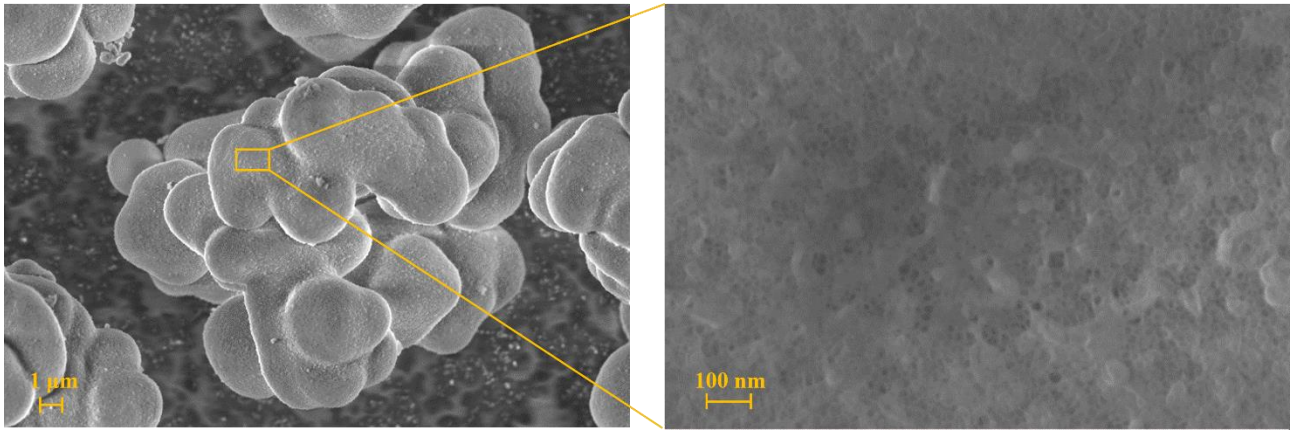

Figure 49. FE-SEM images of $MCF_{0.75}$ sample, metallised with platinum. Magnification: 10.000x on the left and 200.000x on the right. ETH: 3 kV

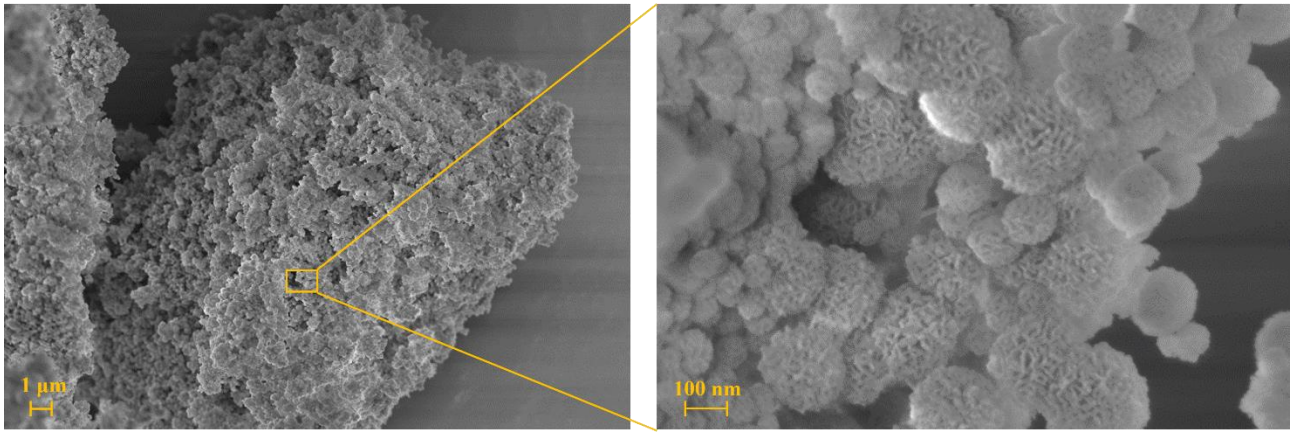

Figure 50. FE-SEM images of DPS sample, metallised with platinum. Magnification: 10.000x on the left and 200.000x on the right. ETH: 3 kV

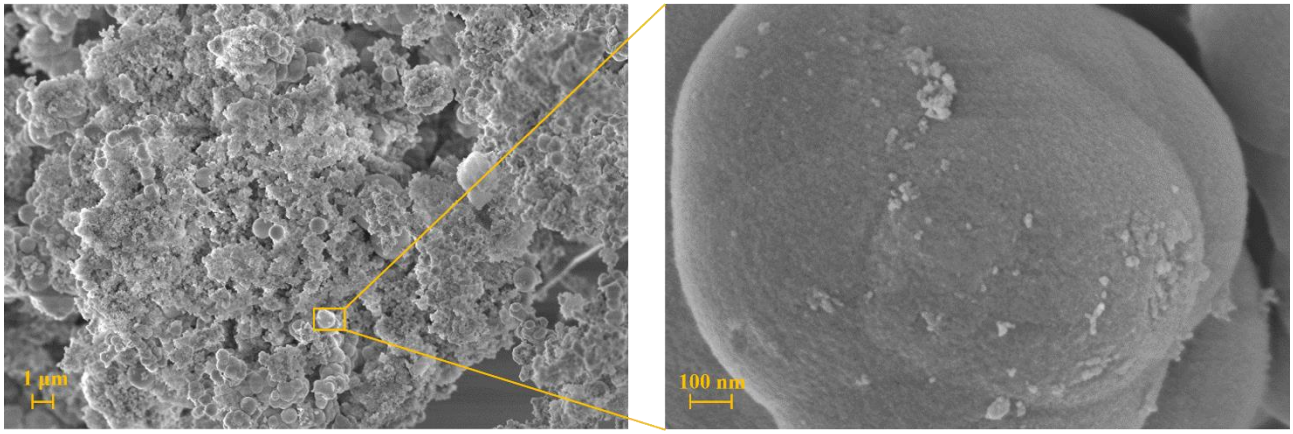

Figure 51. FE-SEM images of $DPS_{0.75}$ sample, metallised with platinum. Magnification: 10.000x on the left and 200.000x on the right. ETH: 3 kV

3.3.3 Surface area and Porosimetric analysis results

Table 4 shows the results of the nitrogen physisorption analysis for the four silica samples chosen. Each material was studied both in its hetero functionalised and non-functionalised form. The data concerning the specific surface area (S_{BET}) were calculated using the BET model equation (Brunauer-Emmett-Teller) previously described, while the cumulative pore volume (V_p) and the mean pore diameter (D_p) were evaluated using the BJH method (Barrett-Joyner-Halenda), which relies on the formerly specified Kevin equation. It can be easily observed that the hetero functionalisation process resulted in the decrease of the observed values for S_{BET} and V_p, in all cases. It is also evident that this decrease in volume was more pronounced in $MCF_{0.75}$ and $SBA\text{-}15_{0.25}$ samples compared to the other two analysed dendritic fibrous nanosilicates. The observed phenomenon may be attributed to the functionalization process, wherein organosilanes, specifically APTES and GPTMS, were covalently bound to the supports. This covalent linkage likely resulted in the partial obstruction of numerous small pores, potentially accounting for the absence of measurable microporosities in the last two samples. It is however true that the micropores area decreased drastically for all the analysed samples, as a consequence of the hetero functionalisation.

Table 4. Results from physisorption analysis, where F marks the functionalised samples.

Sample	**$MCF_{0.75}$**	**$MCF_{0.75}$ F**	**SBA-$15_{0.25}$**	**SBA-$15_{0.25}$ F**	**DPS**	**DPS F**	**$DPS_{0.75}$**	**$DPS_{0.75}$ F**
S_{BET} (m^2/g)	748.69	433.76	634.2	287.5	219.12	169.48	197.85	150.30
Micropores area (t-plot) (m^2/g)	107.29	1.10	144.8	50.15	7.47	-	7.86	-
V_p (cm^3/g)	1.903	0.98	0.73	0.39	0.36	0.20	0.55	0.41
D_p (nm)	10.17	9.23	4.64	5.39	6.32	4.76	11.05	10.81

The functionalization process generally also leads to a decrease in the mean pore diameter, calculated by dividing the cumulative pore volume by the specific surface area.

Figure 52 shows the pore volume distribution as cm^3 for grams of analysed support per nm, for each of the previously mentioned materials. For the reported graphs it is particularly evident that the use, during the synthesis process of the materials, of a greater amount of swelling agent, 1,3,5 trimethylbenzenexylene (TMB), leads to the presence of larger cavities in the final silica support.

The studied $MCF_{0.75}$ and $DPS_{0.75}$ samples show, in fact, a broader range of different pore width in their structure, compared to their counterparts.

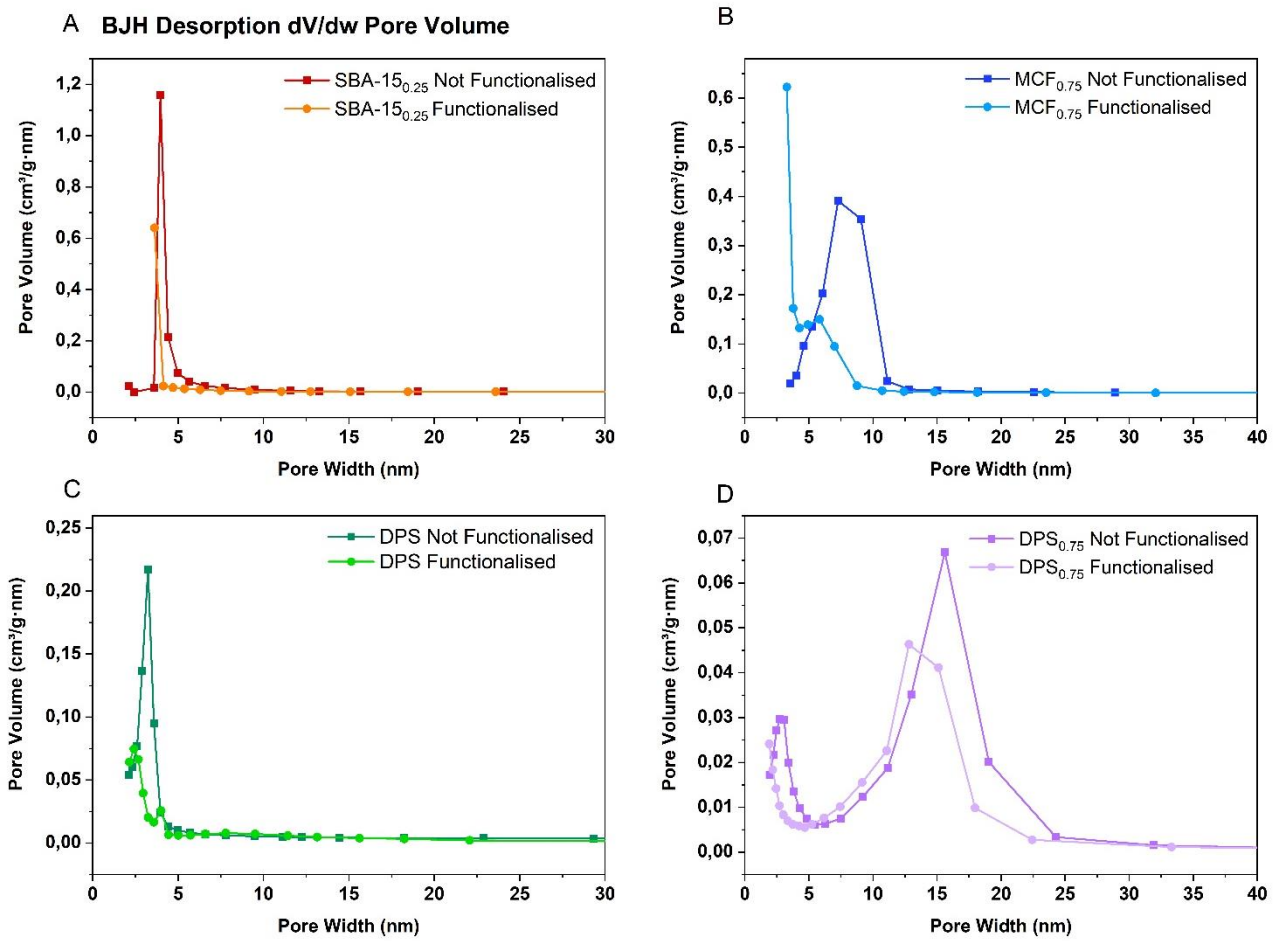

Figure 52. Pore size distribution of non-functionalised (NF) and functionalised (F) supports. A) SBA-15$_{0.25}$ B) MCF$_{0.75}$ C) DPS and D) DPS$_{0.75}$

Figure 53 below shows, on the other hand, the isotherm curves obtained via adsorption and subsequent desorption of liquid nitrogen at -196°C. The presence of hysteresis (isotherm type IV corresponding to *Figure 32*) in each of the obtained curves indicates that the studied support can all be catalogued as mesoporous material according to the IUPAC classification. As described in section 2.3.3 of the present work, it is well known that the hysteresis loop shape is correlated with the pore geometry of the analysed material. It can be noted that $MCF_{0.75}$ and SBA-$15_{0.25}$ samples present a H1 type hysteresis, which is associated with the presence of well-ordered cylindrical pores, typical of the studied supports. Conversely, DPS and $DPS_{0.75}$, are characterised by the presence of a H3 type hysteresis, which is indicative of slit-shaped pores.

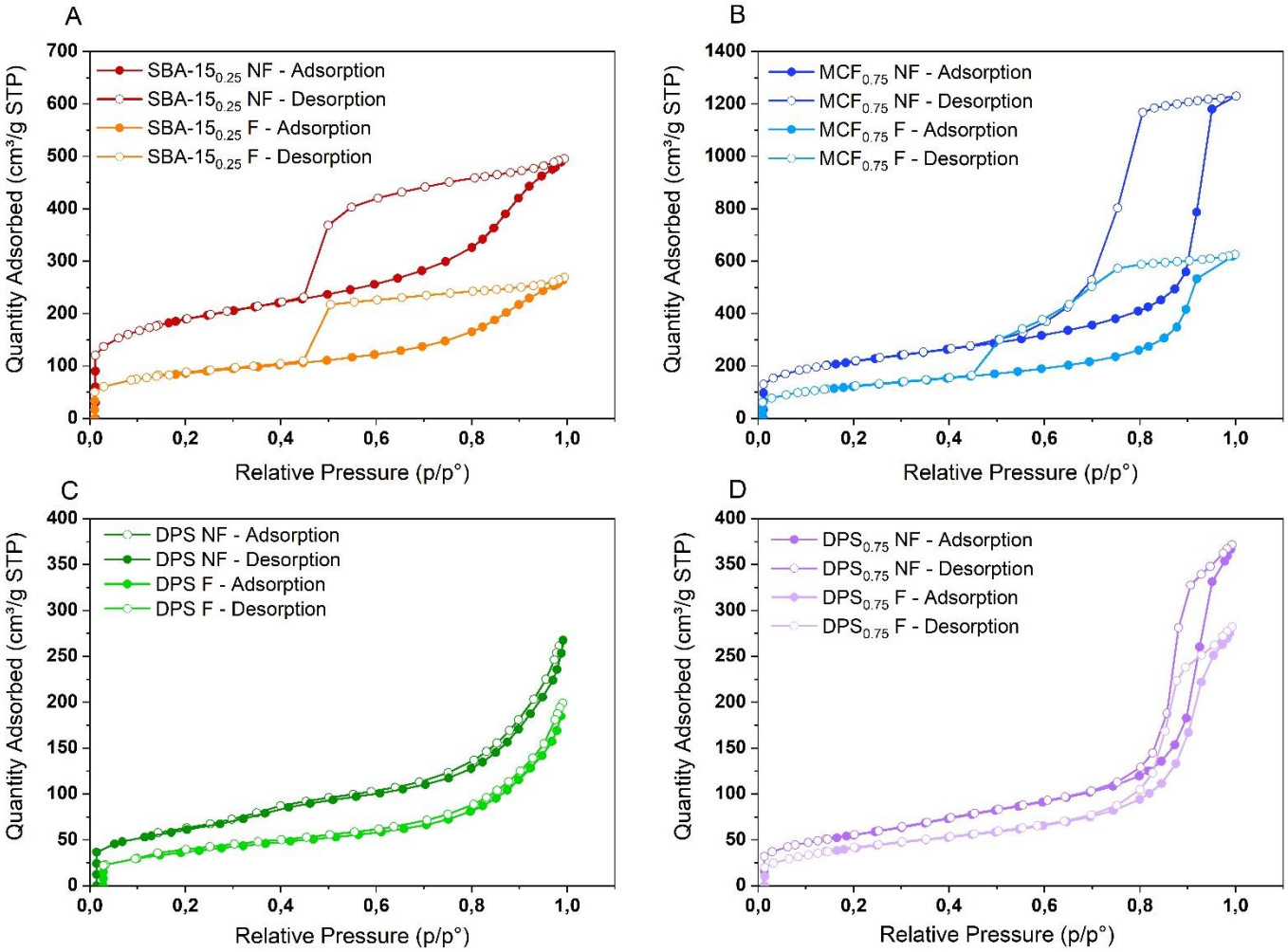

Figure 53. Adsorption and desorption isotherms of non-functionalised (NF) and functionalised (F) supports. A) SBA-15$_{0.25}$ B) MCF$_{0.75}$ C) DPS and D) DPS$_{0.75}$

3.4 Fluorescence Microscopy results

Due to the more favourable activity results obtained for the enzyme immobilised on the SBA-15$_{0.25}$ sample using trehalose as stabilising agent, fluorescence microscopy was used to investigate this material only. This analysis encompassed both the biocatalyst and the hetero functionalised support (modified with APTES and GPTMS) to confirm that the latter does not emit fluorescence in the same wavelength as the marked enzyme. As previously described, for staining of LDH, a kit emitting in the red spectrum was employed.

In *Figure 54*, it is possible to observe the acquired images for the functionalized mesoporous support, respectively under bright field (A), blue channel (B), green channel (C) and red channel (D).

Notably, in Figure (A) several silica clusters can be identified. Images (C) demonstrates that the support exhibits its fluorescence in the green channels, and a week fluorescent signal can also be detected from image (B). More importantly, image (D) confirms the absence of fluorescence in the red channel. This phenomenon pruves that the emitted signal detected for the immobilised sample is only attributable to the dyed Lactate Dehydrogenase and not to the presence of the silica support.

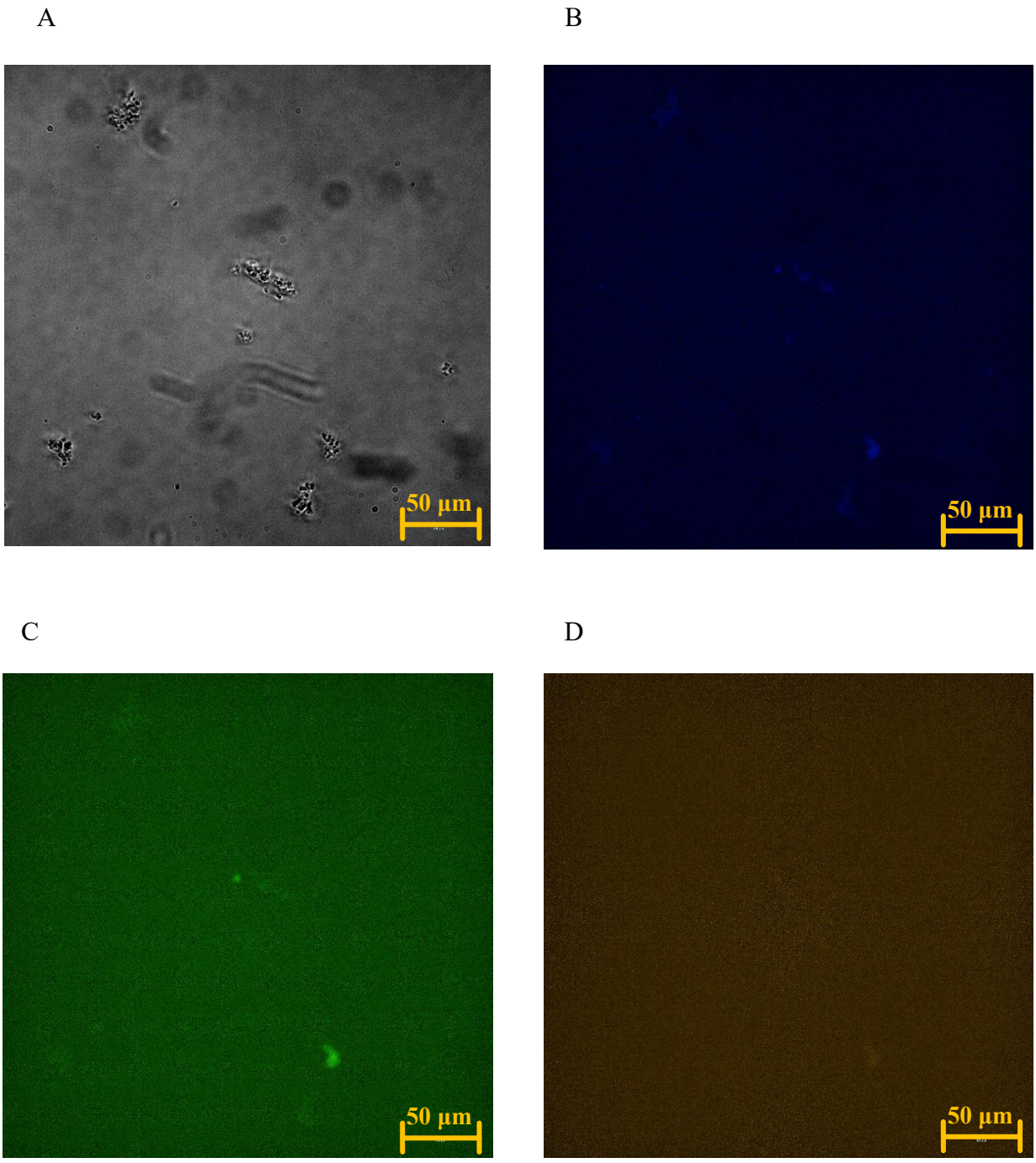

Figure 54. Fluorescence Microscopy images of hetero functionalised SBA-15$_{0.25}$: A) bright field, B) blue channel, C) green channel and D) red channel.

The images obtained from the analysis of Lactate Dehydrogenase immobilised on the chosen mesoporous silica support are collected in *Figure 55*. In particular, (D), which is relative to the images obtained in the red channel, allows us to distinguish the enzyme from the support due to its fluorescence in the red spectrum. It can be noted that the enzyme is present on the support quite homogenously on the silica particles evidenced in the bright field channel.

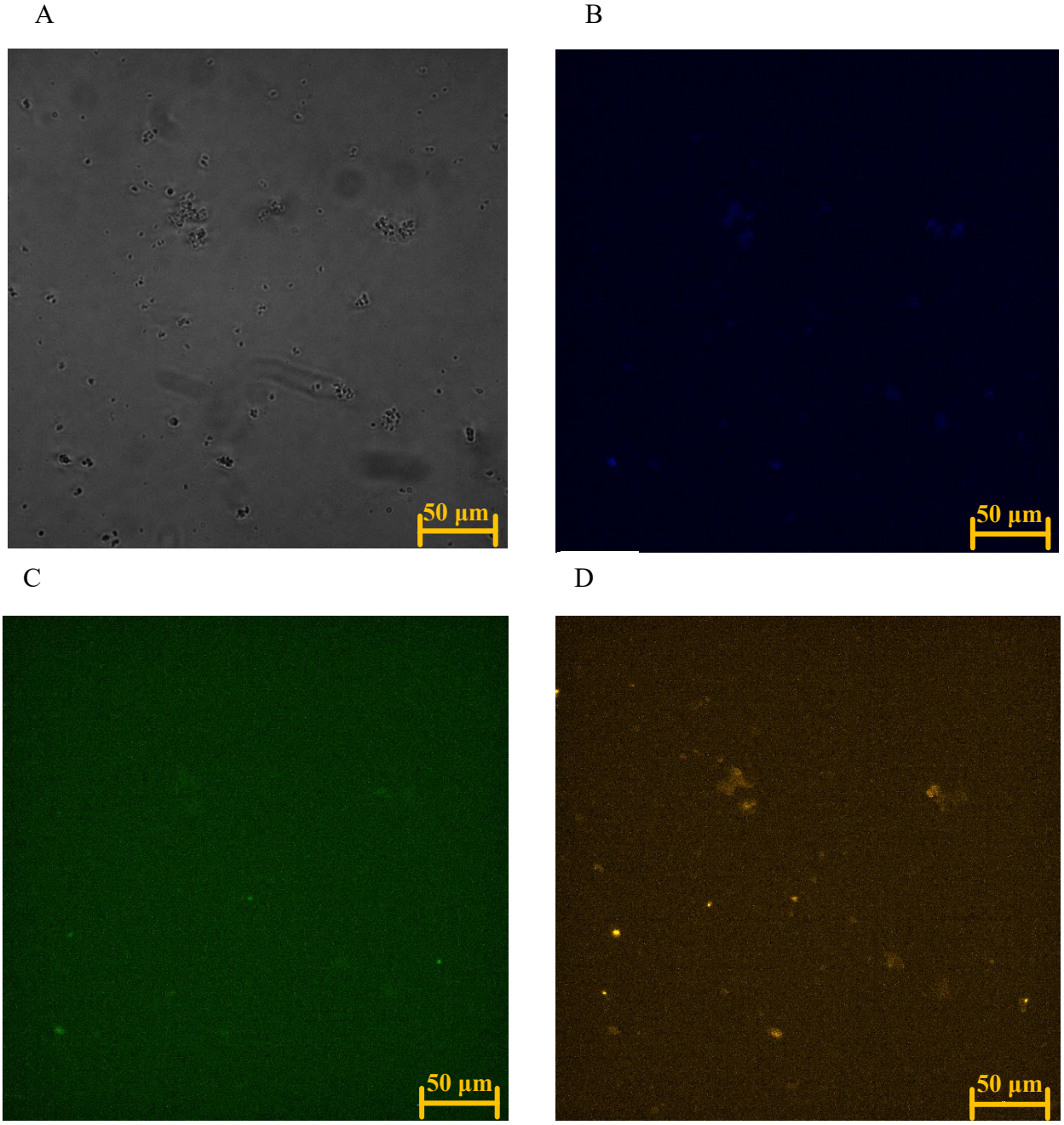

Figure 55. Fluorescence Microscopy images of Lactate Dehydrogenase immobilised on hetero functionalised SBA-15$_{0.25}$: A) bright field, B) blue channel, C) green channel and D) red channel.

3.5 Enzyme inhibition

3.5.1 Results of enzyme inactivation via incubation with denaturation agents

The result of the inactivation tests both on free and immobilised hLDH via incubation in pH 10 0.1 M buffer and in aforementioned ethanol solution are shown in *Figure 56*.

It is easily noticeable how the incubation in the organic solvent solution leads to a more pronounced reduction in enzyme activity for both the free and immobilized forms, in comparison to incubation in the alkaline solution This distinction is exemplified by the initial residual activities observed in the two free enzyme samples. Specifically, for EtHO (as indicated by the light blue graphs), the residual activity plummets to less than 10% almost immediately. Conversely, the initial data collected for the alkaline pH inhibition (orange graphs) displays a residual activity close to 25%.

The immobilization onto functionalized SBA-$15_{0.25}$, the chosen mesoporous silica support, significantly enhances the enzyme's resistance to denaturation caused by extreme pH levels and organic solvents. This enhancement becomes evident when comparing the final residual activity of the free enzyme samples with that of the immobilized counterparts, subjected to the same denaturing agent. For instance, the incubation of the free LDH with a pH 10 buffer solution results in a mere 0.06% residual activity after three hours of incubation. In contrast, when the immobilized sample was exposed to the same conditions, it presented a final residual activity of approximately 55%.

The oscillatory trend and the more pronounced error bars presented by the incubation tests using immobilised enzyme may depend on different factors, the main one being that each spectroscopy analysis performed with the biocatalyst required the continuous suspension of the catalytic powder. The biocatalyst was kept from settling using a magnetic stirred, which could have not been sufficient in some cases. Moreover, the immobilised enzyme denaturation could have been non-homogeneous. It is in fact possible that the enzymes molecules immobilised on the support surface underwent a faster inactivation process compared to the LDH molecules attached to SBA-$15_{0.25}$ internal pores.

While the data collected for the immobilised enzyme presents wider error bars, and displays an oscillatory trend, it is however possible to assert a residual biocatalyst activity much more pronounced than the residual activity measured in the free enzyme tests. Therefore, it can be affirmed that the immobilisation of the protein onto SBA-$15_{0.25}$ leads to the enhanced resistance of the enzyme to denaturation in harsh environmental conditions.

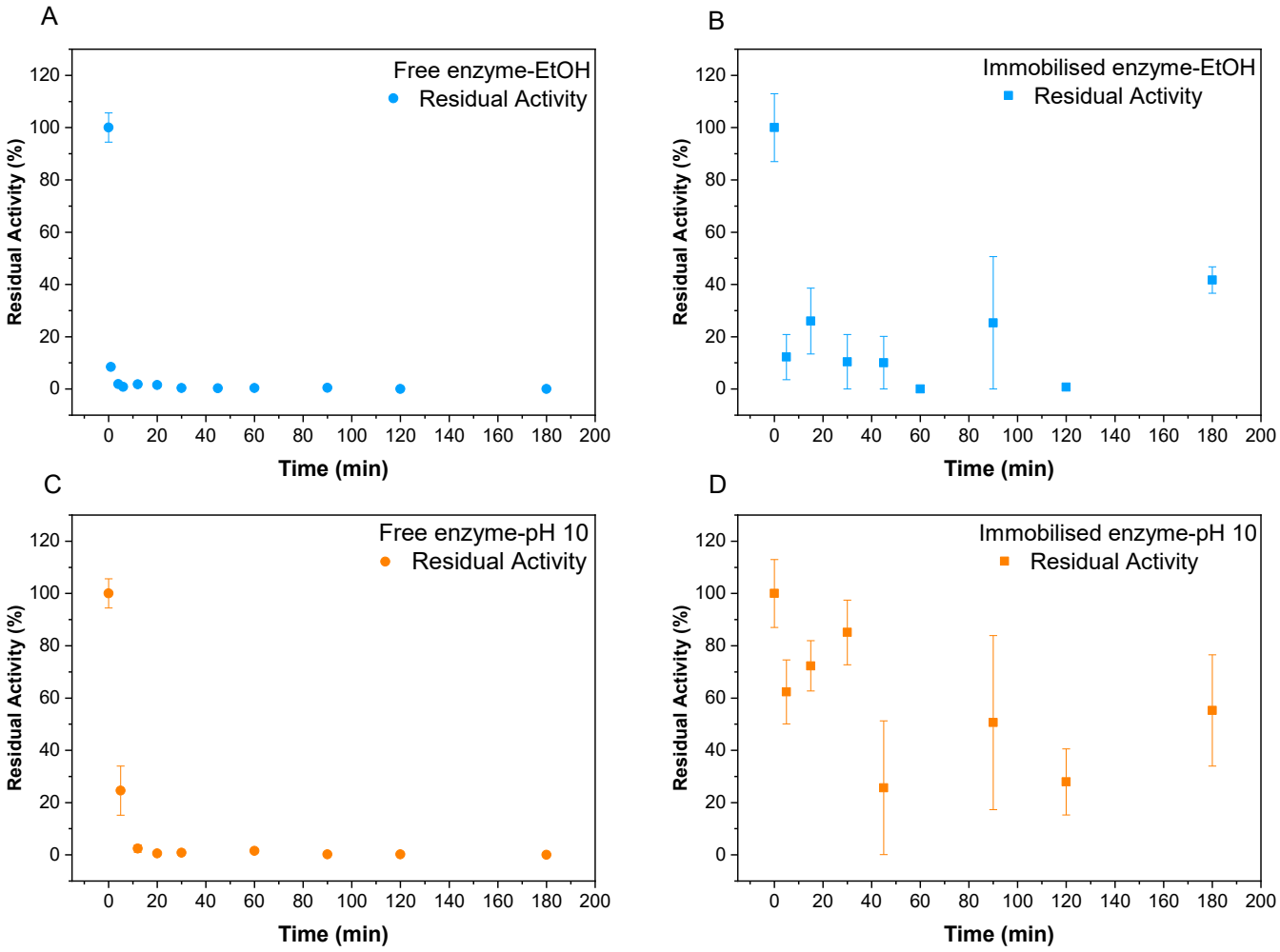

Figure 56. Residual activity compared to non-inhibited samples: A) free enzyme incubated in a solution containing 30% of ethanol B) biocatalyst incubated in the same ethanol solution C) free enzyme incubate at pH 10 D) biocatalyst incubated at pH 10.

3.5.2 Results of enzyme inhibition with NHI-2

Inhibition with NHI-2 and varying substrate concentration

The results of the assays performed on the free form of the enzyme are illustrated in *Figure 57*. The free Lactate Dehydrogenase activity was measured when varying the enzyme substrate (pyruvate) concentration, in presence and in absence of the selected competitive inhibitor. It is evident how the first plot, which describes the increase of the reaction rate when increasing the pyruvate concentration, is perfectly interpolated by the Michaelis Menten equation. The kinetic constants for this first graph were found implementing the Hanes linearisation method, which is generally believed to be more accurate.

The second plot (B) represents the reaction rate when varying the pyruvate concentration but in the presence of the selected anticancer drug NHI-2. It is immediately noticeable how the presence of the inhibitor alters the reaction kinetic, in particular at low concentration of substrate. This phenomenon is fully explained by the fact that the anti-tumoral drug used is competitive with both the substrate and the enzyme cofactor. At high substrate concentrations, the competitivity with the drug is no longer influencing the kinetic since the abundance of pyruvate is prevailing.

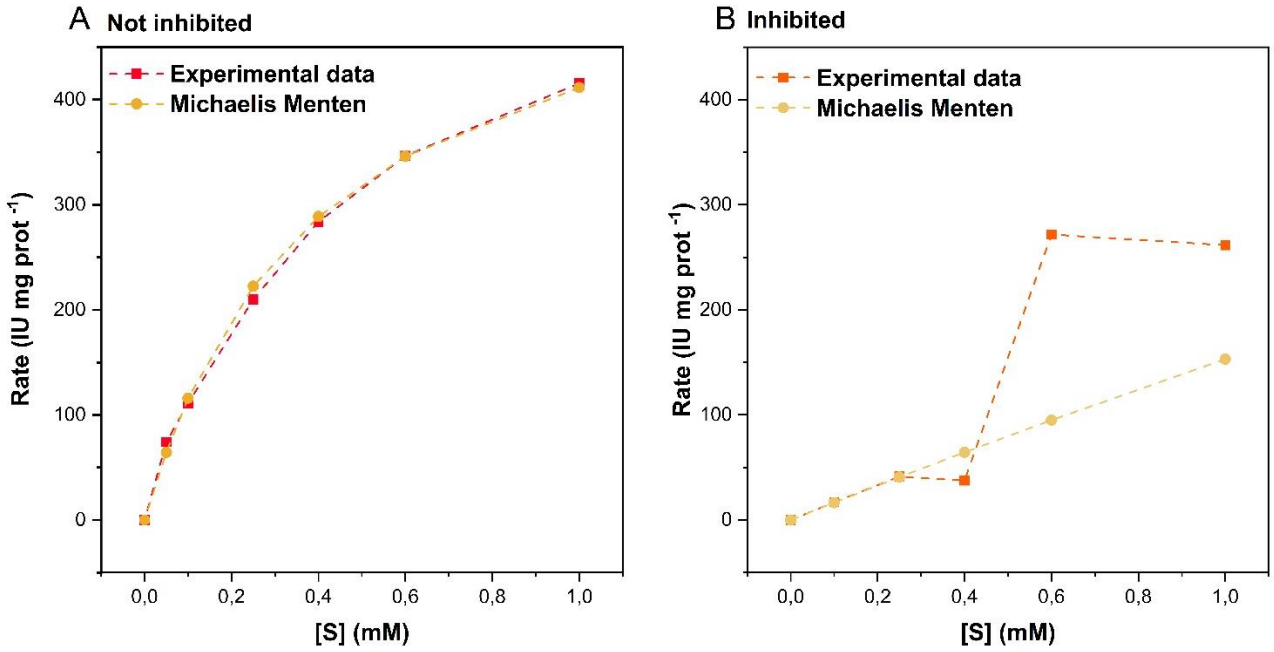

Figure 57. Michaelis Menten equation used to describe the reaction rate of free LDH catalysed reaction when varying pyruvate concentration, A) without inhibitor B) with inhibitor.

The use of the aforementioned linearisation technique of the double reciprocal (Lineweaver-Burk) enabled the linearised representation of the activities measured using the free form of the enzyme, compared in *Figure 58*. Lineweaver-Burk plot was preferred to the Hanes plot for this representation of the competitive inhibition mechanism, due to its simpler interpretation, as previously shown in *Figure 22*. It is in fact evident form this graph how the presence of the inhibitor hampers the linkage between the substrate and the enzyme, lowering their affinity. This phenomenon is reflected in the increase of the Michaelis constant, K_M, which is directly linked with the linearisation plot slope.

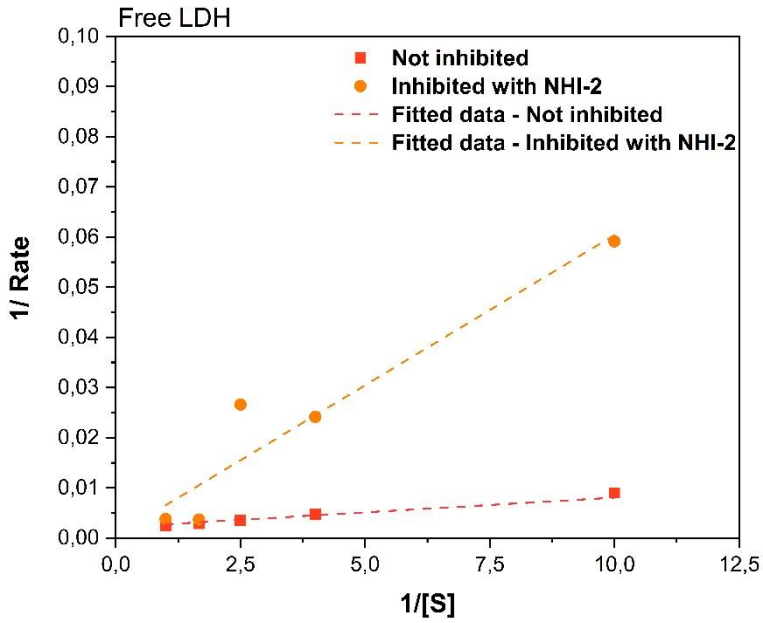

Figure 58.Comparison between the Lineweaver-Burk linearisation plots obtained for the non-inhibited and the inhibited activity assays performed using free LDH at varying Pyruvate concentrations.

The same study was implemented using the enzyme immobilised on the chosen mesoporous support, SBA-$15_{0.25}$. The reaction rate was measured varying the substrate concentration and the data collected were linearised with Lineweaver-Burk linearisation plot, to be able to determine the reaction kinetic parameters. Also in this case, according to the experimental data represented using the double reciprocal plot, it is possible to highlight that the use of NHI-2 as an inhibitor of the reaction kinetic, leads to the increase of K_M. This finding suggests that the anticancer drug used is still effective on the immobilised form of the enzyme.

This result is believed to be very relevant, since the attachment of an enzyme through the formation of covalent bonds with a silica support can alter the protein three-dimensional structure, modifying its binding site for the drug molecule. A modification of LDH structure could have resulted in a non-correct inhibition of the enzyme.

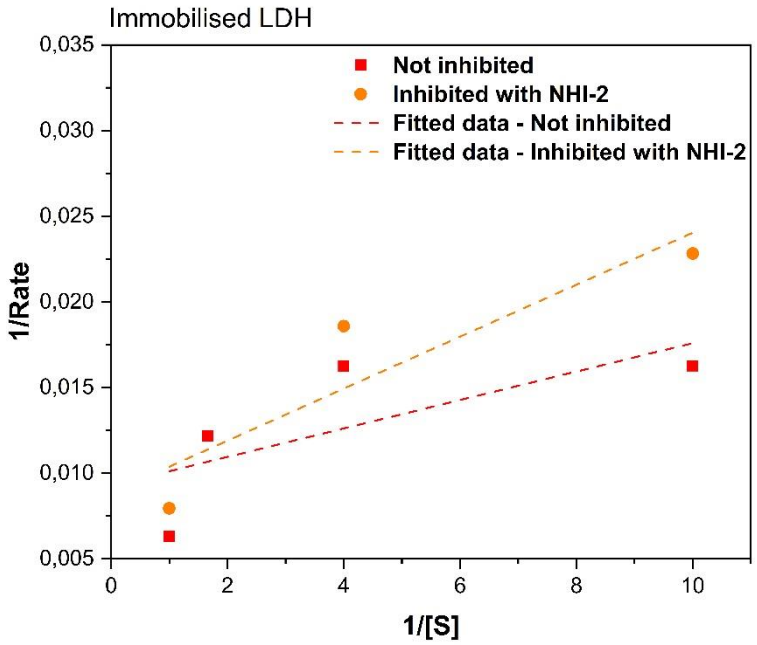

Figure 59. Comparison between the Lineweaver-Burk linearisation plots obtained for the non-inhibited and the inhibited activity assays performed using LDH immobilised on SBA-15$_{0.25}$ support, at varying Pyruvate concentrations.

Inhibition with NHI-2 and varying cofactor concentration

The same kinetic study was conducted by changing the cofactor concentration (NADH) while maintaining the pyruvate concentration stable at a non-limiting amount. The experimental data collected for both the free and the immobilised forms of the enzyme have been analysed purely in their linearised form, as suggested in the literature by Granchi et al. [5]. The Michaelis-Menten equation more correctly represents the substrate variation, while it would be improper to apply it for the analysis of cofactor variation. However, the use of Lineweaver-Burk plot allows for the calculation of the apparent Michaelis-Menten constants, whose values are compared to determine the degree of inhibition in the presented assays.

Figure 60 shows the comparison between the linearisation of the experimental data collected for the catalytic reaction of free LDH in presence and in absence of NHI-2. In this case, the obtained K_M values are very similar, as can be noted from the only slight difference in the slopes of the presented dotted lines. The marginally higher value obtained for the non-inhibited reaction could be explained by the results found in the fourth section of this thesis work, using computational modelling methods. It was found that the active site corresponding to NADH is only partially covered by the binding of NHI-2 to the enzyme surface. This fact could indicate that the free LDH shows the ability to modify its structure, to be able to link the cofactor. [59] This modification could result in the enzyme capability to perform the catalytic conversion of pyruvate to lactate even in the presence of the

anticancer compound, when the substate is present in abundance. This analysis is supported by the results shown in the previous section for the inhibition analysis performed by varying pyruvate concentration. The inhibition effect of NHI-2 was in fact not detected when in presence of an elevated amount of substrate.

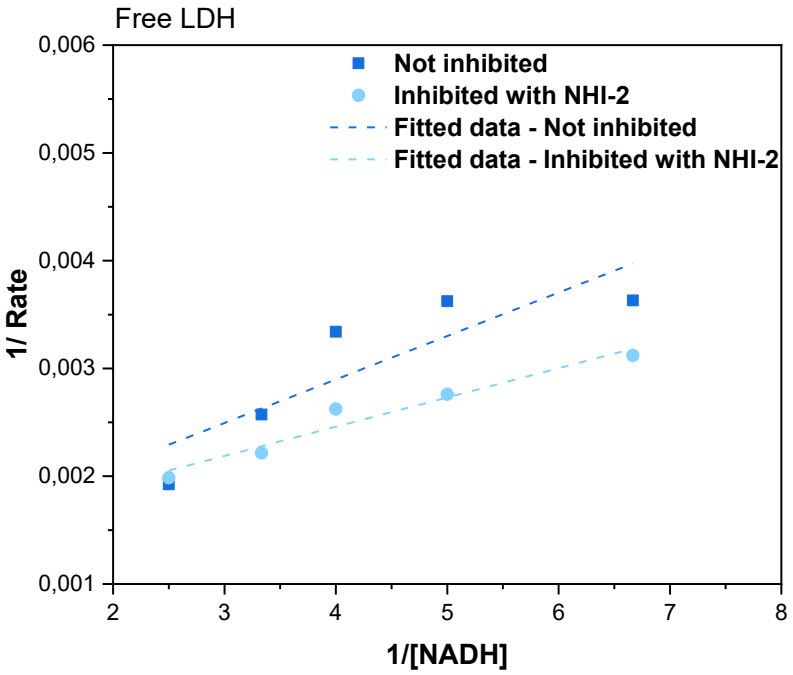

Figure 60. Comparison between the Lineweaver-Burk linearisation plots obtained for the non-inhibited and the inhibited activity assays performed using free LDH at varying NADH concentrations.

Hereafter the results of the same inhibition assays performed on the immobilised form of Lactate Dehydrogenase are reported.

Contrarily to what reported for the free LDH analysis, the covalent bonding of LDH on SBA-$15_{0.25}$ support leads to the rigidification of the protein active sites, which explains the more pronounced inhibition of the catalytic reaction in this second case. [2] The higher apparent K_M value obtained for the reaction in presence of NHI-2 is demonstrated by the more pronounced inclination of the Lineweaver-Burk plot obtained by the linearisation of this assay experimental data. The inhibition of the catalytic reaction was therefore observed for both the analysis performed varying the substrate and the cofactor concentration. This result hence indicates the competitiveness of NHI-2 for both pyruvate and NADH active sites.

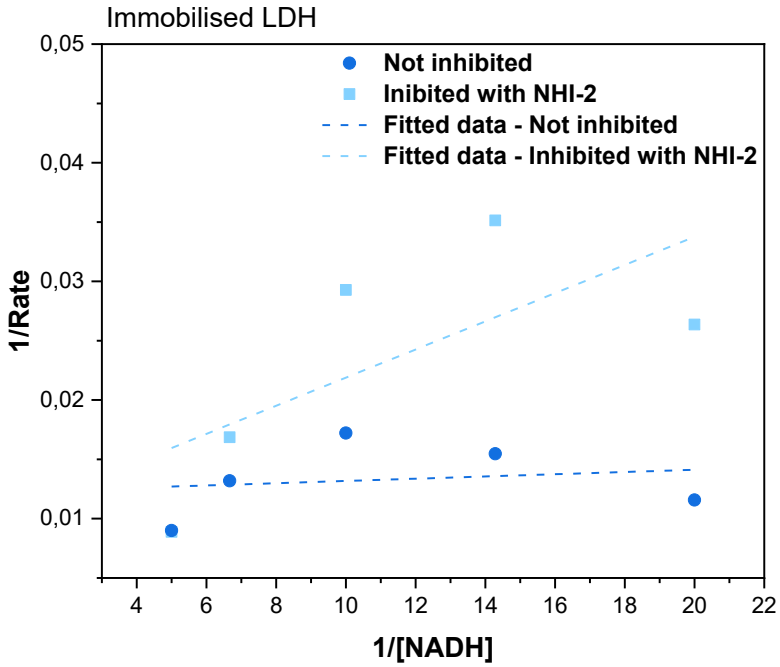

Figure 61. Comparison between the Lineweaver-Burk linearisation plots obtained for the non-inhibited and the inhibited activity assays performed using LDH immobilised on SBA-15$_{0.25}$ support, at varying NADH concentrations.

4. Molecular Modelling

Protein modelling for drug-discovery application

As mentioned in the introductory part of the present thesis work, new anticancer drugs discovery is a very demanding task, requiring an enormous amount of resources and on average more than a decade of time. This research aims to contribute to diminishing these two factors, introducing a novel fast and reliable way of testing molecular compounds with promising antitumoral properties. With a view of optimising the traditional pipeline for new anticancer drug discovery, protein modelling and artificial intelligence could be studied as powerful tools to be associated with enzyme powered biosensors.

In particular, the so-called Computer-aided drug discovery (CADD) techniques, could play a pivotal role for a first potential drugs screening, individuating possible bioactive molecules starting from large compounds libraries. Ideally, the results of this first step could be coupled with the fast testing of the most promising compounds on LDH biosensors, drastically reducing the number of compounds to be tested on expensive and time-consuming tumoral cell lines. CADD techniques can be classified in two main strategies: structure-based drug discovery and ligand-based drug discovery. [87]

Structure-based drug discovery strategies can be implemented when the three-dimensional structure of the target protein is well-known. The complete understanding of the protein structure is made possible by the use of X-ray crystallography and nuclear magnetic resonance (NMR) analyses, largely available nowadays. The most widespread structural-based protocol is the so-called *molecular docking*. [88] This protocol can be implemented via various tools, listed below in *Table 5*, and consists in the accurate modelling of the protein-ligand interaction by predicting the possible binding patterns and interaction affinities present in between the selected molecule and enzyme structure.

Ligand-based drug-discovery strategies, on the other hand, are employed when the protein structure is not completely known or known with low accuracy. This method relies on the principle that ligands with a similar molecular structure will interact with the protein in a similar manner, giving rise to similar biological responses.[87] Thanks to the deep understanding of Lactate Dehydrogenase structure, this second strategy was not implemented in this thesis work and will therefore not be detailed further.

Table 5. Review of the most wide-spread molecular docking software.

Computational tools for molecular docking	Websites
GOLD	https://www.ccdc.cam.ac.uk/solutions/software/gold/
Glide	https://www.schrodinger.com/products/glide
DOCK	https://dock.compbio.ucsf.edu/
AutoDock	https://autodock.scripps.edu/
Discovery Studio	https://www.3ds.com/products-services/biovia/products/molecular-modeling-simulation/biovia-discovery-studio/

4.1 Structure-based drug discovery strategies

The definition of the most suitable docking configuration is a complex task that is carried out differently by each of the presented software, but a general workflow is presented.

As previously mentioned, the structure of the studied protein and of the drug molecules should be known in advance. Several drug databases are available online and can be employed for this first crucial step, such as: DrugBank (http://www.drugbank.ca), PubChem (https://pubchem.ncbi.nlm.nih.gov/) and ChemDB (http://cdb.ics.uci.edu). [89]

Therefore, the first step of the process is the selection of the desired protein structure from the database. Secondly, a docking method is used to individuate the most appropriate protein-ligand complex configuration. There is a wide variety of different docking methods available, subdivisible in three main categories: Systematic search, Stochastic or random search and Deterministic search.

- *Systematic search* methods consist in dividing the chosen molecules, such as a potential anticancer drug, in smaller rigid fragments. Then geometrical matching is implemented to dock the fragment to the active site of the selected protein. This searching algorithm is applied by the cited software DOCK.[90]
- *Stochastic or random search* algorithms rely on the casual generation of different ligand conformations by genetic algorithms. The most suitable compound is then selected based on an evaluation of the energy of the final complex. Notable examples of the implementation of

a random search method are AutoDock and GOLD (Genetic Optimisation for Ligand Docking) software.[91], [92]

- Lastly, *simulation algorithms*, are more complex algorithms that implement Molecular dynamics (MD) as computational techniques for the simulation of the ligand-protein complex in time. This category of algorithms is usually coupled with an energy local minimisation method, which aims to get the formed system to the lower potential energy level. An example of this type of modelling tool is implemented by Discovery Studio visualizer using CHARMM program (https://www.charmm.org/). [93]

All the described algorithms are classified as semi-flexible, due to the fact that they consider only the ligand to be flexible, while the protein is maintained rigid throughout the application of the docking technique.

Finally, after the application of one or a combination of the aforementioned docking methods, several possible enzyme-ligand complexes have been created, and a scoring function needs to be implemented. This last step of a general structure-based drug discovery procedure is pivotal for the selection of the correct binding configuration. In fact, the application of a scoring function is used to rank the different possible configurations proposed by the search tool used. Its aim is to estimate the energy related to each of the complex configurations, and selecting the best one, according to the complex vicinity to the protein natural configuration. [88]

For this thesis work, BIOVIA Discovery Studio software was selected for the implementation of the described molecular docking method. This software was used to model and visualise the interactions between Lactate Dehydrogenase and several fundamental ligands. This study allowed for the consideration of the theoretical consideration on the possible conformation of the protein after the immobilisation and for the demonstration of NHI-2 competitiveness with both the enzyme substrate, pyruvate, and the reaction cofactor, NADH.

4.2 Enzyme immobilisation modelling

As previously mentioned, the presence of the protein residue Lysine is of primal importance for the strong binding of Lactate Dehydrogenase on the chosen functionalised silica support. As Jackson et al. demonstrated for LDH obtained from rabbit muscle, Lysine is homogeneously present on the

selected enzyme. In order to obtain a more detailed understanding of the linkage of the exact protein employed to the supports, a molecular modelling technique was implemented.
Through the use of BIOVIA Discovery Studio (DS) software, it was possible to highlight the presence of Lysine residues in the protein three-dimensional structure, obtained from UniProt [11]. The acquired result is shown in *Figure 62* for the A chain of *h*LDH-A.

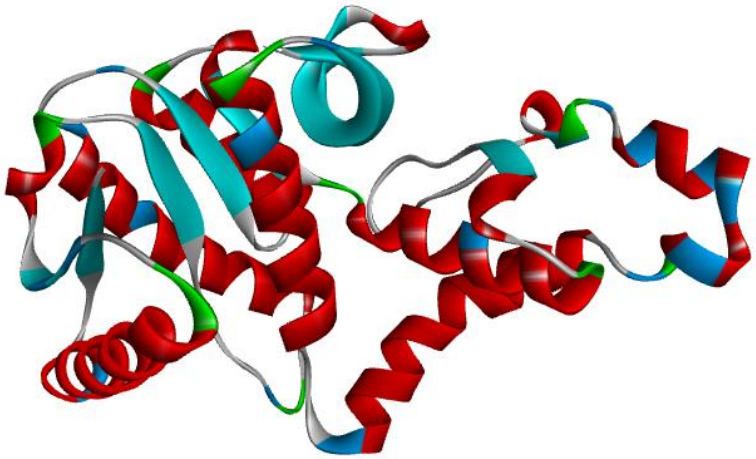

Figure 62. Three-dimensional representation of hLDH-A, where the Lysine residues have been highlighted in blue, while the rest of the colours refer to the protein secondary structure (in red: helixes, light blue: β-sheets, grey: coils, green: turns).

The abundance of Lysine residues in the enzyme structure validates the possibility of a strong enzyme-functionalised support binding. It is in fact evident how the enzyme has different docking points that can form a covalent bond with the support. However, which Lysine residue forms the covalent binding is not irrelevant since the enzyme three-dimensional arrangement is closely linked with its activity. Some enzyme-support configurations will in fact lead to an unactive biocatalyst. It is therefore important to highlight the location of the enzyme active sites that need to face the reaction environment in order to be able to bond the substrate and the NADH.

With the help of DS powerful visualisation tool, the modelling of the interactions between Lactate Dehydrogenase and the enzyme cofactor and substate were implemented. In particular, Discovery Studio enabled the investigation of the three-dimensional structure of LDH, coupled with the ligands' structures, obtained from PubChem online library. By minimizing the global potential energy of the ligand-enzyme complex, the program individuated the most suitable protein binding pockets for both NADH and pyruvate linkage. More specifically, the program individuated the following types of bonds: hydrogen bonds, carbon-hydrogen bonds, halogen bonds, π- donor hydrogen bonds. The program also enabled the visualisation of unfavourable bumps, which are represented in red in the

given simulations. By running the molecular simulation on Discovery Studio software, it was possible to gain information on the protein residues engaged with each ligand, as depicted in *Figure 64* and *Figure 63*. It is important to note that, LDH residues participating to the linkage with NADH are not part of the linkage to the enzyme substrate, as the two described bindings take place simultaneously.

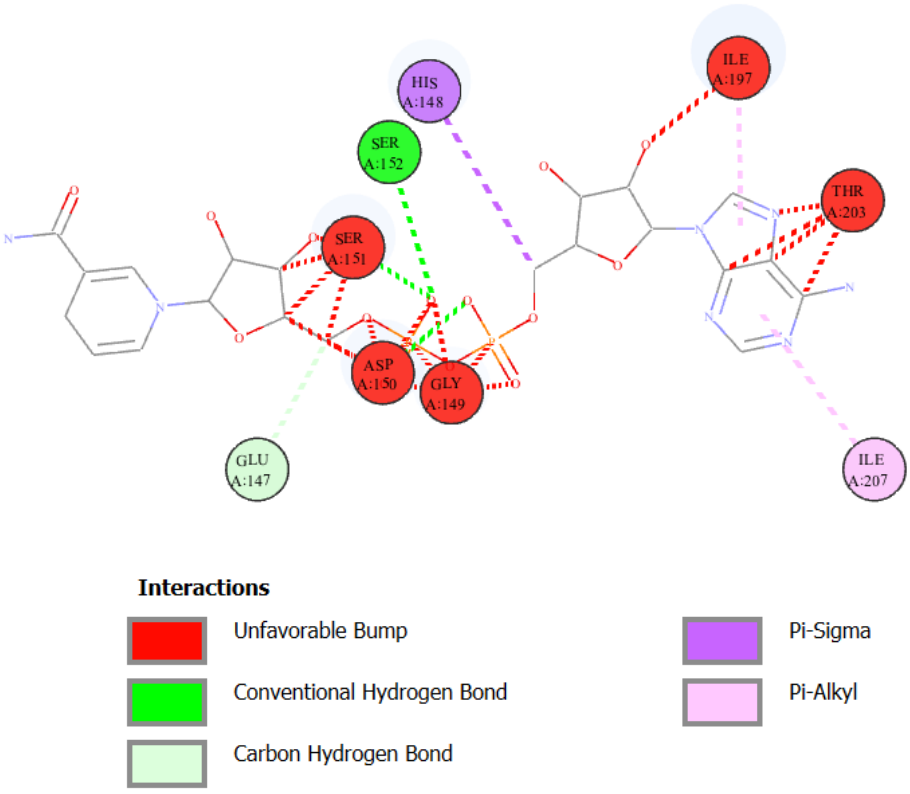

Figure 64. Schematic 2D representation of LDH interaction with NADH. Obtained using Discovery Studio molecular docking software.

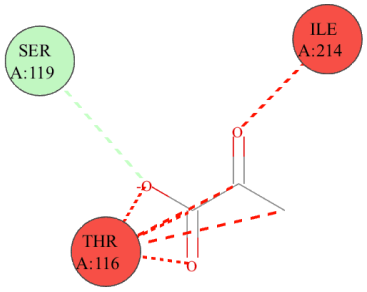

Figure 63. Schematic 2D representation of LDH interaction with pyruvate. Obtained using Discovery Studio molecular docking software.

Using the data collected through the described molecular docking simulation, it was possible to locate each protein residue composing pyruvate (depicted in bright yellow) and NADH (depicted in pink) binding sites on Lactate Dehydrogenase 3D structure. The obtained representations are shown in

Figure 65. Different views of the same enzyme are shown for a better understanding of the highlighted residues positions.

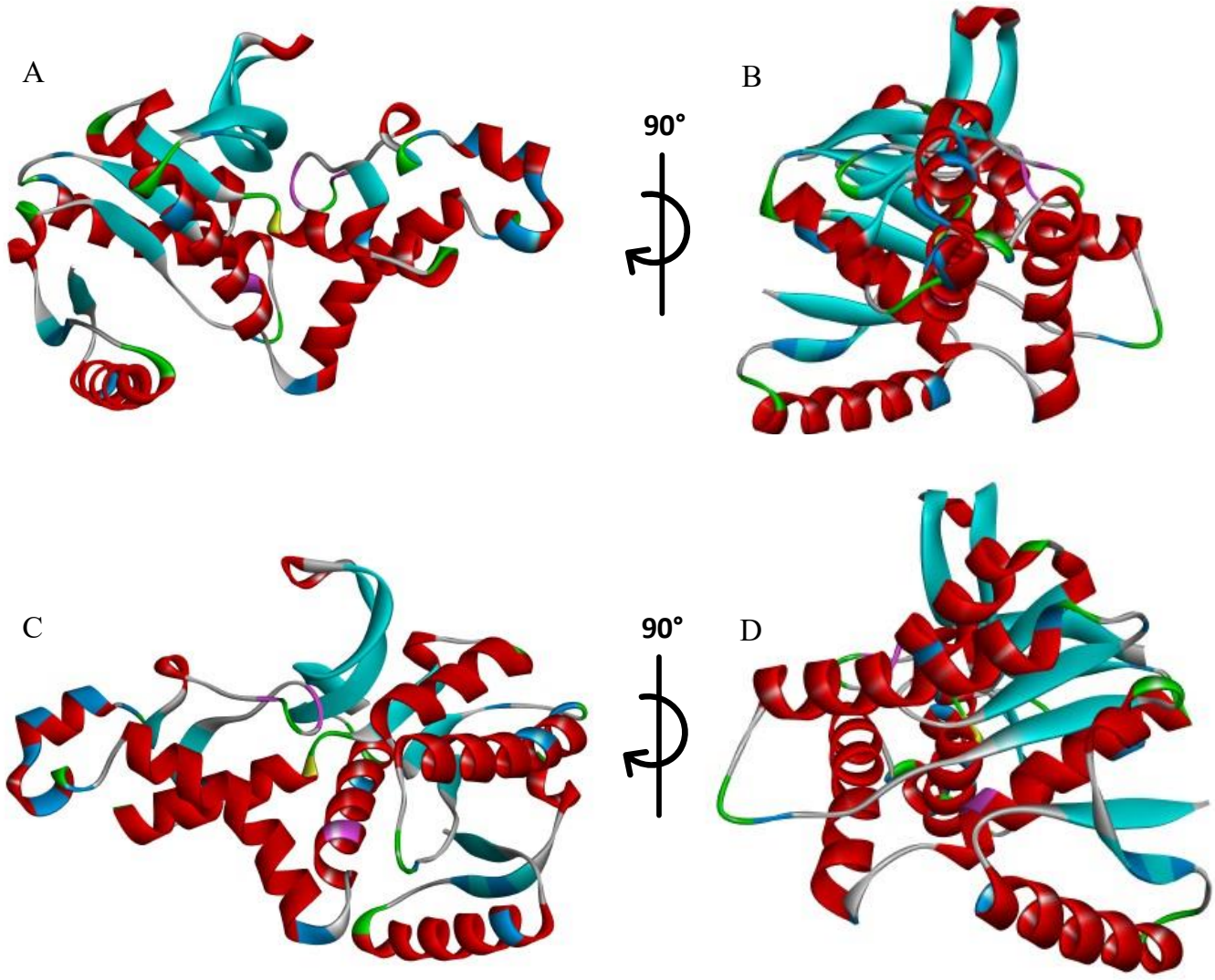

Figure 65. Three-dimensional representation of Lactate Dehydrogenase. Lysine residues are highlighted in blue, while pink and yellow was used to highlight the residues of NADH binding site and pyruvate binding site respectively.

It can be noticed that even if Lysine residues are quite evenly distributed, the active sites for both the cofactor and the substrate are located in the central part of the enzyme. For this graphical analysis it can be derived that covalent bonding with the silica supports leading to the positioning of the protein as depicted in (A) and (C) could result in a not active biocatalyst. (B) and (D) on the other hand, show Lysine residues that are situated on a part of the protein that is more distant to pyruvate and NADH binding sites. These last two orientations could be more favourable for a covalent attachment of the enzyme on the support that does not interfere with protein activity. While it is not possible to select the enzyme orientation when performing its immobilisation on the selected material, this

computational representation could explain one of the reasons leading to the reduced activity of the biocatalyst compared to the free form of the enzyme.

4.3 Enzyme inhibition modelling

With the help of DS powerful visualisation tool, the modelling of the interactions between Lactate Dehydrogenase and the inhibitor used, NHI-2, was implemented. Discovery Studio enabled the representation of the three-dimensional complex formed by LDH and the drug structure, obtained from PubChem (CID 51355147). The small molecule-protein complex was obtained with the same procedure described for the localisation of NADH and pyruvate binding sites. The obtained proposed NHI-2-enzyme interaction structure is presented in its two-dimensional and three-dimensional form in *Figure 66* and *Figure 67* respectively.

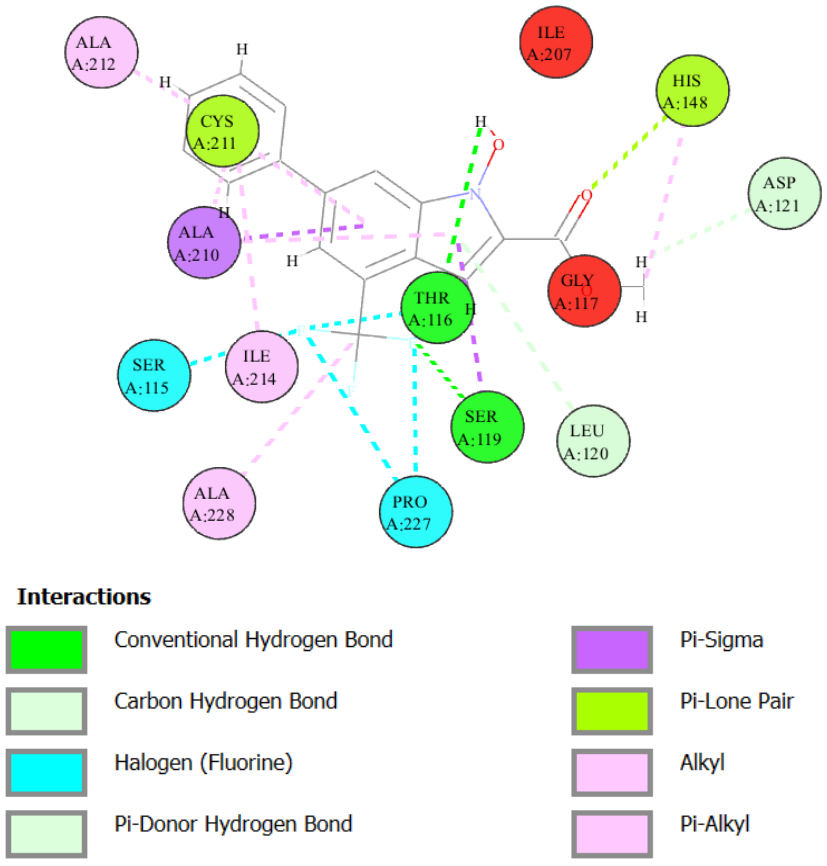

Figure 66. Schematic 2D representation of LDH interaction with the anticancer drug NHI-2. Obtained using Discovery Studio molecular docking software.

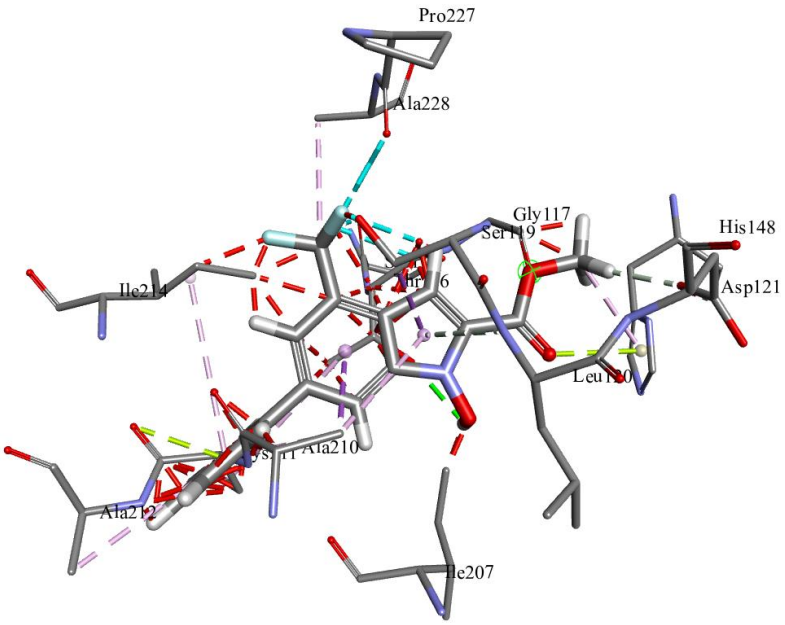

Figure 67. 3D representation of LDH interaction with the anticancer drug NHI-2. Obtained using Discovery Studio molecular docking software.

Following the procedure described by Granchi et al. [5], the obtained representation of NHI-2 binding site on the enzyme was compared with the results found in the molecular docking simulations performed previously for NADH and pyruvate.

For each studied molecule, the found protein residues form the binding site of the relative ligand. Therefore, for NADH, for example, to correctly bind to the enzyme, all the evidenced residues must be free, not involved in any other interactions. As can be easily noted from the schemes shown, NHI-2 binding site involves many residues, including residue His 148, which is also part of the cofactor active site. Another relevant residue is Ser 199, which forms a hydrogen bond with the anticancer drug NHI-2 but is also involved in a carbon-hydrogen bond when the enzyme interacts with pyruvate. The employed computational modelling of the enzyme interactions with the ligands of interests can therefore indicate that NHI-2 acts as a competitive inhibitor with both NADH and pyruvate. In fact, its binding to the enzyme will completely block pyruvate active site, impeding its catalytic conversion to lactate. Similarly, the binding of NHI-2 to the protein leads to the partial blocking of NADH active site, which prevents it from acting as catalytic cofactor for the mentioned reaction.

5. Conclusion and future developments

The here presented research studies the immobilisation of Lactate dehydrogenase on different mesoporous silica supports for the realisation of an LDH-based biosensor, which could enable the quick and reliable testing of numerous anticancer drugs. The comparison between the various biocatalyst synthetised was allowed by the analysis of the catalytic activities, immobilisation yields, and material morphologies, through the use of different assays and characterisation techniques. The performed analysis suggested SBA-$15_{0.25}$ as the best performing support for LDH immobilisation using trehalose as stabilising agent. This immobilisation conditions resulted in a residual relative activity of approximately 15% of the original free enzyme activity.

Inactivation tests were conducted to investigate the enhanced resistance of the immobilized enzyme compared to its free form. SBA-$15_{0.25}$ LDH biocatalyst activity in time was measured in presence of two different denaturising agents: a carbonate buffer solution pH 10 and an organic solvent, ethanol. Results obtained from these assays demonstrated that the covalent binding of Lactate Dehydrogenase on the chosen mesoporous silica support enhances the enzyme stability in presence of denaturising agents. In fact, the incubation of the free enzyme in said solutions led to the complete loss of the activity in approximately 15 minutes, while the immobilised form of LDH showed a residual activity equal to 40-50% of the initial one after 180 minutes of incubation.

The synthetised biocatalyst and free enzyme activities were also studied in the presence of a well-known anticancer drug, NHI-2. These analyses were performed varying the concentration of the reaction cofactor and the enzyme substrate, both in presence and in absence of the chosen drug. Calculations of the kinetic constants describing the catalytic reaction demonstrated that NHI-2 is competitive with both NADH and pyruvate. To further investigate this competitiveness, a molecular docking computational tool was used to model the interaction between the enzyme and the chosen ligands: pyruvate, NADH and the anticancer drug. This modelling technique enabled the visualisation of the protein residues involved in each of the studied bindings, highlighting how the binding site of NHI-2 partially coincides with NADH active site and totally overlaps pyruvate active site on the enzyme. This computational analysis thus demonstrates how the linkage between LDH, and the studied drug prevents the bonding of the substrate and the cofactor, thereby hampering the reaction kinetic.

This finding suggests that the immobilisation of Lactate Dehydrogenase on the SBA-$15_{0.25}$ support does not interfere with NHI-2 inhibition abilities and therefore defines this mesoporous silica support as a valid candidate for the design of an enzymatic biosensor for anticancer drug testing.

The implementation of the described biocatalyst for a rapid pharmaceutical testing could potentially be coupled with different novel computational techniques for the detection of new anticancer compounds in an optimised drug screening pipeline. In recent years in fact, various powerful Artificial Intelligence (AI) tools have been applied in Drug Screening procedures, accelerating the selection procedure of the most promising anticancer drugs. Different AI algorithms can successfully be employed for the rapid screening of extensive compound libraries, being able to identify the drug candidates that exhibit particular selected properties. The implementation of said techniques is believed to reduce the compounds screening period drastically; in fact, it has been shown that the virtual screening of several billion of drugs can be performed in only a couple of days with the help of an AI tool. [94]

For example, AI techniques can be used to select compounds based on their toxicity, bioactivity and bioavailability. Among others, DeepTox is a computational tool that predicts the toxicology of pharmacological compounds based on Deep Learning methods. [89]

As Artificial Intelligence tools are being more and more effectively employed in the pharmacological field for the development of new anticancer drugs, their coupling with a protein-based biosensor could considerably reduce the number of molecules to be tested *in vitro* and consequently could lead to a drastic reduction of *in vivo* drug testing on animals, significantly lowering the cost of a new drug production.

Acknowledgments

In queste ultime righe ci tengo a rivolgere i miei sentiti ringraziamenti al Professor Marco Piumetti, per l'aiuto e il supporto mostratomi nello sviluppo del mio lavoro di tesi. Un sincero ringraziamento va anche a Clarissa Cocuzza, che mi ha accompagnata passo dopo passo nelle lunghe giornate in laboratorio e nella stesura di questo testo; senza la sua costante e attenta guida non sarei riuscita a raggiungere questo importante obiettivo.

Grazie anche alla mia famiglia ed in particolare ai miei genitori, che mi hanno supportata e sopportata durante tutto il mio percorso universitario e in particolare durante questi ultimi mesi di lavoro. Senza il vostro aiuto non sarei riuscita a completare questo impegnativo percorso con la giusta serenità e determinazione.

Un grazie speciale anche a Paolo, con cui ho avuto l'onore di condividere ogni step di questo lungo viaggio, per tutte le parole di incoraggiamento e sostegno che mi hai rivolto in questi anni, spronandomi a migliorarmi sempre e a puntare ad obiettivi sempre più ambiziosi.

Infine, ci tengo a ringraziare Biro, per il suo costante supporto emotivo durante questi ultimi anni universitari, senza il quale sarei sicuramente arrivata a questo obbiettivo molto meno serenamente.

Bibliography

[1] R. L. Siegel, K. D. Miller, N. S. Wagle, and A. Jemal, "Cancer statistics, 2023," *CA Cancer J Clin*, vol. 73, no. 1, pp. 17–48, Jan. 2023, doi: 10.3322/caac.21763.

[2] J. M. Guisan, J. M. Bolivar, F. López-Gallego, and J. Rocha-Martín Editors, "Immobilization of Enzymes and Cells Methods and Protocols Fourth Edition Methods in Molecular Biology 2100." [Online]. Available: http://www.springer.com/series/7651

[3] D. E. Koshland, "APPLICATION OF A THEORY OF ENZYME SPECIFICITY TO PROTEIN SYNTHESIS*," vol. 44, no. 2, pp. 98–104, Feb. 1958, doi: 10.1073/pnas.44.2.98.

[4] N. Majoul, S. Aouida, and B. Bessaïs, "Progress of porous silicon APTES-functionalization by FTIR investigations," *Appl Surf Sci*, vol. 331, pp. 388–391, Mar. 2015, doi: 10.1016/j.apsusc.2015.01.107.

[5] C. Granchi *et al.*, "Discovery of N-hydroxyindole-based inhibitors of human lactate dehydrogenase isoform A (LDH-A) as starvation agents against cancer cells," *J Med Chem*, vol. 54, no. 6, pp. 1599–1612, Mar. 2011, doi: 10.1021/jm101007q.

[6] Farhana A and Lappin SL, *Biochemistry, Lactate Dehydrogenase.* Treasure Island (FL): StatPearls Publishing, 2023. Accessed: Aug. 19, 2023. [Online]. Available: https://www.ncbi.nlm.nih.gov/books/NBK557536/

[7] A. Khan, K. Allemailem, F. Alhumaydhi, S. Gowder, and A. Rahmani, "The Biochemical and Clinical Perspectives of Lactate Dehydrogenase: An Enzyme of Active Metabolism," *Endocr Metab Immune Disord Drug Targets*, vol. 20, Dec. 2019, doi: 10.2174/1871530320666191230141110.

[8] D. B. Millar, V. Frattali, and G. E. Willick, "Quaternary structure of lactate dehydrogenase. I. Subunit molecular weight and reversible association at acid pH," *Biochemistry*, vol. 8, no. 6, pp. 2416–2421, Jun. 1969, doi: 10.1021/bi00834a025.

[9] M. Drent, N. A. M. Cobben, R. F. Henderson, E. F. M. Wouters, and M. Van Dieijen-Visser, "Usefulness of lactate dehydrogenase and its isoenzymes as indicators of lung damage or inflammation," *European Respiratory Journal*, vol. 9, no. 8, pp. 1736 – 1742, 1996, doi: 10.1183/09031936.96.09081736.

[10] J. A. Read, V. J. Winter, C. M. Eszes, R. B. Sessions, and R. L. Brady, "Structural Basis for Altered Activity of M-and H-Isozyme Forms of Human Lactate Dehydrogenase," 2001, doi: 10.1002/1097-0134(20010501)43:2<175::AID-PROT1029>3.0.CO;2.

[11] "UniProt databank L-lactate dehydrogenase." Accessed: Oct. 19, 2023. [Online]. Available: https://www.uniprot.org/uniprotkb/K1T0A2/entry#structure

[12] Rehman I, Farooq M, and Botelho S, "Biochemistry, Secondary Protein Structure.," Treasure Island (FL): StatPearls Publishing. Accessed: Nov. 01, 2023. [Online]. Available: https://www.ncbi.nlm.nih.gov/books/NBK470235/

[13] D.L. Nelson and M.M. Cox, *Introduzione alla biochimica di Lehninger*, Sesta edizione. 2018.

[14] B. Otto Warburg, F. Wind, and N. Negelein, "THE METABOLISM OF TUMORS IN THE BODY." [Online]. Available: http://rupress.org/jgp/article-pdf/8/6/519/1249131/519.pdf

[15] M. V. Liberti and J. W. Locasale, "The Warburg Effect: How Does it Benefit Cancer Cells?," *Trends in Biochemical Sciences*, vol. 41, no. 3. Elsevier Ltd, pp. 211–218, Mar. 01, 2016. doi: 10.1016/j.tibs.2015.12.001.

[16] E. C. Calvaresi *et al.*, “Dual targeting of the warburg effect with a glucose-conjugated lactate dehydrogenase inhibitor,” *ChemBioChem*, vol. 14, no. 17, pp. 2263–2267, Nov. 2013, doi: 10.1002/cbic.201300562.

[17] L. de Bari and A. Atlante, “Including the mitochondrial metabolism of l-lactate in cancer metabolic reprogramming,” *Cellular and Molecular Life Sciences*, vol. 75, no. 15. Birkhauser Verlag AG, pp. 2763–2776, Aug. 01, 2018. doi: 10.1007/s00018-018-2831-y.

[18] Y. Kobayashi *et al.*, “Warburg effect in Gynecologic cancers,” *Journal of Obstetrics and Gynaecology Research*, vol. 45, no. 3, pp. 542–548, Mar. 2019, doi: 10.1111/jog.13867.

[19] International Agency for Research on Cancer, “Global Cancer Observatory (GCO),” 2023. Accessed: Oct. 05, 2023. [Online]. Available: https://gco.iarc.fr/

[20] W. Cui, A. Aouidate, S. Wang, Q. Yu, Y. Li, and S. Yuan, “Discovering Anti-Cancer Drugs via Computational Methods,” *Frontiers in Pharmacology*, vol. 11. Frontiers Media S.A., May 20, 2020. doi: 10.3389/fphar.2020.00733.

[21] L. Wang *et al.*, “Advances of Artificial Intelligence in Anti-Cancer Drug Design: A Review of the Past Decade,” *Pharmaceuticals*, vol. 16, no. 2. MDPI, Feb. 01, 2023. doi: 10.3390/ph16020253.

[22] M. Capula, C. Corno, B. E. L. Hassouni, G. L. I. Petri, and S. Aranđelović, “A brief guide to performing pharmacological studies in vitro: Reflections from the EORTC-PAMM Course ‘Preclinical and Early-phase Clinical Pharmacology,’” *Anticancer Research*, vol. 39, no. 7. International Institute of Anticancer Research, pp. 3413–3418, 2019. doi: 10.21873/anticanres.13485.

[23] M. Piumetti, N. Russo, and M. Piumetti, *Notes on catalysis for environment and energy / Marco Piumetti, Nunzio Russo*. Torino: CLUT, 2017.

[24] P. Zucca and E. Sanjust, “Inorganic materials as supports for covalent enzyme immobilization: Methods and mechanisms,” *Molecules*, vol. 19, no. 9. MDPI AG, pp. 14139–14194, Sep. 09, 2014. doi: 10.3390/molecules190914139.

[25] M. Hartmann and X. Kostrov, “Immobilization of enzymes on porous silicas – benefits and challenges,” *Chem Soc Rev*, vol. 42, no. 15, pp. 6277–6289, Jul. 2013, doi: 10.1039/c3cs60021a.

[26] E. Jackson, F. López-Gallego, J. M. Guisan, and L. Betancor, “Enhanced stability of L-lactate dehydrogenase through immobilization engineering,” *Process Biochemistry*, vol. 51, no. 9, pp. 1248–1255, Sep. 2016, doi: 10.1016/j.procbio.2016.06.001.

[27] D. Roura Padrosa, A. I. Benítez-Mateos, L. Calvey, and F. Paradisi, “Cell-free biocatalytic syntheses of l-pipecolic acid: A dual strategy approach and process intensification in flow,” *Green Chemistry*, vol. 22, no. 16, pp. 5310–5316, 2020, doi: 10.1039/d0gc01817a.

[28] Z. Zhou and M. Hartmann, “Progress in enzyme immobilization in ordered mesoporous materials and related applications,” *Chem Soc Rev*, vol. 42, no. 9, pp. 3894–3912, Apr. 2013, doi: 10.1039/c3cs60059a.

[29] R. Fopase, S. Paramasivam, P. Kale, and B. Paramasivan, “Strategies, challenges and opportunities of enzyme immobilization on porous silicon for biosensing applications,” *J Environ Chem Eng*, vol. 8, no. 5, Oct. 2020, doi: 10.1016/j.jece.2020.104266.

[30] C. Blanco-Llamero, P. García-García, and F. J. Señoráns, “Cross-Linked Enzyme Aggregates and Their Application in Enzymatic Pretreatment of Microalgae: Comparison Between CLEAs and Combi-CLEAs,” *Front Bioeng Biotechnol*, vol. 9, Dec. 2021, doi: 10.3389/fbioe.2021.794672.

[31] N. R. Mohamad, N. H. C. Marzuki, N. A. Buang, F. Huyop, and R. A. Wahab, “An overview of technologies for immobilization of enzymes and surface analysis techniques for immobilized

enzymes," *Biotechnology and Biotechnological Equipment*, vol. 29, no. 2. Diagnosis Press Limited., pp. 205–220, 2015. doi: 10.1080/13102818.2015.1008192.

[32] N. Carlsson, H. Gustafsson, C. Thörn, L. Olsson, K. Holmberg, and B. Åkerman, "Enzymes immobilized in mesoporous silica: A physical-chemical perspective," *Advances in Colloid and Interface Science*, vol. 205. pp. 339–360, Mar. 2014. doi: 10.1016/j.cis.2013.08.010.

[33] S. Hudson, J. Cooney, and E. Magner, "Proteins in mesoporous silicates," *Angewandte Chemie - International Edition*, vol. 47, no. 45. pp. 8582–8594, Oct. 27, 2008. doi: 10.1002/anie.200705238.

[34] D. Chaudhary and S. Sharma, "An overview of ordered mesoporous material SBA-15: synthesis, functionalization and application in oxidation reactions," *Journal of Porous Materials*, Aug. 2017, doi: 10.1007/s10934-016-0311-z.

[35] C. T. Kresge, M. E. Leonowicz, W. J. Roth, J. C. Vartuli, and J. S. Beck, "Ordered mesoporous molecular sieves synthesized by a liquid-crystal template mechanism," *Nature*, vol. 359, no. 6397, pp. 710 – 712, 1992, doi: 10.1038/359710a0.

[36] M. Hartmann, "Ordered mesoporous materials for bioadsorption and biocatalysis," *Chemistry of Materials*, vol. 17, no. 18. pp. 4577–4593, Sep. 06, 2005. doi: 10.1021/cm0485658.

[37] C. T. Kresge, J. C. Vartuli, W. J. Roth, and M. E. Leonowicz, "The discovery of ExxonMobil's M41S family of mesoporous molecular sieves," in *Mesoporous Crystals and Related Nano-Structured Materials*, vol. 148, O. Terasaki, Ed., in Studies in Surface Science and Catalysis, vol. 148. , Elsevier, 2004, pp. 53–72. doi: https://doi.org/10.1016/S0167-2991(04)80193-9.

[38] J. M. Kisler, A. Dähler, G. W. Stevens, and A. J. O'Connor, "Separation of biological molecules using mesoporous molecular sieves," *Microporous and Mesoporous Materials*, vol. 44–45, pp. 769–774, 2001, doi: 10.1016/S1387-1811(01)00259-1.

[39] J. F. Díaz and K. J. Balkus Jr., "Enzyme immobilization in MCM-41 molecular sieve," *J Mol Catal B Enzym*, vol. 2, no. 2–3, pp. 115–126, 1996, doi: 10.1016/S1381-1177(96)00017-3.

[40] A. M. Tope, N. Srinivas, S. J. Kulkarni, and K. Jamil, "Mesoporous molecular sieve (MCM-41) as support material for microbial cell immobilization and transformation of 2,4,6-trinitrotoluene (TNT): A novel system for whole cell immobilization," *J Mol Catal B Enzym*, vol. 16, no. 1, pp. 17–26, 2001, doi: 10.1016/S1381-1177(01)00040-6.

[41] Z. A. Alothman, "A review: Fundamental aspects of silicate mesoporous materials," *Materials*, vol. 5, no. 12. pp. 2874–2902, 2012. doi: 10.3390/ma5122874.

[42] U. Ciesla and F. Schü Th, "Ordered mesoporous materials," *Microporous and Mesoporous Materials*, vol. 27, pp. 131–149, 1999.

[43] Y. Klinthongchai, S. Prichanont, P. Praserthdam, and B. Jongsomjit, "Effect of TMB/P123 ratios on physicochemical properties of mesocellular foam carbon (MCF-C) as catalyst for ethanol dehydrogenation," *Mater Today Chem*, vol. 20, Jun. 2021, doi: 10.1016/j.mtchem.2021.100466.

[44] Y. Wang, M. Noguchi, Y. Takahashi, and Y. Ohtsuka, "Synthesis of SBA-15 with different pore sizes and the utilization as supports of high loading of cobalt catalysts," *Catal Today*, vol. 68, pp. 3–9, 2001, Accessed: Nov. 05, 2023. [Online]. Available: https://doi.org/10.1016/S0920-5861(01)00317-0

[45] H. Chen, H. Liu, R. Wang, X. Jiang, and M. Zhu, "Size-controllable synthesis of dendritic porous silica as reinforcing fillers for dental composites," *Dental Materials*, vol. 37, no. 6, pp. 961–971, Jun. 2021, doi: 10.1016/j.dental.2021.02.015.

[46] M. Kruk, “Access to ultralarge-pore ordered mesoporous materials through selection of surfactant/swelling-agent micellar templates,” *Acc Chem Res*, vol. 45, no. 10, pp. 1678–1687, Oct. 2012, doi: 10.1021/ar200343s.

[47] N. Rahmat, A. Z. Abdullah, and A. R. Mohamed, “A Review: Mesoporous Santa Barbara Amorphous-15, Types, Synthesis and Its Applications towards Biorefinery Production,” *Am J Appl Sci*, vol. 7, no. 12, pp. 1579–1586, 2010.

[48] D. Zhao, Q. Huo, J. Feng, B. F. Chmelka, and G. D. Stucky, “Nonionic Triblock and Star Diblock Copolymer and Oligomeric Surfactant Syntheses of Highly Ordered, Hydrothermally Stable, Mesoporous Silica Structures,” *Journal of the American Chemical Society* , vol. 120, no. 24, pp. 6024–6036, 1998, doi: 10.1021/ja974025i.

[49] L. Qian *et al.*, “Inverse gas chromatography applied in the surface properties evaluation of mesocellular silica foams modified by sized nickel nanoparticles.,” *J Chromatogr A*, vol. 1322, pp. 81–9, 2013, [Online]. Available: https://api.semanticscholar.org/CorpusID:23636262

[50] R. Singh, R. Bapat, L. Qin, H. Feng, and V. Polshettiwar, “Atomic Layer Deposited (ALD) TiO2 on Fibrous Nano-Silica (KCC-1) for Photocatalysis: Nanoparticle Formation and Size Quantization Effect,” *ACS Catal*, vol. 6, no. 5, pp. 2770–2784, May 2016, doi: 10.1021/acscatal.6b00418.

[51] A. Maity and V. Polshettiwar, “Dendritic Fibrous Nanosilica for Catalysis, Energy Harvesting, Carbon Dioxide Mitigation, Drug Delivery, and Sensing,” *ChemSusChem*, vol. 10, no. 20. Wiley-VCH Verlag, pp. 3866–3913, Oct. 23, 2017. doi: 10.1002/cssc.201701076.

[52] B. G. Trewyn, I. I. Slowing, S. Giri, H. T. Chen, and V. S. Y. Lin, “Synthesis and functionalization of a mesoporous silica nanoparticle based on the sol-gel process and applications in controlled release,” *Accounts of Chemical Research*, vol. 40, no. 9. pp. 846–853, Sep. 2007. doi: 10.1021/ar600032u.

[53] J. K. Kaushik and R. Bhat, “Why is trehalose an exceptional protein stabilizer? An analysis of the thermal stability of proteins in the presence of the compatible osmolyte trehalose,” *Journal of Biological Chemistry*, vol. 278, no. 29, pp. 26458–26465, Jul. 2003, doi: 10.1074/jbc.M300815200.

[54] A. Blanco and G. Blanco, “Chapter 8 - Enzymes,” in *Medical Biochemistry*, A. Blanco and G. Blanco, Eds., Academic Press, 2017, pp. 153–175. doi: https://doi.org/10.1016/B978-0-12-803550-4.00008-2.

[55] E. Seibert and T. S. Tracy, “Fundamentals of Enzyme Kinetics,” in *Enzyme Kinetics in Drug Metabolism: Fundamentals and Applications*, S. Nagar, U. A. Argikar, and D. J. Tweedie, Eds., Totowa, NJ: Humana Press, 2014, pp. 9–22. doi: 10.1007/978-1-62703-758-7_2.

[56] K. A. Johnson and R. S. Goody, “The original Michaelis constant: Translation of the 1913 Michaelis-Menten Paper,” *Biochemistry*, vol. 50, no. 39, pp. 8264–8269, Oct. 2011, doi: 10.1021/bi201284u.

[57] H. Lineweaver and D. Burk, “The Determination of Enzyme Dissociation Constants,” *J. Am. Chem. Soc.*, vol. 56, no. 3, pp. 658–666, 1934, Accessed: Nov. 05, 2023. [Online]. Available: https://doi.org/10.1021/ja01318a036

[58] “Enzyme Kinetics and Diagnostic Uses of Enzymes.” Accessed: Oct. 12, 2023. [Online]. Available: https://themedicalbiochemistrypage.org/enzyme-kinetics-and-diagnostic-uses-of-enzymes/

[59] M. Piumetti, A. Illanes, N. Lygeros, M. Piumetti, A. Illanes, and N. Lygeros, *Molecular dynamics and complexity in catalysis and biocatalysis / Marco Piumetti ; [with contributions by Andrés Illanes, Nik Lygeros]*. Cham: Springer, 2022.

[60] E. Buxbaum, “Inhibition and Inactivation of Enzymes,” in *Fundamentals of Protein Structure and Function*, E. Buxbaum, Ed., Cham: Springer International Publishing, 2015, pp. 141–161. doi: 10.1007/978-3-319-19920-7_6.

[61] G. Hegyi *et al.*, *Introduction to Practical Biochemistry*. Eötvös Loránd University, 2013.

[62] H. P. Erickson, “Size and shape of protein molecules at the nanometer level determined by sedimentation, gel filtration, and electron microscopy,” *Biological Procedures Online*, vol. 11, no. 1. pp. 32–51, 2009. doi: 10.1007/s12575-009-9008-x.

[63] O. Alptekin, S. S. Tükel, D. Yildirim, and D. Alagöz, “Characterization and properties of catalase immobilized onto controlled pore glass and its application in batch and plug-flow type reactors,” *J Mol Catal B Enzym*, vol. 58, no. 1–4, pp. 124–131, 2009, doi: 10.1016/j.molcatb.2008.12.004.

[64] S. C. Liew, “Electromagnetic Waves ,” Centre for Remote Imaging, Sensing and Processing. Accessed: Oct. 26, 2023. [Online]. Available: https://crisp.nus.edu.sg/~research/tutorial/em.htm

[65] H. and W. R. L. Rodriguez-Saona Luis and Ayvaz, “Infrared and Raman Spectroscopy,” in *Food Analysis*, S. S. Nielsen, Ed., Cham: Springer International Publishing, 2017, pp. 107–127. doi: 10.1007/978-3-319-45776-5_8.

[66] M. Jafari, “Application of Vibrational Spectroscopy in Organic Electronics,” 2017.

[67] J. Coates, “Interpretation of Infrared Spectra, A Practical Approach,” *Encyclopedia of Analytical Chemistry*, pp. 10815–10837, 2006, Accessed: Nov. 05, 2023. [Online]. Available: https://doi.org/10.1002/9780470027318.a5606

[68] S. Khan, S. Khan, L. Khan, A. Farooq, K. Akhtar, and A. M. Asiri, “Fourier Transform Infrared Spectroscopy: Fundamentals and Application in Functional Groups and Nanomaterials Characterization,” in *Handbook of Materials Characterization*, 2018, pp. 317–344. doi: 10.1007/978-3-319-92955-2_9.

[69] DISAT-Carbon Group, “Field Emission SEM,” Politecnico di Torino. Accessed: Sep. 22, 2023. [Online]. Available: https://areeweb.polito.it/ricerca/carbongroup/fac_fesem.html

[70] C. Temiz, “Scanning Electron Microscopy,” in *Electron Microscopy*, M. Mhadhbi, Ed., Rijeka: IntechOpen, 2022, p. Ch. 1. doi: 10.5772/intechopen.103956.

[71] M. Abd Mutalib, M. A. Rahman, M. H. D. Othman, A. F. Ismail, and J. Jaafar, “Scanning Electron Microscopy (SEM) and Energy-Dispersive X-Ray (EDX) Spectroscopy,” in *Membrane Characterization*, 2017, pp. 161–179. doi: 10.1016/B978-0-444-63776-5.00009-7.

[72] K. A. Cychosz and M. Thommes, “Progress in the Physisorption Characterization of Nanoporous Gas Storage Materials,” *Engineering*, vol. 4, no. 4. Elsevier Ltd, pp. 559–566, Aug. 01, 2018. doi: 10.1016/j.eng.2018.06.001.

[73] K. S. W. Sing, “Reporting physisorption data for gas/solid systems with special reference to the determination of surface area and porosity (Recommendations 1984),” vol. 57, no. 4, pp. 603–619, 1985, doi: doi:10.1351/pac198557040603.

[74] M. Thommes *et al.*, “Physisorption of gases, with special reference to the evaluation of surface area and pore size distribution (IUPAC Technical Report),” *Pure and Applied Chemistry*, vol. 87, no. 9–10, pp. 1051–1069, Oct. 2015, doi: 10.1515/pac-2014-1117.

[75] Andy Connelly, “BET surface area,” WordPress.com. Accessed: Sep. 20, 2023. [Online]. Available: https://andyjconnelly.wordpress.com/2017/03/13/bet-surface-area/

[76] M. Thommes *et al.*, “Physisorption of gases, with special reference to the evaluation of surface area and pore size distribution (IUPAC Technical Report),” *Pure and Applied Chemistry*, vol. 87, no. 9–10, pp. 1051–1069, Oct. 2015, doi: 10.1515/pac-2014-1117.

[77] “Gas adsorption: Determination of the specific surface area (BET surface area).” Accessed: Sep. 20, 2023. [Online]. Available: https://www.3p-instruments.com/measurement-methods/bet-surface-area/

[78] S. Brunauer, P. H. Emmett, and E. Teller, “Adsorption of Gases in Multimolecular Layers,” *J Am Chem Soc*, vol. 60, no. 2, pp. 309 – 319, 1938, doi: 10.1021/ja01269a023.

[79] C. Cocuzza, E. Antoniono, C. Ottone, V. Cauda, D. Fino, and M. Piumetti, “Preparation of a Mesoporous Biosensor for Human Lactate Dehydrogenase for Potential Anticancer Inhibitor Screening,” *ACS Biomater Sci Eng*, Oct. 2023, doi: 10.1021/acsbiomaterials.3c00582.

[80] J. H. Billman and A. C. Diesing, “Reduction of Schiff Bases with Sodium Borohydride,” *J. Org. Chem.*, vol. 22, no. 9, pp. 1068–1070, 1957, Accessed: Nov. 05, 2023. [Online]. Available: https://doi.org/10.1021/jo01360a019

[81] “51146 Atto 550 Protein Labeling Kit,” 2018.

[82] S. L. Zhang, Y. He, and K. Y. Tam, “Targeting cancer metabolism to develop human lactate dehydrogenase (hLDH)5 inhibitors,” *Drug Discovery Today*, vol. 23, no. 7. Elsevier Ltd, pp. 1407–1415, Jul. 01, 2018. doi: 10.1016/j.drudis.2018.05.014.

[83] C. Granchi *et al.*, “Discovery of N-hydroxyindole-based inhibitors of human lactate dehydrogenase isoform A (LDH-A) as starvation agents against cancer cells,” *J Med Chem*, vol. 54, no. 6, pp. 1599–1612, Mar. 2011, doi: 10.1021/jm101007q.

[84] C. Granchi *et al.*, “Assessing the differential action on cancer cells of LDH-A inhibitors based on the N-hydroxyindole-2-carboxylate (NHI) and malonic (Mal) scaffolds †”, doi: 10.1039/b000000x.

[85] N. Markoglou and I. W. Wainer, “Chapter 7 - Immobilized enzyme reactors in liquid chromatography: On-line bioreactors for use in synthesis and drug discovery,” in *Handbook of Analytical Separations*, vol. 4, I. D. Wilson, Ed., Elsevier Science B.V., 2003, pp. 215–234. doi: https://doi.org/10.1016/S1567-7192(03)80008-6.

[86] M. Hiraoui, M. Guendouz, N. Lorrain, A. Moadhen, L. Haji, and M. Oueslati, “Spectroscopy studies of functionalized oxidized porous silicon surface for biosensing applications,” *Mater Chem Phys*, vol. 128, no. 1–2, pp. 151–156, Jul. 2011, doi: 10.1016/j.matchemphys.2011.02.052.

[87] W. Cui, A. Aouidate, S. Wang, Q. Yu, Y. Li, and S. Yuan, “Discovering Anti-Cancer Drugs via Computational Methods,” *Frontiers in Pharmacology*, vol. 11. Frontiers Media S.A., May 20, 2020. doi: 10.3389/fphar.2020.00733.

[88] V. Salmaso and S. Moro, “Bridging molecular docking to molecular dynamics in exploring ligand-protein recognition process: An overview,” *Frontiers in Pharmacology*, vol. 9, no. AUG. Frontiers Media S.A., Aug. 22, 2018. doi: 10.3389/fphar.2018.00923.

[89] W. Chen, X. Liu, S. Zhang, and S. Chen, “Artificial intelligence for drug discovery: Resources, methods, and applications,” *Molecular Therapy - Nucleic Acids*, vol. 31. Cell Press, pp. 691–702, Mar. 14, 2023. doi: 10.1016/j.omtn.2023.02.019.

[90] T. J. A. Ewing, S. Makino, A. G. Skillman, and I. D. Kuntz, “DOCK 4.0: Search strategies for automated molecular docking of flexible molecule databases,” *J Comput Aided Mol Des*, vol. 15, no. 5, pp. 411–428, 2001, doi: 10.1023/A:1011115820450.

[91] G. M. Morris *et al.*, “AutoDock4 and AutoDockTools4: Automated docking with selective receptor flexibility,” *J Comput Chem*, vol. 30, no. 16, pp. 2785–2791, Dec. 2009, doi: https://doi.org/10.1002/jcc.21256.

[92] G. Jones, P. Willett, R. C. Glen, A. R. Leach, and R. Taylor, “Development and validation of a genetic algorithm for flexible docking11Edited by F. E. Cohen,” *J Mol Biol*, vol. 267, no. 3, pp. 727–748, 1997, doi: https://doi.org/10.1006/jmbi.1996.0897.

[93] Dassault Systèmes, “SIMULATIONS - INCLUDES THE HIGHLY VERSATILE CHARMM MOLECULAR MECHANICS SIMULATION PROGRAM.” Accessed: Oct. 31, 2023. [Online]. Available: https://www.3ds.com/products-services/biovia/products/molecular-modeling-simulation/biovia-discovery-studio/simulations/

[94] H. C. S. Chan, H. Shan, T. Dahoun, H. Vogel, and S. Yuan, “Advancing Drug Discovery via Artificial Intelligence,” *Trends in Pharmacological Sciences*, vol. 40, no. 8. Elsevier Ltd, pp. 592–604, Aug. 01, 2019. doi: 10.1016/j.tips.2019.06.004.